Spring 5-6-2017

Targeted Delivery of Drug Combinations Via Nanocarriers for Cancer Treatment

Kruti Soni
University of Nebraska Medical Center

TARGETED DELIVERY OF DRUG COMBINATIONS VIA NANOCARRIERS FOR CANCER TREATMENT

by

Kruti S. Soni

A DISSERTATION

Presented to the Faculty of

The Graduate College in the University of Nebraska

In Partial Fulfillment of the Requirements

For the Degree of Doctor of Philosophy

Department of Pharmaceutical Sciences

Under the Supervision of Professor Tatiana K. Bronich

University of Nebraska Medical Center

Omaha, Nebraska

January 2017

Supervisory Committee:

Dr. Jered Garrison

Dr. Ram Mahato

Dr. Vimla Band

TABLE OF CONTENTS

In loving memory of my father,
my constant source of inspiration

ACKNOWLEDGEMENT

This is a moment of great pleasure for me as I have come to the end of an extremely challenging and enriching journey of my life. The past 4.5 years of my life have shown me extreme highs and lows; I have learnt to come to terms with all that life has thrown at me, whether it be losses or gains, and move on. I am extremely glad that I have survived this journey and accomplished what I started, albeit as a very different and hopefully better person at the end of it. However, as they say, nothing worth achieving can ever be accomplished alone and I do have quite a few people to be grateful for being there and helping me see this through till the end.

First and foremost, my sincerest gratitude goes to my mentor, Dr. Tatiana Bronich. She has always shown great faith in me, especially at times when I did not have it in myself and that helped me keep going. Her constant pushing to be productive helped me stay focused and motivated during tough times and I wouldn't have reached the end of my Ph.D. without her faith in me. I have learnt a lot from her both personally and professionally and hope to eventually imbibe in myself her qualities of critical thinking, perseverance, attention to the smallest detail and problem solving approach. She has been extremely supportive and accommodating and I am thankful to her for letting me complete my work at my own pace. I am also thankful to her for always being readily available for discussing results and troubleshooting experiments or giving feedback on abstracts and fellowship drafts in spite of keeping a busy schedule. I have gained many valuable skills under her mentorship.

My gratitude also extends to Dr. Luis Marky for being extremely generous with his time and knowledge. The discussions with him on my experiments and results were some of the best learning experiences and very enjoyable part of my Ph.D. work. The members of my advisory committee, Dr. Jered Garrison, Dr. Vimla Band and Dr. Ram Mahato have

provided me with valuable feedback on my research during committee meetings for which I am very grateful. I sincerely appreciate Dr. Samuel Cohen and Lora Arnold for helping me out with the pathological evaluation of my slides, especially for doing things very quickly at short notices in spite of having a hectic schedule. I would like to thank our collaborator, Dr. Prakash Radhakrishnan and Thomas Caffrey for their help with the animal experiments of our project. I am also thankful to Dr. Nilesh Wagh for teaching me many basic laboratory techniques during my first rotation at UNMC.

Another very important person in this journey is Dr. Swapnil Desale. I am extremely fortunate to have had a chance to work under him and learn all the technical skills that were necessary for my Ph.D. work. Working with him was always fun. He has always helped me out in my times of stress and constantly motivated me to focus on the right things. He is a true friend and a true critic and has always been there at every turning point of my career, giving great advice from his own experiences. More than anything, he has been extremely patient in answering my endless questions. I am glad that we have been in touch even after he moved out of Omaha and I am certain that our friendship will only get stronger with time. Dr. Jinjin Zhang is the kindest and the most hardworking person I have seen, who was always ready to help in any way she could. She has been a true source of inspiration. Both Swapnil and Jinjin have been great seniors to work with and with them around, the lab environment was always positive, energetic and friendly to work in. I wish them both plenty of success and happiness in life. Dr. Hangting Hu has been a kind friend in this journey. I am extremely grateful to Dr. Fan Lei for helping me with polymer synthesis and animal studies in the last phase of my Ph.D. His sincere and dedicated efforts helped me complete the experiments in a timely manner. I thank him for not only being a dependable colleague but also a great friend, who made the long and hectic working hours fun and manageable. I would also like to thank other present and

past members of our lab, Dr. Svetlana Romanova, Dr. Shaheen Ahmed, Dr. Anya Brynskikh, Xinyuan Xi, Dr. Chantey Morris, and Tong Liu for being wonderful coworkers as well as the administrative staff including Katina Winters, Jamie Arbaugh, Christine Allmon and Keith Sutton for their support. A special thanks to Christine for always having solutions to everything I ask for and processing all requests at the speed of light! I would like to acknowledge the technical assistance from UNMC core facilities in my research and financial support from NIH and UNMC Graduate Assistantship and Fellowship.

Omaha has given me many great friends without whom this journey would have been very dull. A special thanks to Sugandha and Aastha for always being there and keeping me upbeat during bad times. I wouldn't have survived the tough days without their emotional support and the times we spent together are some of my fondest memories. My list of friends would be incomplete without mentioning Swati, Rashmi, Rhishikesh, Shashank, Niodita, Seema, Pravin, Shalis, Prathamesh, Aditya, Shrey and many more people who have been a family away from home and I wish them the very best with their future endeavors.

Last but not the least, my wonderful family, who has supported me in everything I did and never let me compromise on my dreams even when the situations were tough. My uncle, Mukesh Soni for keeping us strong during the darkest times and my wonderful cousin and his wife, Aditya and Shweta and Anand and Priyanka and my late aunt for being my support system. My deepest gratitude and respects to my mother for letting me go away from her at a time when she needed me the most and staying strong through it and my wonderful little brother, Chintan, for being my best friend and a constant source of joy. I cannot imagine my life without all of them.

Kruti Soni

January, 2017

TARGETED DELIVERY OF DRUG COMBINATIONS VIA NANOCARRIERS FOR CANCER TREATMENT

Kruti Soni, Ph.D.

University of Nebraska Medical Center, 2017

Advisor: Tatiana K. Bronich, Ph.D.

Combination therapy is preferred over monotherapy to treat cancer as it can show better therapeutic outcomes and also delay the onset of resistance by targeting multiple cell-survival pathways in cancer cells. Rationally developed combinations with monoclonal antibodies and small molecule drugs in the form of antibody-drug conjugates or antibody nanoparticle conjugates allow us to take advantage of the cellular targeting of the potent cytotoxic agents, thereby widening the scope for dose reduction while maintaining the required therapeutic response. This can in turn improve patient tolerability by reducing the off target toxicities. For the therapy of ErbB2 positive breast cancer, the monoclonal antibody, Trastuzumab, is the FDA approved therapy. The receptor tyrosine kinase, ErbB2 is a viable target in 20-25 % breast cancer patients due to its overexpression. Its degradation is associated with slower progression of the disease and increased survival times. While the monoclonal antibody Trastuzumab (Herceptin™) is the first line therapy in such patients, monotherapy with Trastuzumab has shown little benefit and therefore must be given with chemotherapeutic agents. Such combinations also help in delaying the development of resistance to Trastuzumab, since multiple cellular pathways can be targeted simultaneously. ErbB2 is a client protein of heat shock protein 90 and 17-N-allylamino-17-demethoxygeldanamycin (17-AAG) is a potent inhibitor of HSP90. Previous work in our lab has demonstrated strong synergy of action between 17-AAG and a model cytotoxic agent doxorubicin. In order to further improve the efficacy of the therapy, our

goal was to replace doxorubicin with a more potent, clinically relevant agent paclitaxel (PTX), which has been shown to have strong synergistic antitumor effect with 17-AAG in ErbB2-driven breast cancers. Since synergy of such therapy is often sequence and dose ratio specific, co-delivery of the drugs via the same vehicle is desirable as well as beneficial. For this purpose, polymeric micelles prepared from a biodegradable block copolymer were chose. Polypeptides have an inherent property to assemble into supramolecular structures in solution. The formation of supramolecular structures is a controlled and organized process that depends by and large on the nature of the polypeptide and conditions of the solvent it is exposed to. Formation of amphiphilic copolymers based on such polypeptides can allow for tailoring the assembly process to a predefined nanoscale supramolecular structure, which can then be used as drug delivery vehicles. The overall process of self-assembly of such amphiphilic copolymers can then be regarded as a complex phenomenon of structural organization that is governed by the nature of constituent hydrophilic and hydrophobic blocks, their relative lengths, as well as properties of the solvent-phobic block that is the driving force for self-assembly. The inherent biocompatibility and biodegradability of polypeptides is of additional advantage for their biological applications. For the purpose of the current study, amphiphilic block copolymer with following composition was chosen: polyethylene glycol (PEG) as the hydrophilic, stealth imparting block and polyleucine (PLeu) as the hydrophobic part and the initiator of micelle formation in aqueous environment. The variables explored in the current study were altering the ratio of lengths of constituent blocks as well as chirality of PLeu block and the temperature of solvent used for preparation of micelles via the film rehydration method. The impact of all these variables on the thermodynamic stability as well as type of secondary structures formed and the influence of these attributes on the ability of the micelles to encapsulate a combination of hydrophobic drugs into their core are also described. Dual drug-loaded micelles thus prepared could load 17-AAG and PTX

in a ratio 2:1 by weight. The formulation showed a high level of synergy on BT-474 cells that express a high amount of ErbB2 while the synergy was negligible in ErbB2low MCF-7 cells. The strong synergy also observed when the formulation was tested in an orthotopic breast cancer mouse model developed using ErbB2 overexpressing BT-474 cells, and an arrest in the growth of tumors in animals treated with dual drug-loaded micelles was observed, while both 17-AAG and PTX were used at sub therapeutic doses of 10 mg and 5 mg equivalents per kg body weight. The lower doses also helped avoid toxicity associated with the therapy. We also show the importance of simultaneously delivering the two drugs via a single carrier system as opposed to cocktail of individual drug-loaded micelles administered at equivalent doses, which has a better therapeutic outcome than the cocktail therapy. These combination drug-loaded micelles were developed as a platform for chemotherapy with Trast. The triple therapeutic system of Trast with combination drug-loaded micelles containing 17-AAG and PTX exhibited an even stronger anticancer effect, with complete regression of tumors at the end of treatment, which reached a palpable size again after day 45 with much slower progression than other treatment controls.

Pancreatic cancer (PC) is one of the most lethal malignancies, due to aggressive tumorigenicity, early metastasis and development of drug resistance to standard care chemotherapy. Since its approval in 1997, Gemcitabine (Gem) has been the first-line treatment for advanced disease. However, there is no standard second-line therapy after Gem failure. FOLFIRINOX, a combination of four agents, folinic acid, fluorouracil, irinotecan and oxaliplatin was approved by the FDA in 2010. The rationale for this combination was based on these drugs having a different mechanism of action, and, more importantly, non-overlapping toxicities. In cases that could tolerate FOLFIRINOX, an overall improvement in the survival times as well as quality of life was noted. However,

even the toxicities are non-overlapping, the cumulative toxicity profile for FOLFIRINOX can become the dose limiting factor. In the first trial itself, 50.8% of the patients needed dose adjustment. The common toxicities observed with FOLFIRINOX include Febrile neutropenia, Thrombocytopenic bleeding, ≥ grade 3 platelets, Grade 2 persistent neurotoxicity, Grade 3 persistent neurotoxicity OR Grade 4 neurotoxicity and many more non-hematological toxicities. Most of the toxicities are severe enough to require discontinuation of the treatment or switching to lower doses or alternative agents. The combination of Gem with Cisplatin (CDDP) has been explored in clinical trials for metastatic disease. As a part of FOLFIRINOX, platinum compounds showed significant efficacy. Cisplatin acts by damaging the DNA. It is known to first get converted into the aqua form within the cell, which happens by the replacement of the labile chloro groups with water molecules. This active form is then able to form covalently linked adducts with the DNA. This initial assault then goes on to activate a series of signaling pathways that ultimately lead to apoptosis and cell death. The DNA adducts thus formed can cause distortion of the DNA and subsequent recognition by various cellular proteins. This leads to problems in DNA synthesis and replication and is reported to cause a prolonged G2 cell-cycle phase arrest. However, the exact mechanism of activation of the apoptotic pathways remains unclear. On the other hand, gemcitabine is a deoxycytidine analog. Its mechanism of activation involves conversion into its triphosphate form, which can then be incorporated into the DNA as a false nucleotide. Usually, one more deoxynucleotide can be incorporated into the DNA before the synthesis stops. Another minor mechanism of action of gemcitabine is its ability to inhibit ribonucleotide reductase, which plays a key role in the repair mechanism of the DNA. Many studies report the benefit of administration of gemcitabine prior to that of cisplatin; the reason cited for this is the increase in the formation of Pt-DNA adducts when the DNA had already been damaged and exposed due to the incorporation of deoxycytidine or active gemcitabine. The gemcitabine in turn

inhibits the repair of the formed Pt-DNA adducts as well as reduces the efficacy of nucleotide excision repair by its ability to inhibit the action of ribonucleotide reductase. On the other hand, when Pt compounds are administered prior to gemcitabine, the formed Pt-DNA adducts can no longer allow for the incorporation of gemcitabine and that leaves no scope for gemcitabine to act. Our preliminary in vitro studies with the free drugs on T3M4 Simple Cells (*COSMC* deleted cells) showed that synergy of the combination is schedule-dependent, and Gem administration followed by CDDP showed the most potent cytotoxic activity. However, this combination proved to be only marginally effective in actual practice due to combined increased toxicity of both the agents. We have shown that encapsulation of CDDP in polymeric nanogels with cross-linked ionic cores enhanced its tumor accumulation and improved its safety profile. Additionally, sustained release profile of CDDP from nanogels allows for the administration of free Gem and CDDP loaded nanogels in a single injection while still retaining schedule-dependent synergy of the combination. Pancreatic ductal adenocarcinoma cells are known to express truncated O-glycans (Tn and STn antigens) and it was shown that decorating the nanogels with an antibody directed against this antigen further enhanced their uptake by tumor cells while reducing off-target accumulation in an in vivo pancreatic cancer model.

LIST OF FIGURES

LIST OF TABLES

LIST OF ABBREVIATIONS

17-AAG	17-N-allylamino-17-demethoxygeldanamycin
^{1}H-NMR	Proton Nuclear Magnetic Resonance
5-FU	5-Fluorouracil
ABC	ATP-binding cassette
ADC	Antibody Drug Conjugates
ADCC	Antibody dependent cellular cytotoxicity
ALP	Alkaline Phosphatase
ALT	Alanine Aminotransferase
ANOVA	One way analysis of variance
ATP	Adenosine triphosphate
CD	Circular Dichroism
CDC	Complement-dependent cytotoxicity
CDDP	cis-dichlorodiamminoplatinum (II)
CI	Combination Index
CMC	Critical Micelle Concentration
DAB+	3,3'-Diaminobenzidine
D_{eff}	Effective hydrodynamic diameter
DLS	Dynamic Light Scatterig
DMEM	Dulbecco’s Modified Eagle's Medium

DMSO	Dimethyl Sulfoxide
DNA	Deoxyribonucleic acid
DOX	Doxorubicin
DSC	Differential Scanning Calorimetry
EDC	1-Ethyl-3-(3-dimethylaminopropyl)carbodiimide
EDTA	Ethylene Diaminetetraacetic acid
EGFR	Epidermal Growth Factor Receptor
EPR	Enhanced Permeability and Retention
FACS	Fluorescence-activated Cell Sorting
FBS	Fetal Bovine Serum
FDA	Food and Drug Administration
Fmoc	9-Fluorenylmethyloxycarbonyl
Gem	Gemcitabine
GPC	Gel Permeation Chromatography
H&E	Hematoxylin and Eosin
HER2	Human Epidermal growth factor receptor 2
HPLC	High Pressure Liquid Chromatography
HSP90	Heat Shock Protein 90
IACUC	Institutional Animal Care and Use Committee
IC_{50}	Half Maximal Inhibitory Concentration

ICP-MS	Inductively Coupled Plasma-Mass Spectrometer
IV	Intravenous
mAb	Monoclonal Antibody
MALS	Multi-angle light scattering
MDR	Multi-drug resistance
mPEG	Methoxy Polyethylene Glycol
mTOR	Mechanistic target of rapamycin
MUC	Mucin
MW	Molecular Weight
MWCO	Molecular Weight Cut-off
NCA	N-carboxyanhydride
NG	Nanogel
NHS	N-Hydroxysuccinimide
PBS	Phosphate Buffered Saline
PDI	Polydispersity index
PEG	Polyethylene Glycol
PEG-PLeu	Polyethylene Glycol-*block*-polyleucine
PgP	P-glycoprotein
PLeu	Polyleucine
Pt	Platinum

PTX	Paclitaxel
RBC	Red Blood Cells
RP-HPLC	Reverse Phase-high Pressure Liquid Chromatography
RPMI	Roswell Park Memorial Institute medium
SD	Standard Deviation
SEC	Size Exclusion Chromatography
SEM	Standard Error of the Mean
THF	Tetrahydrofuran
UV	Ultraviolet–visible Spectroscopy
VEGF	Vascular endothelial growth factor
WBC	White Blood Cells

LIST OF CONTRIBUTIONS

1. Chapter 2 – Dr. Swapnil Desale and Dr. Svetlana Romanova assisted with monomer synthesis. Modified polymer for Trast conjugated micelles was synthesized by Dr. Fan Lei. Drs. Swapnil Desale and Fan Lei assisted throughout the animal studies. Dr. Luis Marky, Dr. Calliste Reiling and Dr. Alexander Lushnikov for help with Differential Scanning Calorimetry and Circular Dichroism experiments, Dr. Bhopal Mohapatra for help with implantation of estrogen pellets, Rhishikesh Thakare for assisting with LC-MS/MS method optimization, Fei Yu for help with MALS measurements and Xinyuan Xi for help with animal necropsy. Dr. Samuel Cohen performed the histopathological analysis of tissue samples.
2. Chapter 3 - The synthesis of nanogels was initially described by Dr. Bronich and Sirisha Bontha. Further work on this system was performed by Drs. Nataliya Nukolova and Jong Oh Kim. TKH-2 antibody was provided by Dr. Prakash Radhakrishnan. Thomas Caffrey and Dr. Prakash Radhakrishnan assisted with the animal experiment. Xinyuan Xi helped with animal necropsy. Paul Grandgenett, Maria Steele, Kamiya Mehla, Kelly O'Connell helped with surgery to develop the orthotopic mouse model of pancreatic cancer. Platinum measurements were done at core facility of University of Nebraska Medical Center by Dr. Chantey Morris.
3. Major contributions in all chapters were made by Kruti Soni. The overall project was designed under the guidance of Dr. Tatiana K. Bronich. Dr. Prakash Radhakrishnan helped in the design of pancreatic cancer animal experiment.
4. This work was supported by the DOD grant W81XWH-11-1-0167 (Dr. Tatiana K. Bronich). We acknowledge the assistance of the Nanomaterials Core facility of the Center for Biomedical Research Excellence (CoBRE) Nebraska Center for Nanomedicine supported by the Institutional Development Award (IDeA) from the

National Institute of General Medical Sciences of the National Institutes of Health under grant number 4P20GM103480-09. Partial support for the work described in Chapter 3 was by LB506 and Pancreas Spore Career Development Award. The Salary support for Kruti Soni was provided by research assistantship from Nebraska Center for Nanomedicine (NCN), a Center of Biomedical Research Excellence (COBRE) (2012-2015) and the Program of Excellence Graduate Assistantship from UNMC (2015-2017).

CHAPTER 1

Introduction

1.1 Therapeutic approaches in cancer

The National Cancer Institute defines cancer as a group of diseases arising due to defects in the genes responsible for the control of cell division. It can be inherited or caused due to environmental factors or exposure to known carcinogens. Latest statistics indicate that nearly 40 percent of men and women would be diagnosed with cancer during their lifetime and the rates of mortality resulting from cancer is on the rise. It is a disease with heterogeneity that makes it difficult to have a standard therapy that can be equally effective even within the same type of cancer. The complexity of the disease arises from the fact that each individual's cancer can have a unique combination of genetic changes, which continue to diversify as the cancer progresses. This makes it very difficult to combat the disease with a single therapeutic approach. Hence, a variety of combination approaches are adopted, which are summarized in fig. 1.1. Briefly, they consist of 1) Surgery: this is the most preferred option where feasible; most of the tumor mass is removed surgically, and is followed by adjuvant therapies like radiation or chemotherapy to eradicate the remaining cells in the tissue. However, surgery is not an option for very deep-seated tumors at sites that are inaccessible or if there is extensive metastasis. 2) Immunotherapy: it involves taking help of the immune system directly or indirectly to fight cancer. Some of the approaches in immunotherapy include use of monoclonal antibodies that specifically mark cancer cells for clearance by the immune system, adoptive transfer of T cells to boost the body's natural immunity, cytokines like interferons and interleukins and vaccines for prophylactic purposes. 3) Radiation: radiation can be used at multiple

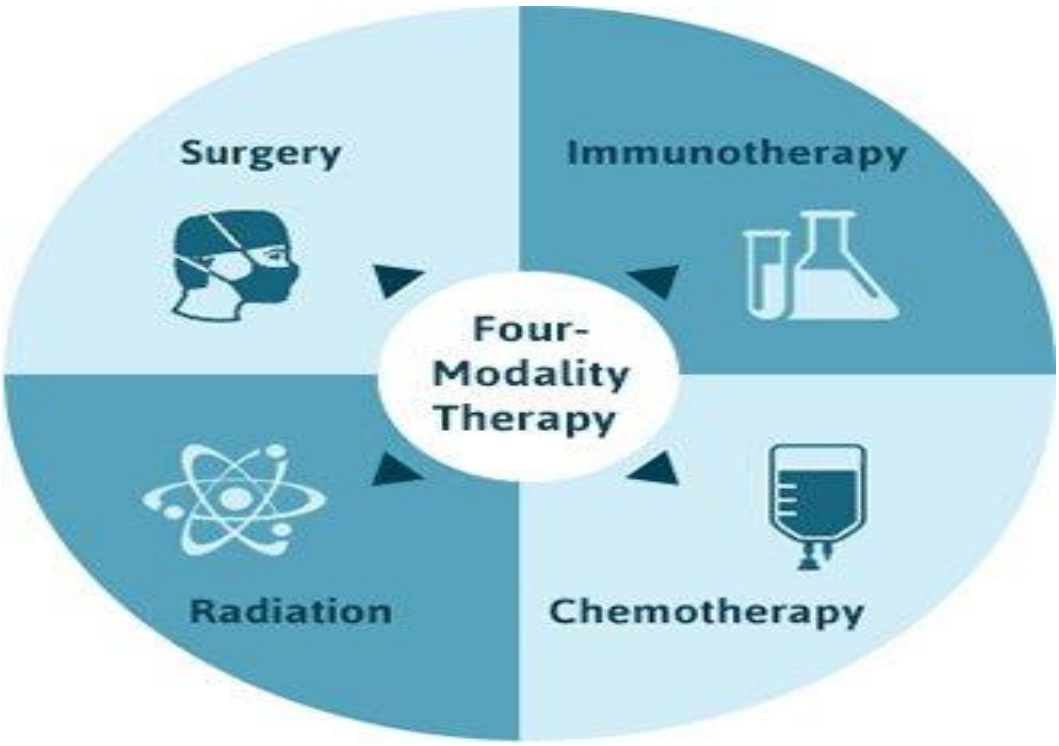

Figure 1. Therapeutic approaches for cancer treatment

stages of the disease; before surgery, it can be used to shrink the tumor for ease of removal, intraoperatively, for better access to the tumor site and avoid exposure to healthy areas or after the surgery, to kill the residual cancer cells. 4) Chemotherapy: it is the most popular form of therapy and can be given post-surgery or even as a stand-alone treatment option. There are multiple chemotherapeutic agents with different mechanisms of action that can be employed for the purpose. Like radiation, it can either be used prior to surgery to reduce the tumor volume or post-surgery to kill the residual cancer cells. Chemotherapy can involve the use of either single or multiple agents depending on the severity of the disease as well as its response to treatment. Overall, the type of therapeutic approach adopted to combat cancer depends on subtype of the disease as well as its sensitivity to the approach adopted as well as its feasibility. Often, the side effects can also be a limiting factor for the use of a specific approach and can depend on individual susceptibilities.

1.2 Chemotherapy – the need for combination therapy

1.2.1 Chemotherapy

Therapeutic approaches in cancer have traditionally involved the use of cytotoxic agents and the majority of them act via induction of apoptosis in the cancer cells. This apoptosis is induced via damage to a key cell organelle like the DNA or by hampering the cell division process like microtubule inhibition or by affecting the synthesis of key proteins for normal cellular function. These approaches are summarized in Fig. 2. [1]. Apoptotic signals are generated within the cells when chemotherapeutic agent causes an injury that can make the cell dysfunctional. This process can be divided into 3 phases. Phase I is where the injury first occurs. The site of injury depends on the type of drug used and maybe either the DNA, RNA or microtubules. The cell realizes the extent of damage caused by the initial assault in Phase II, by mechanisms that are yet to be discovered. For example, treatment of some T-cell leukemia lines with doxorubicin results in upregulation of the ligand to the Fas receptor, which may mediate the ability of doxorubicin to kill these cells [2]. This response depends on the sensitivity of the cell to the injury and lack of defense or corrective mechanisms decide the extent of sensitivity. Phase III is the final phase where apoptotic signaling is initiated. For example, γ-radiation causes the induction of the pro-apoptotic Bax in radiosensitive but not in radio-resistant cells. This may drive cells to apoptosis [3]. In this phase, the cells undergo the orderly breakdown of macromolecules through the operation of proteases, endonucleases, transglutaminases, and possibly lipases. Other cell types may preferentially execute programs of cell cycle arrest and damage repair in response to these same signals. Although such a decision point appears critical in imparting selectivity of responses to similar stimuli, little is known concerning its existence, components, or regulation. The conclusion remains that if the cell senses the

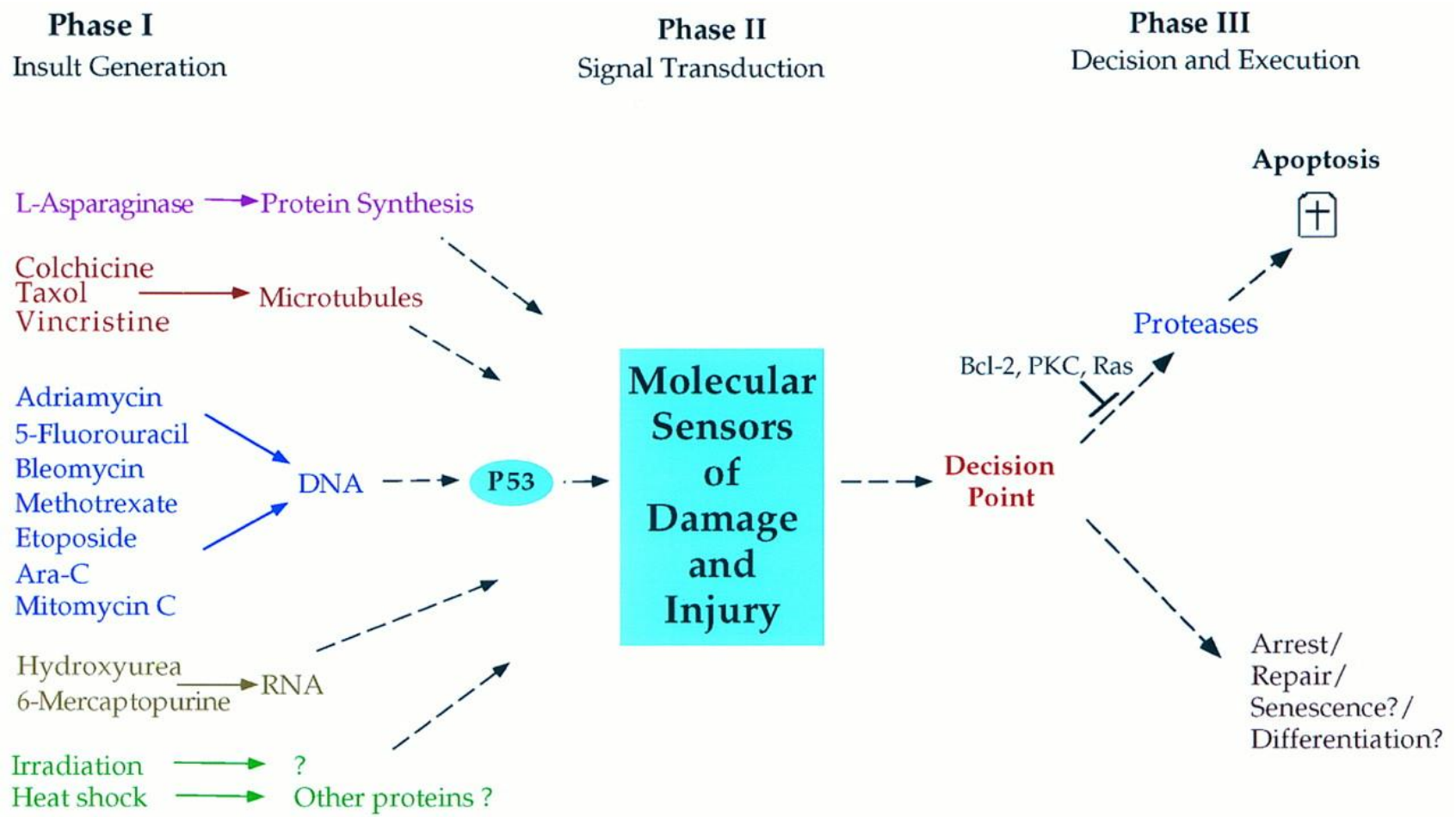

Figure 2. Summary of the different hypothetical phases in the induction of apoptosis by chemotherapeutic agents. Adapted from (Hannun).

damage to be irreversible, it undergoes apoptosis and subsequent death. Thus, the above listed process can be described as a general mechanism of action for single drugs that is monotherapy in cancer.

1.2.2 Development of resistance

The development of resistance to monotherapy is a very common phenomenon that is quick to occur, while many cells are inherently resistant to apoptosis. These cancers may very well have disarmed regulatory mechanisms that survey damage or injury. This is supported by the frequent mutations in p53, which appears to play a critical role in the response to DNA damage. Other mutations may exist that also allow these cancer cells to escape suicide. If chemotherapeutic agents act primarily to induce apoptosis, then it becomes obvious that these cancer cells may be a priori resistant to cell death in response to these agents. If this is the case, then the hematologic and germ cell malignancies may be the exceptional malignancies. For some reason these cancers may have traded the increased susceptibility to apoptosis for some survival or growth advantage. What the era of cytotoxic chemotherapy may have accomplished is to segregate cancers into two groups: those that are prone to apoptosis and those that are resistant [1]. Various mechanisms have been proposed to explain the mechanism of resistance development [4]. Altered Membrane Transport is probably one of the most significant forms of resistance against the variety of currently used antineoplastic agents. It is by the action of a group of membrane proteins which extrude cytotoxic molecules, keeping intracellular drug concentration below a cell-killing threshold. These ATP-dependent multidrug transporters belong to the ubiquitous superfamily of ATP-binding cassette (ABC) proteins. The ABC proteins have been grouped into 7 subclasses ranging from ABCA to ABCG [5-7] based upon genomic organization, order of domains and sequence homology. The MDR1 gene, which encodes P-glycoprotein (P-gp; MDR1, ABCB1) [8-11], a phosphorylated and

glycosylated 170-kDa protein of 1,280 amino acids, is the most widely observed mechanism in clinical transport-associated MDR [11-14]. Genetic responses may also decide the fate of therapy. Cells can compensate for the action of inhibitors by overexpressing the target protein; the administered concentration of the drug would then be insufficient to show desired inhibitory effects. P-gp activity is also related to the status and level of activity of the MDR1 gene. Rifampicin can induce MDR1 expression. Induction of intestinal P-gp by rifampicin has been shown to be the major mechanism responsible for reduced digoxin levels during concomitant rifampicin therapy; in healthy male volunteers, the oral bio-availability of digoxin decreased by 30% and intestinal P-gp levels were induced 3.5-fold during rifampicin therapy [15,16]. Many drugs act by damaging the DNA or by inhibition of the enzymes responsible for DNA repair. To compensate, cells can enhance the activity of repair enzymes. Excision repair cross-complementing protein (ERCC1), most likely a DNA-binding protein, is another example of a DNA repair protein that may be involved in recognition of cisplatin damage; its expression is elevated in cisplatin- and carboplatin-resistant cells compared with that in cells sensitive to cisplatin [17,18]. The target molecules in the cells can undergo alterations in such a manner that their binding affinity to the drug molecules is reduced to the extent that the drugs are no longer effective. A classic example of this phenomenon is anti-estrogen therapy in breast cancer by agents like tamoxifen. The cells lose estrogen receptors overtime and the initially responsive cancer then becomes non-responsive, although a temporary response to other estrogen receptors like aromatase inhibitors might be seen temporarily [19,20]. Target molecules may also disappear from cancer cells as a result of the loss of the corresponding gene. Chromosomal losses are a common feature of cancer. Duesberg et al. [21,22] have suggested that it is the aneuploid nature of cancer cells that best explains the development of MDR. Another physiological response to the presence of drugs is the overexpression of drug-metabolizing enzymes or carrier molecules; e.g. the increased production of glutathione

[23] or ubiquitin contributes to inactivation of the drug by forming conjugates that are excreted. Resistance to cisplatin in ovarian carcinoma cells is associated with increased expression of dihydrodiol dehydrogenase [24]. Serum levels of interleukin (IL)-6 have been found to be elevated in patients with various types of cancer. Conze et al. [25] demonstrated that autocrine production of IL-6 by breast cancer cells could promote resistance to chemotherapy. Cells sensitive to chemotherapy did not express appreciable IL-6, whereas high levels were detectable in multidrug-resistant cells. Studies on breast cancer cells have also suggested involvement of the extracellular matrix in drug resistance [26]. It is known that out of different pathways, apoptosis can also be mediated by activation of the Fas/Fas-L pathway, which is the extrinsic pathway of induction of apoptosis. These authors showed that ligation of b1 integrins by their extracellular matrix ligands inhibits apoptosis mediated by paclitaxel and vincristine, which activate this pathway. These agents act by causing release of mitochondrial cytochrome c. Integrin mediated protection from the drug-induced apoptosis and inhibition of cytochrome c release were dependent on the activation of the PI3 kinase/Akt pathway. Song et al. [27] have shown that chemo resistance may be induced by extracellular factors in tumor-bearing organs. Comparing chemo sensitivity and proteins in different tumors and different culture systems, they found elevated levels of acidic and basic fibroblast growth factors in the media of solid and metastatic tumors. These conditioned media induced broad-spectrum resistance to drugs (paclitaxel, doxorubicin and 5-FU) with diverse structures and mechanisms of action. Application in combination, of these two growth factors, could produce a 10-fold increase in drug resistance, whereas suramin, a known inhibitor of fibroblast growth factors, was able to reverse this resistance. Thus, with monotherapy, cells can in general adopt several mechanisms to develop resistance.

1.2.3 Approaches to overcome resistance - combination therapy

As discussed above, cancer cells can develop multiple pathways of overcoming the toxic effects of a single anticancer drug. The most logical way to overcome resistance therefore is the use of a combination of drugs that can target multiple, distinct pathways so that the cells cannot find a mechanism to cope with the damage. The general guidelines for choosing drugs in combination therapy are: 1) drugs that target different pathways synergistically so as to achieve maximum benefit and explore the possibility of reducing the dose of individual agents [28,29]; 2) the drugs do not have overlapping toxicities and the combination is not antagonistic; 3) a combination that can be administered since early onset of the disease where the drugs have similar administration cycles so that there is minimum gap between treatments for recovery of sensitive healthy tissue [4,28-30]. The many advantages of combination therapy are summarized in Fig 1.3. [31]. Many approaches may be used to assess the extent of synergy that drug combinations have, the Chou and Talalay analysis being the most popular amongst them [32]. Synergy essentially allows us to see better response than sum of effects of individual drugs. This effect may be seen irrespective of whether the drugs act on the same pathway or different ones [32]. Chiang et al. have shown that an mTOR inhibitor, RAD001 has strong synergy with gem or PTX in a heterogeneous group of non-Hodgkin lymphoma cell lines. Their observations indicated that mTOR inhibition sensitized the cells to apoptosis induced by gemcitabine or PTX, and this ultimately activated caspase-dependent apoptosis to a greater extent than monotherapy with PTX or gem [33]. As described earlier, one of the main reasons for the development of resistance is the presence of efflux pumps and P-gp, multidrug resistance protein 1 (MRP1) and breast cancer resistance protein (BCRP) are some of the most overexpressed efflux pumps in human cancers [34].

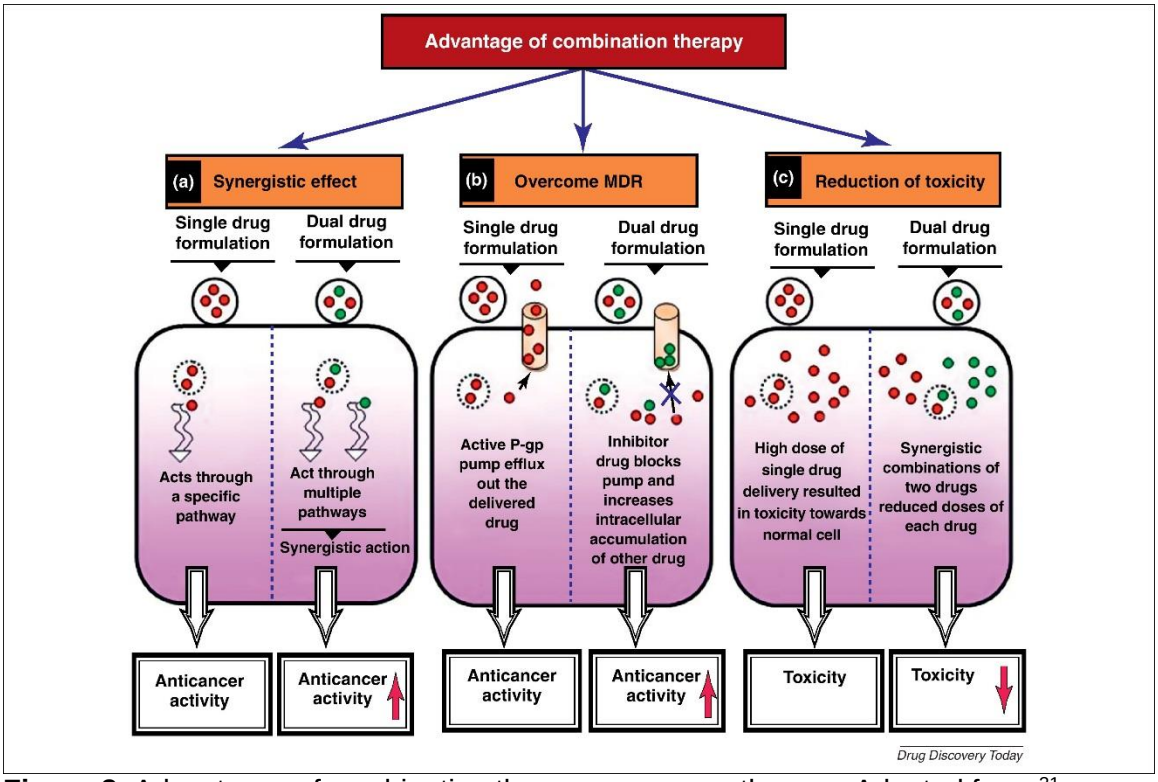

Figure 3. Advantages of combination therapy over monotherapy. Adapted from [31].

Thus, it is logical to co-administer P-gp inhibitors with cytotoxic agents to prevent or reverse MDR [35]. Recently, Hubensack *et al.* showed a significant elevated concentration of paclitaxel in the brain domain of nude mice when administrated with elacridar and tariquidar (both are third-generation P-gp inhibitors), caused by downregulation of P-gp expressed at the blood–brain barrier [36]. In another Phase I clinical trial, zosuquidar was co-delivered with daunorubicin and cytarabine to older acute myeloid leukemia patients and the results demonstrated increased anticancer activity experienced by patients overcoming drug resistance [37]. Since synergistic effects are much greater than the additive effect of individual components, it is possible to keep the disease in check with much lower doses of individual drugs. This helps spare healthy tissues from chemotherapy-related toxicities and increases patient tolerance. It was shown that one such combination of carboplatin and gem in a small group pf patients with metastatic ovarian cancer administered at sub therapeutic doses resulted in significant antitumor activity without any

signs of hematological toxicity [38]. In another study, Bava *et al.* co-administered the herbal drug curcumin with the cytotoxic anticancer drug paclitaxel with a view to reducing the dose-limiting toxicity exerted by paclitaxel on systemic delivery, and they demonstrated that combination therapy not only reduced the dose of paclitaxel but also demonstrated increased anticancer cytotoxic activity compared with paclitaxel alone in HeLa cells [39]. In conclusion, synergistic combinations can increase patient compliance for treatment as they have the potential to reduce toxic effects, lower frequency of administration and delay the onset of MDR [32,40,41].

1.2.3.1 Types of combination therapies in clinical practice

Combination therapy is a broad term that covers the application of more than one technique or agent that can be injurious to cancer cells. The most common approaches involve combination of various cytotoxic drugs, inhibitors of oncogenic pathways, chemotherapeutic drugs with radiotherapy or hormone therapy or immunotherapy. These approaches are summarized in fig 1.4. For hormone dependent breast cancer, different methods are adopted to reduce or stop the effect of estrogen on cancer cells. Aromatase is an enzyme responsible for the production of estrogens. Therefore, inhibitors of aromatase can stop the production of estrogen and have been used intensely for the treatment of breast cancer. Similarly, the use of various hormone receptor inhibitors (such as tamoxifen and raloxifene) can block the overexpressed cancer cell receptor and prevent its activation for consequent uncontrolled proliferation. Recent studies have suggested that endocrine therapy can be used with adjuvant bisphosphonate therapy (using zoledronic acid) for the treatment of breast cancer. Zoledronic acid prevents aromatase-inhibitor-associated bone loss in post-menopausal women with breast cancer and it represented a cost-effective treatment for the prevention of bone loss and/or fracture [42]. Combination of chemotherapy and radiotherapy is one of the most promising

strategies for current cancer therapeutics. It has been shown to improve patient survival and the locoregional control of various cancers when compared with radiotherapy alone [43]. In the early 1970s, the combination of 5-fluorouracil (5-FU) and mitomycin C with radiotherapy demonstrated improved results for patients with locally advanced stages of anal cancer [44]. A randomized Phase II clinical trial was performed to examine the combination of radiotherapy and a prostate-specific-antigen-based vaccine in prostate cancer patients and the results have shown that radiotherapy makes the tumor more susceptible to vaccines [45]. Different monoclonal antibodies can also be used to block oncogenic signaling. Antibodies can also be used to activate the immune system to kill the cancer cells through the activation of complement system or by direct cytotoxic effect which is termed as antibody-dependent cellular cytotoxicity (ADCC) [46]. Studies conducted by Tanabe *et al.* have demonstrated that the combinations of mitomycin C and methotrexate showed significant antitumor activity in metastatic breast cancer patients pretreated with anthracycline and taxanes [47]. In another study, Arkenau *et al.* showed that, after curative resection of stage III colon cancer, adjuvant treatment with 5-FU plus leucovorin is generally well tolerated and the long-term follow-up study demonstrated that this combination administered for 12 cycles significantly reduced tumor relapse and improved survival [48]. The other combinations of drugs in cancer therapeutics include a combination of paclitaxel with carboplatin or with vinorelbine for the treatment of nonsmall-cell lung cancer [49]. Among different combination therapies the most practiced and well researched therapy method is co-treatment with multiple chemotherapeutic drugs. Therefore, current trends in anticancer research have progressively concentrated on the development of new combinations of anticancer drugs with a view to overcoming the limitations frequently associated with conventional chemotherapy [31].

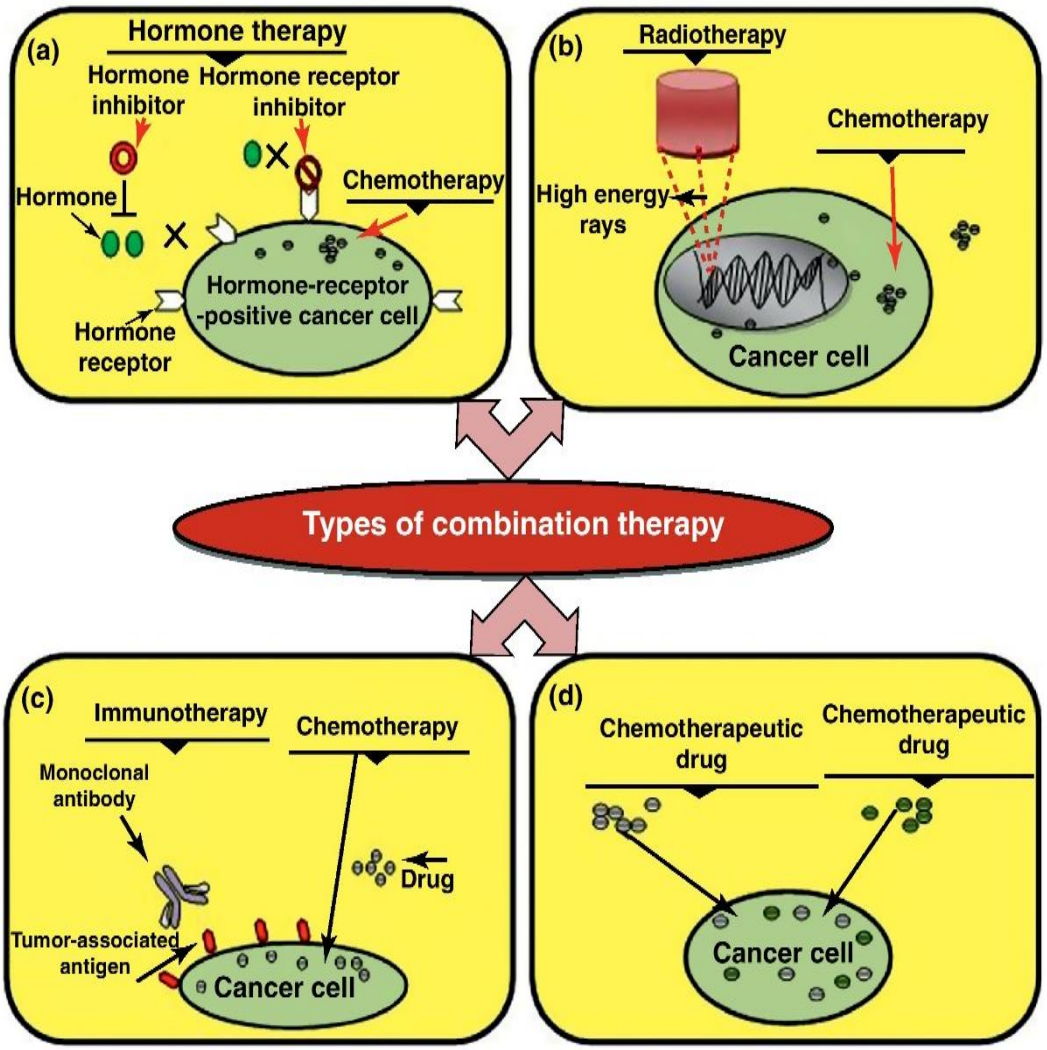

Figure 4. Different approaches of combination therapy for the treatment of cancer. Adapted from [31].

1.2.3.2. Combination therapy in breast cancer

Breast cancer is one of the most commonly encountered gynecological malignancies in women and claims many lives worldwide. About 1 in 8 U.S. women (12%) is prone to develop breast cancer during her lifetime. Latest cancer statistics indicate that in 2016, an estimated 246,660 new cases of invasive breast cancer are expected to be diagnosed in women in the U.S. (Source: Breastcancer.org). Despite excellent advances in medical diagnostics and early detection, it has been observed that up to five percent of the patients diagnosed with breast cancer already have metastatic disease at the time of diagnosis,

while around thirty percent of the cases with primary tumor are expected to progress to metastatic disease (EarlyBCTCG). While medical advances have improved the overall survival of patients with breast cancer, the disease itself is known to be very heterogeneous and has profound complexity at the genetic level, which makes it a great challenge to find a treatment solution that can be effective in the vast majority of the cases [50]. Overexpression or aberrant activity of many growth factor receptors is associated with oncogenic signaling. Especially receptors of the ErbB family, including EGFR, ErbB2 (also known as HER2/neu) and ErbB3 are present in many cases of breast cancer and have become popular therapeutic targets for intervention as well as development of novel therapeutic candidates. The best drug in class is the monoclonal antibody, Trastuzumab (Herceptin™; Genentech; against ErbB2) or Cetuximab (Erbitux™; Eli Lilly and Company; against EGFR) and the tyrosine kinase inhibitors, Lapatinib (Tykerb; Glaxo Smithkline; dual EGFR/Her2 inhibitors) or Erlotinib (Tarceva; Genentech; against ErbB2) are currently used clinically. For combinatorial approach, antibody-drug conjugates (ADC) are gaining popularity. Trastuzumab-DM1 (also developed by Genentech) is an anti-mitotic fungal toxin chemically conjugated to anti-ErbB2 monoclonal antibody. An alternative strategy involves targeted delivery of conventional chemotherapeutic drugs (such as Doxorubicin, Paclitaxel or Campothecin) encapsulated in liposomal or polymer micelle based nanoparticles that are conjugated with anti-ErbB2 or anti-EGFR antibodies or ligands are being explored at a laboratory and pre-clinical stage. Both approaches use the overexpression of EGFR and ErbB2 as addresses to specifically deliver cytotoxic cargo. This may be particularly useful as a strategy for overcoming resistance to currently approved ErbB-directed targeted therapies. However, for both antibody-drug conjugates as well as targeted nanoparticulate drug-delivery systems, the extent of endocytosis of the receptor and its distribution between recycling versus lysosomal pathways can limit successful delivery of the chemotherapeutic payload into ErbB2 or EGFR overexpressing

breast cancers. Considering a scope of thesis, this section is intended to focus on use of clinical combination therapy for the treatment of ErbB2-driven breast cancer. Trastuzumab is the current first line therapy for ErbB2-driven breast cancer. It is a humanized monoclonal antibody that binds to its receptor and inhibits its oncogenic signaling that results in ADCC [51-53]. Trastuzumab is well established in palliative as well as adjuvant treatment of Her2-positive breast cancer. In the neoadjuvant setting, phase II studies incorporating trastuzumab reported pCR rates in the range of 18–39% [54-56]. In a randomized study, Budzar et al. [57] treated patients with 4 cycles of paclitaxel followed by 4 cycles of FEC (fluorouracil, epirubicin, and cyclophosphamide) with or without weekly trastuzumab for 24 weeks. After the inclusion of only 42 patients, a significant difference in terms of pCR rate in favour of trastuzumab was observed, and the trial was terminated (66.7 vs. 25%; p = 0.02). Although, Trastuzumab in combination with chemotherapy has shown effectiveness in many patients, challenges due to intrinsic or acquired therapeutic resistance have prompted the development of Trastuzumab-MCC-DM1 (T-DM1; Genentech), which is an antibody-drug conjugate (ADC). DM1 is a Maytansanoid (a derivative of Maytansine; a Vinca alkaloid), which functions as an antimitotic drug [58,59]. DM1 is chemically conjugated to Trastuzumab via a non-reducible Succinimidyl-4-(Nmaleimidomethyl) cyclohexane-1-carboxylate (MCC) crosslinker, which was optimized based on a systematic comparison of various reducible and non-reducible crosslinkers in in vitro studies (intracellular drug release) and in vivo pharmacokinetics and toxicity studies [60-62]. While the mechanism(s) of Trastuzumab resistance remains unclear, several studies indicate that it is not due to loss of ErbB2 overexpression [63,64]; consequently the rationale for T-DM1 design was to use ErbB2 as an address to deliver the cytotoxic drug specifically to ErbB2-overexpressing breast cancers. T-DM1 demonstrated potent and selective activity against a panel of ErbB2 overexpressing breast cancer cell lines (including several Trastuzumab-resistant model cell lines) as compared to normal or

ErbB2-low cancer cell lines [65,66]. Most importantly, the drug exhibited favorable pharmacokinetics, low toxicity in mice and also inhibited growth of Trastuzumab-sensitive as well as resistant ErbB2-overexpressing human breast cancer cell xenografts in mice [65]. Although it was presumed that the cytotoxicity was a result of internalization of the ADC direct data demonstrating internalization of the ADC was lacking. The importance of this is underscored by recent studies that have shown that ErbB2 receptor is not efficiently internalized [67,68]. Given the numerous studies, which suggest that ErbB2 receptor is either internalization resistant or rapidly recycles back to the cell surface [67], data on the site of action of T-DM1 is critical in order to improve designs for optimizing the intracellular delivery of the Maytansanoid. This will especially become important in cases where patient-specific mutations or alterations in the activities of regulators of endocytic trafficking (discussed above) could potentially cause refractoriness or reduce the efficacy of T-DM1. For example, one factor that is hypothesized to contribute to the low rate of endocytosis is the constitutive association of ErbB2 with Heat Shock Protein 90 (HSP90) [68]. It has been demonstrated that HSP90 ATPase inhibitors such as 17-allylaminodemethoxy geldanamycin (17-AAG) induced rapid downregulation of cell surface ErbB2 which is mediated by ubiquitin modification of ErbB2 (Zhou, Xu). Subsequent work has shown that 17-AAG indeed promotes the delivery of surface ErbB2 to the lysosome [59,69], an organelle where molecules such as T-DM1 are intended to go. Several HSP90 inhibitors are currently in phase I and II clinical trials and could potentially be combined with T-DM1. In yet another attempt, NeoSphere, a 4-arm phase II trial focused on the effects of combining trastuzumab with taxanes and also pertuzumab. Patients were randomly assigned to docetaxel plus trastuzumab, docetaxel plus pertuzumab, an alternative Her2-targeting antibody, and docetaxel plus the combination of both antibodies or of trastuzumab and pertuzumab alone without a chemotherapy backbone, for a total of 12 weeks. While the triple-combination arm yielded highest pCR

rates (46%), this study was the first to report a clinically meaningful activity of a chemotherapy-free combination regimen in the neoadjuvant setting with a pCR rate of 17% [70], underscoring the importance of dual Her2 targeted therapy for improved outcomes.

1.2.3.3. Combination therapy in pancreatic cancer

Pancreatic cancer is one of the most lethal cancers known with extremely poor prognosis. It is estimated that 74 percent of the patients diagnosed with pancreatic cancer die within the first year of diagnosis, and most diagnosis is done at a much later stage, when cancer already shows distant metastasis. Average life expectancy after metastasis is between three to six months, and the five-year survival rate is only 2 percent. Since its approval in 1997, gemcitabine has been the first-line therapy for patients with unresectable locally advanced or metastatic disease as it showed benefit over 5-FU [71]. However, the response is only marginal; one year survival rates are no more than 17 to 23 percent post gemcitabine monotherapy [71-73]. Since then, efforts have been directed towards development of better therapeutic approach to combat the disease. Platinum- and Capecitabine- based combination therapy has shown distinct advantages over gemcitabine alone [74-76]. Yet another study reported the benefits of Gemcitabine with nab-PTX [77] this study reported significant improvement in survival rates as well as median survival times (by 3.4 months over gemcitabine alone). This trend continued in secondary end points like progression-free survival, which improved by as much as 31% as compared to gemcitabine alone and response rate that almost tripled. All in all, these studies show the benefit of combination therapy over gemcitabine alone, especially when dealing with advanced stages of pancreatic cancer. FOLFIRINOX, a combination of four agents, folinic acid, fluorouracil, irinotecan and oxaliplatin was approved by the FDA in 2010 [72]. The rationale for this combination was based on these drugs having a different

mechanism of action, and, more importantly, non-overlapping toxicities [78]. FOLFIRINOX was the choice of treatment by nearly 18% oncologists for patients with metastatic disease [79]. The study compared either gemcitabine or FOLFIRINOX (only in patients that did not show preexisting neutropenia) as the first-line therapy and the other as the second-line therapy in case of non-responders or recurrences. Platinum compounds were also used as the second-line therapy in some cases. The end result obtained showed that first-line therapy of with FOLFIRINOX had significant advantages over gemcitabine therapy. In cases that could tolerate FOLFIRINOX, an overall improvement in the survival times as well as quality of life was noted [80]. However, even the toxicities are non-overlapping, the cumulative toxicity profile for FOLFIRINOX can become the dose limiting factor. In the first trial itself, 50.8% of the patients needed dose adjustment. The common toxicities observed with FOLFIRINOX include Febrile neutropenia, Thrombocytopenic bleeding, ≥ grade 3 platelets, Grade 2 persistent neurotoxicity, Grade 3 persistent neurotoxicity OR Grade 4 neurotoxicity and many more non-hematological toxicities. Most of the toxicities are severe enough to require discontinuation of the treatment or switching to lower doses or alternative agents. Thus, although highly effective over gemcitabine monotherapy, very few patients actually qualify for FOLFIRINOX therapy and even fewer are able to continue it beyond two to three cycles. To find a balance between the need for combination therapy and avoidance of dose-limiting toxicities, the alternative has been to look at two-drug combinations. As a part of FOLFIRINOX, platinum compounds showed significant efficacy. Cisplatin, like all other platinum compounds, acts by damaging the DNA. It is known to first get converted into the aqua form within the cell, which happens by the replacement of the labile chloro groups with water molecules. This active form is then able to form covalently linked adducts with the DNA. This initial assault then goes on to activate a series of signaling pathways that ultimately lead to apoptosis and cell death [81]. The DNA adducts thus formed can cause distortion of the DNA and subsequent

recognition by various cellular proteins. This leads to problems in DNA synthesis and replication and is reported to cause a prolonged G2 cell-cycle phase arrest. However, the exact mechanism of activation of the apoptotic pathways remains unclear. On the other hand, gemcitabine is a deoxycytidine analog [82,83]. Its mechanism of activation involves conversion into its triphosphate form, which can then be incorporated into the DNA as a false nucleotide. Usually, one more deoxynucleotide can be incorporated into the DNA before the synthesis stops. Another minor mechanism of action of gemcitabine is its ability to inhibit ribonucleotide reductase, which plays a key role in the repair mechanism of the DNA. Many studies report the benefit of administration of gemcitabine prior to that of cisplatin; the reason cited for this is the increase in the formation of Pt-DNA adducts when the DNA had already been damaged and exposed due to the incorporation of deoxycytidine or active gemcitabine [83]. The gemcitabine in turn inhibits the repair of the formed Pt-DNA adducts as well as reduces the efficacy of nucleotide excision repair by its ability to inhibit the action of ribonucleotide reductase [84,85]. On the other hand, when Pt compounds are administered prior to gemcitabine, the formed Pt-DNA adducts can no longer allow for the incorporation of gemcitabine and that leaves no scope for gemcitabine to act. This is yet another classic example of how the synergy of action/cytotoxic effect of a combination is not a random event, but something that is highly regulated by the mechanism of action of the drugs involved. This mechanism of action then forms the rational basis for selection of the sequence in which the drugs should be administered for optimal efficacy of the combination. In spite of a strong basis for the synergy of action, this combination was also found to have a dose-limiting toxicity and therefore offers the potential for development of nanoparticle-based formulation approaches that can control the sequence of action as well as mitigate toxicities associated with free drugs.

1.3 Antibody conjugates for combination therapy

Antibody-based therapeutics have become an important class of agents for cancer therapy. The idea of antibodies as therapeutics stems from the idea of 'magic bullets' as conceptualized by Paul Ehrlich nearly a century ago and was given a practical and adaptable form with the development of the hybridoma technology by Kohler and Milstein [86], that eventually allowed for the development of highly target specific monoclonal antibodies, directed against a specific receptor. Chimeric humanized IgG antibodies overcame the challenges associated with the administration of a foreign protein into the human body, which involved recognition and clearance by the immune system as a foreign substance and resulted in less than adequate therapeutic response [87-89]. Most therapeutic antibodies are humanized with an IgG1 isotype that is useful for regulation of effect via the Fc region based recognition. Current advances in the antibody production technology are directed towards the making of antibodies with more specificity and alterations in the glycosylation as well as amino-acid sequence for specific tumor antigens.

There are several mechanisms by which mAbs can exert therapeutic vary and can exhibit more than one mode of action. They can activate the immune system and cause cell death via either complement-dependent cytotoxicity of antibody dependent cellular cytotoxicity (ADCC). ADCC involves interaction with two cell types at the same time – the Fc region binds with Fc domain on the surface of immune cells [90] whereas the complementarity determining region binds with its complementary antigen on the target cell such as a cancer cell. Although proven to be effective in vitro, ADCC has been difficult to find operational in the in vivo setting. Clyne and Ravetch [53] found that deletion of the Fc receptor in an Fc-receptor mouse model resulted in diminished antitumor activity of clinically effective mAbs. This data suggested Fc receptor interactions play an important role in the anticancer activity of these mAbs and speculations revolve around the role of

mononuclear phagocytes or natural killer cells as being the effector cell population, and an example of this is the antibody rituximab. However, very little infiltration of host leukocytes was seen when such mAbs were administered to murine models. Alternatively, it may be hypothesized that the immediate effect of such mAb is some damage to the tumor that increases tumor antigen presentation and recruitment of a more specific T-cell response [91,92]. This is known as the ADCC-mediated adaptive immune switch. CDC is more commonly seen with IgM, IgG1 as well as IgG3 subclasses. This effect is a cascade that is set in motion by the formation of antigen-antibody complexes. The ultimate effect is the formation of a membrane attack complex that creates pores in the cell membrane, allowing for free passage of water and solutes out of the cell [93]. However, one of the most prominent modes of action of antibodies in cancer is causing changes in signal transduction. Carcinogenesis is usually associated with an overexpression of certain growth factor receptors, probably due to the high rate of cellular turnover. The activation of signaling of such receptors occurs via the binding of their respective ligands in the extracellular space and promotes cell division and survival. Interfering with the signaling can help sensitize and/or reverse resistance to chemotherapeutic drugs. By extension, antibodies against the EGFR family are some of the most potent agents available. Most antibodies physically bloc the receptor binding site and thereby prevent the binding of the growth factor on its target receptor, e.g. cetuximab [94] while others like pertuzumab inhibit the heterodimerization of the receptor upon binding of ligand to the receptor [95]. Antibodies are mostly designed to be directed at hampering the signaling that is most crucial to cell survival. Within a solid tumor, these can include antigens associated with the tumor stroma, like fibroblasts, vasculature or growth factors like VEGF or EGFR. However, monotherapy with mAbs are as prone to development of resistance as those with small molecules. However, development of combination therapy centered on mAbs has many advantages. mAbs can be used to deliver cytotoxic payloads specifically to the tumor cells,

thereby reducing toxicity to healthy tissues (Wu). Antibodies can be used to deliver chemotherapeutic agents, radioisotopes or other proteins like enzymes. This dissertation focuses on different ways of delivering chemotherapeutic agents using mAbs, viz., ADCs and antibody-nanoparticle conjugates.

1.3.1 Antibody-drug conjugates

ADCs are conjugates of mAbs to cytotoxic agents that allow for more specific delivery of the cytotoxic agents and potentially widen the therapeutic window of the therapeutic system. This can be achieved due to the high binding affinity of mAbs to certain antigens that are over expressed on malignant cells. In other words, mAbs act as the vehicles for the delivery of cytotoxic payloads to cancer cells. ADCs are developed with the aim of enhancing therapeutic efficacy by synergy of action between the mAb and the small molecule drugs conjugated with it. These small molecule payloads have much higher efficacy but lack target specificity. Thus, ADCs serve to combine the best of both the worlds [96-98]. ADCs can be envisioned as prodrugs also, wherein the cytotoxic agent can be cleaved from the linker and released in its active form post internalization of the ADC, as guided by the mAb. Therefore, the choice and design of linker is an area of substantial research, to ensure the release of the cytotoxic agent only when it is internalized into the cancer cells and not in circulation .Before reaching their target cancer cells, the ADCs have to cross many hurdles within the circulation. Thus, the mode of action of ADCs is a complex process involving multiple steps and different types of challenges at each level [99]. In circulation, the ADC is expected to have a distribution profile similar to that of the mAb itself. As mentioned earlier, the chemical stability of the linker is of utmost importance in order to avoid the release of the cytotoxic agent in circulation and avoiding damage to healthy tissues. At the same time, the most crucial consideration is ensuring that the mAb does not lose its binding affinity to the target receptor. mAbs are complex proteins with

secondary and tertiary structures formed due to hydrogen bonding, hydrophobic interactions and many other such forces. Conjugation of a liner can disturb the delicate higher order structure of the mAb and cause it to lose the confirmation necessary for antigen binding. Without binding to the target receptor, internalization of the ADC is not possible. Upon successful internalization, retention and trafficking to the right subcellular compartment is necessary to achieve therapeutic effect. It is also important to achieve enough internalization of the ADC to be in the therapeutic range. Given the unpredictable nature of internalization kinetics of receptors, the cytotoxic agents chosen are often quite potent. This allows for therapeutic effect to be seen even with small amounts of ADCs being internalized as well as allows for smaller number of drug molecules to be conjugated per mAb. This also helps in increasing the stability of the final ADC construct. However, in practicality, the molar ratio of cytotoxic agents to mAb is usually quite high. This excessive payload can alter the surface properties of mAb and cause it to be recognized by the immune system, this leads to rapid clearance of the ADC from circulation and does not allow for effective therapeutic concentration of the ADC to remain in circulation. In general, 2-4 drugs per mAb are considered to be appropriate [100,101]. At the same time, care needs to be taken to avoid masking of the antigen binding sites. Given the complexity of this process, conjugation of nanoparticles loaded with cytotoxic agents offers an attractive alternative strategy. Nanoparticles can be tailored to encapsulate cytotoxic agents of different types. More importantly, with limited points of conjugation to the mAb, nanoparticles can help deliver much higher number of drug molecules per mAb. This can allow for much greater flexibility in terms of adjusting the dose ration between the drugs and the mAbs. In spite of these shortcomings, ADCs are a popular choice for combination therapy in cancer and several ADCs are either in clinical trials or already approved for use by the FDA. Table 1 lists the ADC currently in clinical trials [102].

Agent	Status	Indication	Antigen	Cytotoxic
Vandortuzumab vedotin	Phase I	Hormone refractory prostate cancer	STEAP1	Monomethyl auristatin E
Vorsetuzumab mafodotin SGN-75	Phase I	Metastatic renal carcinoma	CD70	Monomethyl auristatin F
AMG595	Phase I	Glioblastoma	EGFRvIII	DM1
IMGN853	Phase I	Epithelial ovarian cancer	Folate receptor 1	DM4
Enfortumab vedotin	Phase I	Bladder, breast, lung, pancreatic cancer	Cell surface protein nectin 4	Monomethyl auristatin E
Vintafolide	Phase I/IIb	Nonsmall cell lung cancer, ovarian cancer	Folate receptor	Vinblastine
ABT-414	Phase I/II	Glioblastoma	EGFRvIII	Monomethyl auristatin F
Sacituzumab govitecan IMMU-132	Phase I/II	Triple negative BC epithelial cancers	TROP-2	SN38
Indusatumab vedotin	Phase II	Gastrointestinal, pancreatic cancer	Guanylyl cyclase C	Monomethyl auristatin E
Glembatumumab vedotin	Phase II	Metastatic BC advanced melanoma, recurrent or refractory osteosarcoma	Glycoprotein NMB	Monomethyl auristatin E
PSMA-ADC	Phase II	Hormone refractory prostate cancer	PSMA	Monomethyl auristatin E
Lifastuzumab vedotin	Phase II	Platinium-resistant ovarian cancer	SLC34A2	Monomethyl auristatin E
Lorvotuzumab mertansine	Phase II	Small-cell lung, ovarian cancer	CD56	DM1

Table 1. Antibody-drug conjugates in clinical trial. BC, breast cancer; EGFR, epidermal growth factor receptor; Glycoprotein NMB, hematopoietic growth factor inducible neurokinin-1 type (HGFIN); PSMA, prostate-specific membrane antigen; SLC34A2, solute carrier family 34 sodium phosphate member 2; STEAP1, six transmembrane epithelial antigen of the prostate 1: a membrane protein overexpressed in prostate cancer; TROP-2, tumor-associated calcium signal transducer 2. Adapted from [102].

1.3.2 Antibody-nanoparticle conjugates

Out of the many advantages that nanoparticles offer as drug delivery systems, one of the most important ones remain the solubilization of hydrophobic drugs without the use of toxic cosolvents and most nanoparticles can hold more than one type of drug, thus making

them ideal candidates for combination therapy. Several types of nanoparticles are currently in clinical trials, but the most popular type remains nanoparticles made from polymers. Table 2 lists some of the formulations based on polymeric nanoparticles that are in clinical trial for anticancer therapy. These include, but are not limited to, polymerosomes, micelles, hydrogels and nanogels [95,103].

1.3.2.1 Liposomes:

Liposomes have been widely used for the delivery of chemotherapeutic agents, genes, proteins, or any combinations thereof. While natural biolipids impart low stability to liposomes, synthetic amphiphilic copolymers help achieve much higher stability. Liposomes mimic the natural cell membrane properties, it is relatively easy for liposomes to gain entry into the intracellular space [104]. Active targeting of liposomes can be achieved by conjugation of active ligands ion their surface. PEG is the most commonly used spacer that can be functionalized at both ends and conjugate the liposomes to mAbs or other targeting ligands [105]. Either whole antibodies or specific fragments like Fc or Fab can be used to prepare targeted drug delivery systems, while the chemotherapeutic agents can be loaded either in the lipid bilayer (for hydrophobic drugs) or in the aqueous interior for the hydrophilic drugs. For the therapy of HER2+ breast cancer, HER-2 targeted DOX-loaded immunoliposomes (MM-302) have been in clinical trials [106-108]. Such active targeting strategies have shown differential uptake in cancer cells and spared healthy tissues from toxicity [109,110]. Another example of targeted liposomes in clinical trials is that of DOX-loaded PEGylated immunoliposomes targeted with the F(ab') fragment of a tumor-specific human mAb-GAH for patients with metastatic cancer in Phase 1 trials [111].

Formulation	Product	Description	Cancer indication	Phase
Micelles	NK105	PTX	Breast	III
	IG-001	PTX	Breast	I
	Genexol PM	PTX	Bladder, ureter	II
	BIND-014	DTX	Advanced solid	I
	SP1049	DOX	Gastroesophageal	II
	NK911	DOX	Various solid tumor	II
	NC-6300	Epirubicin	Various solid tumor	I
	NK012	SN-38	Breast	II
	NC6004	CDDP	Pancreatic	III
	NC4016	Oxaliplatin	Bowel	I
Hydrogels	Histrelin hydrogel	Histrelin	Prostate	III
	DEBDOX	DOX	Hepatocellular	IV
Microbubbles	Definity®	None	Ocular Melanoma	0
Nanoemulsion	BF-200 ALA	Aminolevulinic Acid	Basal cell	I/II
Conjugates	XMT-1001	CPT	Small cell lung, non-small cell lung	I
	CRLX101	CPT	Solid tumors	II
	CT-2103	PTX	Fallopian tube, ovarian, primary peritoneal cavity	II
	CT-2103	PTX	Glioblastoma multiforme	II
	NKTR-102	Irinotecan	Breast	III
Nanoparticles	BIND-014	DTX	Prostate	II
	BIND-014	DTX	Metastatic solid	I
	ProLindac™	diaminocyclohexane-platinum	Ovarian	II
Supermolecules	CRLX101	CPT	Non-small cell lung	II
	CALAA-01	siRNA	Solid	I
Combination therapy	Atu027 + gemcitabine		Pancreatic	II
	CT-2103 + carboplatin		Non-small cell lung	III
	NKTR-102 + Cetuximab		Colorectal	II
	Microbubble + platinum + gemcitabine		Gastrointestinal	I/II

Table 2. List of polymeric nanoparticles in clinical trials indicating the phase and type of cancer. (Li)

1.3.2.2 Polymerosomes:

Polymerosomes were developed as the more stable alternatives to liposomes, to overcome shortcomings of short circulation half-lives, low drug encapsulation efficiency and short storage shelf life. Like liposomes, polymerosomes can also deliver both hydrophobic and hydrophilic drug molecules and can be tuned in terms of size, shape, permeability, etc [112,113]. At the same time, they can encapsulate drugs like PTX and DOX, that have opposite solubility profiles, like polymerosomes prepared from pH-sensitive degradable copolymers PEG–PTMBPEC [poly(2,4,6-trimethoxy benzylidenepentaerythritolcarbonate)] and PEG-PLA [9,114]. They can also encapsulate superparamagnetic iron oxide into their aqueous cores for diagnostic as well as therapeutic functions and can be surface functionalized with the appropriate mAb [84].

1.3.2.3 Hydrogels and nanogels:

Nanogels are three-dimensional hydrogel materials in the nanoscale size range formed by crosslinked swellable polymer networks with a high capacity to hold water, without actually dissolving into the aqueous medium. Nanogels can be composed of a variety of naturally occurring polymers, synthetic polymers or a combination thereof. Their characteristics such as size, charge, porosity, amphiphilicity, softness, and degradability can be fine-tuned by varying the chemical composition of the nanogels. They are mostly spherical particles but the current advancement in synthetic strategies allow for the fabrication of nanogels of different shapes [103,115,116]. The versatility of their architecture allows for incorporation of a plethora of guest molecules ranging from inorganic nanoparticles to biomacromolecules like proteins and DNA with suitable modifications of the materials used for their construction, without compromising their gel-like behavior [117-123]. As the nanogel structure can be readily adjusted to integrate features of different materials and, thus, offer advantages for combinatorial encapsulation of drugs with varying

physicochemical properties such as small molecules, proteins and nucleic acids. Fahmy and coworkers developed liposomal nanogels of drug-complexed cyclodextrins and cytokine-encapsulating biodegradable polymers that can deliver small hydrophobic molecular TGF-β inhibitor and water-soluble protein cytokine (IL-2) in a sustained fashion to the tumor microenvironment [124]. They demonstrated that synergistic effects of simultaneously delivered IL-2 and TGF-β inhibitor on activation of the innate arm of the immune system led to delayed tumor growth and enhanced survival of melanoma tumor-bearing mice after systemic administration. Similarly, pDNA and proteins were successfully co-encapsulated using pH- and temperature-sensitive carbohydrate-based nanogels [114]. The nanogels had a core–shell structure with a crosslinked hydrophobic core that could be loaded with proteins and the shell contained carbohydrate residues that allowed for the complexation of DNA. These nanogels were capable of loading larger-than-normal amounts of cargo by using a heating and cooling cycle. Owing to the ability of nanogels to encapsulate high amounts of biomacromolecules and prevent them from degradation, they have been also widely explored for the delivery of proteins and peptides. In their pioneering work, Akiyoshi et al. reported that the nanogel of self-assembled cholesterol-modified pullulan (CHP) forms a complex with various kinds of proteins spontaneously, primarily through hydrophobic interactions [125,126]. The amount of protein complexed by such nanogels depends on the molecular weight and hydrophobicity of the protein. The application of polysaccharide-based nanogels for delivering proteins and other macromolecular therapeutics has recently been summarized in a review article [127]. In another interesting work reported by Chen et al. RAFT polymerization was used to prepare disulfide crosslinked nanogels based on PEG-*b*-poly(2-(hydroxyethyl) methacrylate-*co*-acryloyl carbonate) for loading (~ 50% wt.) and triggered intracellular release of proteins [9]. The *in vitro* release studies showed that release of fluorescently-labeled cytochrome C was minimal under physiological conditions while complete release of the protein from

nanogel was observed in the presence of 10 mM dithiothreitol over 22 h. Cytochrome C-loaded reduction-sensitive nanogels demonstrated apparently better apoptotic activity than free cytochrome C and reduction-insensitive controls.

1.3.2.4 Polymeric micelles:

Polymeric micelles are self-assembled systems made from an amphiphilic copolymer with a characteristic core-shell structure, wherein the hydrophilic shell surrounds the hydrophobic core. These hydrophobic cores can hold hydrophobic drugs [128]. Depending on the chemical nature of the polymer used for their preparation, micelles can encapsulate drugs via hydrophobic interactions, electrostatic interactions, coordination bonds or even covalent linkages. The design of a polymer that can assemble into stable micelles with a suitable size, surface charge and drug-loading capacity is a challenging task. Moreover, it is essential that after completion of its function of delivering the drugs to the tumor tissue, the polymer must degrade, be biocompatible and cause no harm to the healthy tissues of the body [95]. Very few polymers are currently approved by the FDA for in vivo use due to the above constraints and there is scope for more research in the area of development of better polymers for preparation of micellar carriers.

1.3.2.4.1 Preparation, self-assembly and properties of polymeric micelles

The process of self-assembly of amphiphilic block copolymers is governed by a variety of factors, including, but not limited to, the method of preparation, temperature of preparation, the lengths of constituent blocks, etc [129]. In direct dissolution method, the polymer is simply mixed with an aqueous medium to form micelles [130]. Film rehydration method involves formation of a thin film of the polymer by removal of a low boiling solvent from the polymer solution and subsequent rehydration of this thin film by water. The dialysis method also involves the use of a cosolvent; the solution of the polymer in the organic solvent is

dialyzed against water. This leads to the gradual exchange of the cosolvent with water and micellization starts once enough water is present to reach the critical micelle concentration of the polymer. The size and polydispersity of the micelles depends not only on the method employed, but also the type of cosolvent used and the manner I which that solvent interacts with the polymer [131]. The same method that is used for the preparation of the micelle can also be used for drug encapsulation. In most cases, the drugs are also readily soluble in the cosolvent used and are spontaneously incorporated into the micelles while the polymer chains assemble into micelles. Different methods may yield slightly different encapsulation efficiencies and loading capacities; besides, loading capacity can also depend on the nature of the drug molecule as well as the initial feed ratio of the free drug [132]. The corona or shell forming hydrophilic block is most popularly composed of PEG to impart stealth properties to the micelles. The hydrophobic block can be composed of a variety of entities. The CMC of the value depends on the relative proportion of hydrophilic to hydrophobic blocks. For example, if the hydrophilic block length is kept constant and the hydrophobic block length is increased, the CMC of the resultant polymers would decrease [133]. The lower the CMC, the better is the stability of the micelles in vivo. However, the disassembly of the micelles into unimers is crucial for drug release and subsequent clearance of the polymer from the body [134-137]. One of the most important of any nanocarrier system that dictate the in vivo performance is the size. Smaller the size of the micelles, farther they can penetrate into the tumor. Moreover, a larger size also causes faster and higher clearance of the micelles from circulation by the RES system. Like the rest of the parameters, size is also a function of the ratio of the hydrophilic to hydrophobic blocks of the constituent polymer [128,138]. The uniformity of the starting polymer dictates the polydispersity of the micelles thus formed. A narrow size distribution is important to achieve more predictable and consistent pharmacokinetic profile of the micelles upon in vivo administration [129,139].

1.3.2.4.2 Micelles as drug delivery systems

Multi-drug delivery is very often realized by the step-wise physical loading of an anticancer agents in a polymeric micelle. Multi-drug polymeric micelles may release physically loaded drug(s) by disassembly of polymeric micelles in blood and/or by diffusion. Drug release tends to be rapid in vivo, and in vitro results must be interpreted with caution due to poor in vitro/in vivo correlation. Thus, while EPR targeting of solid tumors is feasible with physically loaded drug, it is regarded as challenging, and research on multidrug polymeric micelles for tumor targeting deserves more attention. Another way for multi-drug loading is via chemical conjugation, a reversible covalent linkage is required between an anticancer agent and a block copolymer. Drug release from multi-prodrug polymeric micelles may occur by simple hydrolysis or stimuli- /environment dependent release and may be tuned by choice of chemical linkage, e.g., esters, and spacer groups [46,140]. Shin et al attempted to physically co-incorporate three hydrophobic drugs, PTX, rapamycin, and 17-AAG in Poly(ethylene glycol)-block-poly(d,l-lactic acid) (PEG-*b*-PLA) micelles using a simple solvent evaporation method in various drug(s)-in-micelle combinations (Fig. 5) [141]. Three drug-loaded PEG-b-PLA micelles had a 10–10,000-fold increase in aqueous solubility of PTX, rapamycin, and 17-AAG (up to 7.2, 3.3, and 7.3 mg/mL, respectively). PEG-b-PLA micelles delayed release of three drugs compared to single drug-loaded micelles in vitro. Simultaneous delivery of PTX, rapamycin, and 17-AAG via 3-in-1 PEG-b-PLA micelles (particle size of ca. 30–40 nm) at 60, 30, and 60 mg/kg, respectively IV injection caused durable antitumor responses in A549 human non-small cell lung cancer and MDA-MB-231 human breast cancer xenograft models with acceptable acute toxicity.

Na et al studied the antitumor effects of 5-fluorouracil, CDDP, CPT-11, oxaliplatin,

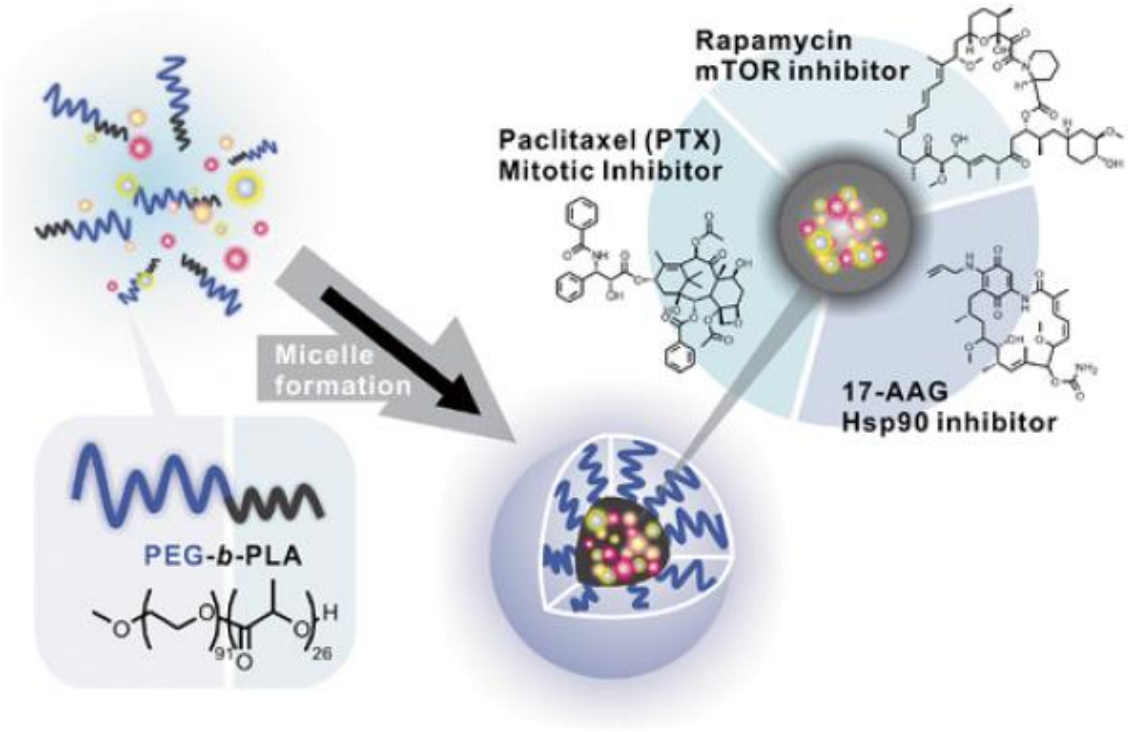

Figure 5. Multi-drug loaded PEG-*b*-PLA micelles for the delivery of PTX, 17-AAG and rapamycin. Adapted from [141].

etoposide, mitomycin-C, doxorubicin and PTX by determination of in vitro cytotoxicity to CT-26 colorectal tumor cells or in vivo following a subcutaneous transplant in BALB/c mice. Single agent and combination in vivo studies were performed using drug-loaded polymeric micelles composed of poly(γ-benzyl l-glutamate) and poly(ethylene oxide) (GEG) or poly(l-lactide)/poly(ethylene glycol) (LE) diblock copolymer. When tumor cells were exposed to doxorubicin concurrently with etoposide or paclitaxel, evidence of synergy was observed in CT-26 cells in vitro. Doxorubicin and paclitaxel loaded into GEG or LE copolymers at a high concentration (19.5 and 16.7 wt%, respectively) were almost completely released (83.2% and 93.7%, respectively) by day 3. When tumor-bearing mice were treated in combination with doxorubicin–paclitaxel or doxorubicin–etoposide, substantial antitumor activity was evident compared with single therapy. These data suggest that chemotherapy using micelle-loaded anticancer drugs represents a promising

potential as a carrier system in modulating drug delivery. In another study, Wang at al reported core-shell-type micelles that were doubly emulsified from an amphiphilic copolymer methoxy poly(ethylene glycol)-poly(lactide-co-glycolide) (mPEG-PLGA) [142]. These micelles offered advantages over other nanocarriers, as they were easy to fabricate by improved double emulsion method, biocompatible, and showed high loading efficacy. More importantly, these micelles could co-deliver hydrophilic doxorubicin and hydrophobic PTX. The drugloaded micelles possessed a better polydispersity, indicating that they are more readily subject to controlled size distribution. Co-delivery nanocarrier suppressed tumor cells growth more efficiently than the delivery of either doxorubicin or PTX at the same concentrations, indicating a synergistic effect. Moreover, the drug-loaded micelles with a DOX/PTX concentration ratio of 2:1 showed the highest anti-tumor activity to three different types of tumor cells. Kabanov and collaborators reported amphiphilic poly(2-oxazoline)s (POx)-based micelles as a promising high capacity delivery platform for multidrug cancer chemotherapy [143]. A variety of binary and ternary drugs combinations of PTX, docetaxel, 17-AAG, etoposide and bortezomib were solubilized in defined polymeric micelles achieving unprecedented high total loading capacities of up to 50 wt% drug per final formulation. Multi-drug loaded POx micelles showed enhanced stability in comparison to single-drug loaded micelles. Drug ratio dependent synergistic cytotoxicity of micellar etoposide /17-AAG was observed in MCF-7 cancer cells and of micellar bortezomib /17-AAG in MCF-7, PC3, MDA-MB-231 and HepG2 cells. Katragadda et al developed a micellar nanocarriers for concomitant delivery of PTX and 17-AAG for cancer therapy (Katragadda). PTX and 17-AAG were simultaneously loaded into polymeric micelles by a solvent evaporation method. Two candidate nanocarrier constructs, PEG–PLA-based micelles and PEGdistearoylphosphatidylethanolamine/ tocopheryl polyethylene glycol 1000 (PEGDSPE/ TPGS)-based mixed micelles, were assessed for the release kinetics of the loaded drugs. Compared to PEG–PLA micelles, entrapment of paclitaxel and 17-

AAG into PEGDSPE/ TPGS mixed micelles resulted in significantly prolonged release half-lives. Paclitaxel/17-AAG-loaded PEG-DSPE/TPGS mixed micelles were as effective in blocking the proliferation of human ovarian cancer SKOV-3 cells as the combined free drugs. There are plenty of other examples of use of micelles a carrier of drug combinations. This section only covers the most relevant examples. For detailed information about the application of polymeric micelles as a multi-drug vehicles, please see the review by Cho et al [144].

1.3.2.5. In vivo behavior of nanoparticles

Nanoparticles are macromolecular systems specifically designed to achieve long circulation half-lives of their cargo in vivo, along with their ability to deliver this cargo at the desired site. To realize this, a nanogel, or any nanoparticulate system has to overcome many barriers, especially when administered via routes other than intravenous, like oral, intradermal, pulmonary, intraocular, etc. Depending on the route of administration, nanoparticles are designed specifically to overcome associated barriers and reach the circulation intact. Nanoparticles prolong circulation half-life of their cargo by 1) preventing their fast clearance especially in the case of small molecules and 2) prevent quick degradation or metabolism which is more relevant for biomolecules. One of the most important obstacles to achieving prolonged circulation is opsonization of the nanoparticles followed by their clearance via organs of the MPS like liver and spleen, where they are taken up by the resident monocytes and macrophages [145]. PEGylation of the nanogel surface imparts them with ‘stealth’ properties by making the surface more hydrophilic, shielding a charge that the core might carry and establishing a steric hindrance for interaction with serum proteins, although this is highly dependent on the size of nanogel, its shape, molecular weight and surface density of the PEG used [146,147]. While PEGylation endows nanosystems with long circulation properties and reduces MPS uptake, eventually

opsonization and macrophage clearance still occurs [148]. A number of studies have demonstrated that PEGylation of nanoparticles tends to shift their accumulation towards the spleen instead of the liver as compared to their non-PEGylated counterparts [149]. A unique feature that helps nanoparticles partially escape splenic filtration process is their softness and deformability. This is can be explained by an example in nature, namely erythrocytes, which in spite of having a size range in microns are easily able to pass through the splenic filtration bed that has a pore size of few hundred nanometers, due to their flexibility and deformability [147,150]. In fact, old RBCs are cleared from circulation mainly because they lose their flexibility. This biomimetic property of the nanoparticles can be highly advantageous for their in vivo application. For example, Lyon and colleagues have recently reported that soft spherical acrylamide-based nanoparticles deform and pass through membrane pores several times smaller than their hydrodynamic diameter under physiological pressures [151]. Also, varying the moduli of similar nanoparticles has been shown to affect their mechanism and rate of uptake in macrophages [152]. Merkel et al. reported that decreasing the modulus of microgel particles altered their biodistribution properties, allowing them to bypass several organs, such as the lung, that entrapped their more rigid counterparts, resulting in increasingly longer circulation times (Merkel). Convincing evidence for the prolonged circulation time of soft PEG-based hydrogel nanoparticles compared to hard nanoparticles of the same size was recently provided by Mitragori and coworkers [153]. The deformability of the nanoparticles can be modulated by varying the crosslink density within the particle matrix as well as by varying the size of the crosslinking moiety [154]. Incorporation of electrolyte moieties into the polymer network of hydrogel particles to increase the swelling ratio is another straightforward and quite efficient way to decrease the modulus [116]. However, the distribution of charged groups on the surface of a particle can accelerate the clearance of particle. To address this drawback, DeSimone's group has recently developed a strategy to generate highly-

swollen polyelectrolyte gel particle with near-neutral charge while retaining charged group in the interior [9]. Fraction of nanoparticles that escapes clearance by the mechanisms discussed above is then distributed into various organs by the circulating blood. Nanoparticles are usually too big to pass through the tight junctions of the normal endothelium but can efficiently accumulate in solid tumors or inflamed tissues that have unique structural features such as defective leaky and loosely compacted vasculature and impaired lymphatic drainage leading to the well-characterized enhanced permeability and retention effect (EPR) [155,156]. In addition to EPR, bioconjugation of nanoparticles to targeting ligands allows directing them to specific receptors or molecules differentially overexpressed on the diseased cells/tissues thus improving their retention at the targeted site as well as facilitating their cellular uptake [157]. Various small molecules, peptides, aptamers, antibodies or antibody fragments have been explored for targeted delivery of nanoparticles and other nanomedicines in tissue- or cell-specific manner [158]. Ligand-mediated targeting influences the overall biodistribution profile of the nanoparticles as compared to their nontargeted counterparts and the bias of distribution is towards to those tissues that have a high expression of the receptor. This can help avoid excess accumulation of the nanoparticles at off target sites and reduce the associated side effects. After extravasation from the blood compartment, nanoparticles have to diffuse through the tissue matrix in the interstitial space [159] and reach the targeted cells, where they are internalized by a number of different endocytotic mechanisms, depending on the size, shape, softness, charge and other surface properties of the nanoparticles and the type of cells and receptor being targeted. Internalization of the nanoparticles can occur via more than one pathway, making it a highly complex process. But in general, endocytosis eventually confines the particles into intracellular vesicles, from where they are trafficked into endosomes and ultimately lysosomes. At each of these stages, nanoparticles are exposed to varying pH of endosomal/lysosomal lumen, degrading enzymes or reducing

environments, which are often utilized as stimuli for the release of cargo held within the nanoparticles. Nanogel carriers can also be designed to target specific intracellular organelles or escape them, depending on the type of cargo that they carry. For example, it is essential for the nanoparticles to undergo endosomal/lysosomal escape so that the encapsulated siRNA or oligonucleotides can be released in their active form in the cytosol where they are supposed to show their therapeutic effect [118]. This has brought growing interest in the use of nanoparticles made of bioresponsive polymers to promote escape by osmotic effects, membrane binding or membrane fusion or using pH-sensitive or reducible crosslinkers to facilitate nanogel destabilization following internalization and enhance delivery efficiency [114,160,161]. Degradability of the nanoparticles is also essential to minimize toxicities associated with the accumulation of the carrier in the body.

1.4Conclusion

Polypeptides have an inherent property to assemble into supramolecular structures in solution. The formation of supramolecular structures is a controlled and organized process that depends by and large on the nature of the polypeptide and conditions of the solvent it is exposed to. Formation of amphiphilic copolymers based on such polypeptides can allow for tailoring the assembly process to a predefined nanoscale supramolecular structure, which can then be used as drug delivery vehicles. The overall process of self-assembly of such amphiphilic copolymers can then be regarded as a complex phenomenon of structural organization that is governed by the nature of constituent hydrophilic and hydrophobic blocks, their relative lengths, as well as properties of the solvent-phobic block that is the driving force for self-assembly. The inherent biocompatibility and biodegradability of polypeptides is of additional advantage for their biological applications. For the purpose of the current study, amphiphilic block copolymer with following composition was chosen: polyethylene glycol (PEG) as the hydrophilic,

stealth imparting block and polyleucine (PLeu) as the hydrophobic part and the initiator of micelle formation in aqueous environment. The variables explored in the current study were altering the ratio of lengths of constituent blocks as well as chirality of PLeu block and the temperature of solvent used for preparation of micelles via the film rehydration method. The impact of all these variables on the thermodynamic stability as well as type of secondary structures formed and the influence of these attributes on the ability of the micelles to encapsulate a combination of hydrophobic drugs into their core are also described. The primary purpose of designing this micellar carrier was for combination therapy of ErbB2 positive breast cancer. The receptor tyrosine kinase, ErbB2 is a viable target in 20-25 % breast cancer patients due to its overexpression. Its degradation is associated with slower progression of the disease and increased survival times. While the monoclonal antibody Trastuzumab (Herceptin™) is the first line therapy in such patients, monotherapy with Trastuzumab has shown little benefit and therefore must be given with chemotherapeutic agents. Such combinations also help in delaying the development of resistance to Trastuzumab, since multiple cellular pathways can be targeted simultaneously. ErbB2 is a client protein of heat shock protein 90 and 17-N-allylamino-17-demethoxygeldanamycin (17-AAG) is a potent inhibitor of HSP90. Previous work in our lab has demonstrated strong synergy of action between 17-AAG and a model cytotoxic agent doxorubicin. In order to further improve the efficacy of the therapy, our goal was to replace doxorubicin with a more potent, clinically relevant agent paclitaxel (PTX), which has been shown to have strong synergistic antitumor effect with 17-AAG in ErbB2-driven breast cancers. Since synergy of such therapy is often sequence and dose ratio specific, co-delivery of the drugs via the same vehicle is desirable as well as beneficial. Dual drug-loaded micelles thus prepared could load 17-AAG and PTX in a ratio 2:1 by weight. The formulation showed a high level of synergy on BT-474 cells that express a high amount of ErbB2 while the synergy was negligible in ErbB2 low MCF-7 cells. The strong synergy

was also observed when the formulation was tested in an orthotopic breast cancer mouse model developed using ErbB2 overexpressing BT-474 cells, and an arrest in the growth of tumors in animals treated with dual drug-loaded micelles was observed, while both 17-AAG and PTX were used at sub therapeutic doses of 10 mg and 5 mg equivalents per kg body weight. The lower doses also helped avoid toxicity associated with the therapy. We also show the importance of simultaneously delivering the two drugs via a single carrier system as opposed to cocktail of individual drug-loaded micelles administered at equivalent doses, which has a better therapeutic outcome than the cocktail therapy. These combination drug-loaded micelles were developed as a platform for chemotherapy with Trast. The triple therapeutic system of Trast with combination drug-loaded micelles containing 17-AAG and PTX exhibited an even stronger anticancer effect and this system was one step further in the process of optimizing a carrier system that can be used for combination drug delivery using small molecules and monoclonal antibodies.

1.5 References

1. Hannun, Y. A. Apoptosis and the dilemma of cancer chemotherapy. *Blood* **1997***, 89*, 1845-1853.

2. Friesen, C.; Herr, I.; Krammer, P. H.; Debatin, K. Involvement of the CD95 (APO–1/Fas) receptor/ligand system in drug–induced apoptosis in leukemia cells. *Nat. Med.* **1996***, 2*, 574-577.

3. Yuan, Z. M.; Huang, Y.; Whang, Y.; Sawyers, C.; Weichselbaum, R.; Kharbanda, S.; Kufe, D. Role for c-Abl tyrosine kinase in growth arrest response to DNA damage. *Nature* **1996***, 382*, 272-274.

4. Luqmani, Y. A. Mechanisms of drug resistance in cancer chemotherapy. *Med. Princ Pract.* **2005***, 14 Suppl 1*, 35-48.

5. Kast, C.; Gros, P. Epitope insertion favors a six transmembrane domain model for the carboxy-terminal portion of the multidrug resistance-associated protein. *Biochemistry (N. Y.)* **1998***, 37*, 2305-2313.

6. Kast, C.; Gros, P. Topology mapping of the amino-terminal half of multidrug resistance-associated protein by epitope insertion and immunofluorescence. *J. Biol. Chem.* **1997***, 272*, 26479-26487.

7. Dean, M.; Hamon, Y.; Chimini, G. The human ATP-binding cassette (ABC) transporter superfamily. *J. Lipid Res.* **2001***, 42*, 1007-1017.

8. Juliano, R. L.; Ling, V. A surface glycoprotein modulating drug permeability in Chinese hamster ovary cell mutants. *Biochimica et Biophysica Acta (BBA)-Biomembranes* **1976***, 455*, 152-162.

9. Chen, C.; Chen, C. A PNIPAM-based fluorescent nanothermometer with ratiometric readout. *Chemical Communications* **2011***, 47*, 994-996.

10. Ueda, K.; Cardarelli, C.; Gottesman, M. M.; Pastan, I. Expression of a full-length cDNA for the human "MDR1" gene confers resistance to colchicine, doxorubicin, and vinblastine. *Proc. Natl. Acad. Sci. U. S. A.* **1987***, 84*, 3004-3008.

11. Gottesman, M. M.; Fojo, T.; Bates, S. E. Multidrug resistance in cancer: role of ATP–dependent transporters. *Nature Reviews Cancer* **2002***, 2*, 48-58.

12. Endicott, J. A.; Ling, V. The biochemistry of P-glycoprotein-mediated multidrug resistance. *Annu. Rev. Biochem.* **1989***, 58*, 137-171.

13. Higgins, C. F. ABC transporters: from microorganisms to man. *Annu. Rev. Cell Biol.* **1992***, 8*, 67-113.

14. Gottesman, M. M.; Pastan, I.; Ambudkar, S. V. P-glycoprotein and multidrug resistance. *Curr. Opin. Genet. Dev.* **1996***, 6*, 610-617.

15. Fromm, M. F.; Kauffmann, H.; Fritz, P.; Burk, O.; Kroemer, H. K.; Warzok, R. W.; Eichelbaum, M.; Siegmund, W.; Schrenk, D. The effect of rifampin treatment on intestinal

expression of human MRP transporters. *The American journal of pathology* **2000***, 157*, 1575-1580.

16. Greiner, B.; Eichelbaum, M.; Fritz, P.; Kreichgauer, H. P.; von Richter, O.; Zundler, J.; Kroemer, H. K. The role of intestinal P-glycoprotein in the interaction of digoxin and rifampin. *J. Clin. Invest.* **1999***, 104*, 147-153.

17. Rosell, R.; Taron, M.; Ariza, A.; Barnadas, A.; Mate, J. L.; Reguart, N.; Margelí, M.; Felip, E.; Méndez, P.; García-Campelo, R. In *In Molecular predictors of response to chemotherapy in lung cancer;* Seminars in oncology; Elsevier: 2004; Vol. 31, pp 20-27.

18. Chu, G. Cellular responses to cisplatin. The roles of DNA-binding proteins and DNA repair. *J. Biol. Chem.* **1994***, 269*, 787-790.

19. Miller, W. Biological rationale for endocrine therapy in breast cancer. *Best Practice & Research Clinical Endocrinology & Metabolism* **2004***, 18*, 1-32.

20. Campos, S. M. Aromatase inhibitors for breast cancer in postmenopausal women. *Oncologist* **2004***, 9*, 126-136.

21. Duesberg, P.; Stindl, R.; Hehlmann, R. Explaining the high mutation rates of cancer cells to drug and multidrug resistance by chromosome reassortments that are catalyzed by aneuploidy. *Proc. Natl. Acad. Sci. U. S. A.* **2000***, 97*, 14295-14300.

22. Duesberg, P.; Stindl, R.; Hehlmann, R. Origin of multidrug resistance in cells with and without multidrug resistance genes: chromosome reassortments catalyzed by aneuploidy. *Proc. Natl. Acad. Sci. U. S. A.* **2001***, 98*, 11283-11288.

23. Gamcsik, M. P.; Dubay, G. R.; Cox, B. R. Increased rate of glutathione synthesis from cystine in drug-resistant MCF-7 cells. *Biochem. Pharmacol.* **2002***, 63*, 843-851.

24. Deng, H. B.; Parekh, H. K.; Chow, K.; Simpkins, H. Increased expression of dihydrodiol dehydrogenase induces resistance to cisplatin in human ovarian carcinoma cells. *J. Biol. Chem.* **2002***, 277*, 15035-15043.

25. Conze, D.; Weiss, L.; Regen, P. S.; Bhushan, A.; Weaver, D.; Johnson, P.; Rincon, M. Autocrine production of interleukin 6 causes multidrug resistance in breast cancer cells. *Cancer Res.* **2001***, 61*, 8851-8858.

26. Aoudjit, F.; Vuori, K. Integrin signaling inhibits paclitaxel-induced apoptosis in breast cancer cells. *Oncogene* **2001***, 20*, 4995-5004.

27. Song, S.; Wientjes, M. G.; Gan, Y.; Au, J. L. Fibroblast growth factors: an epigenetic mechanism of broad spectrum resistance to anticancer drugs. *Proc. Natl. Acad. Sci. U. S. A.* **2000***, 97*, 8658-8663.

28. Mayer, L. D.; Janoff, A. S. Optimizing combination chemotherapy by controlling drug ratios. *Mol. Interv.* **2007***, 7*, 216-223.

29. Zoli, W.; Ricotti, L.; Tesei, A.; Barzanti, F.; Amadori, D. In vitro preclinical models for a rational design of chemotherapy combinations in human tumors. *Crit. Rev. Oncol.* **2001***, 37*, 69-82.

30. Harasym, T. O.; Tardi, P. G.; Harasym, N. L.; Harvie, P.; Johnstone, S. A.; Mayer, L. D. Increased preclinical efficacy of irinotecan and floxuridine coencapsulated inside liposomes is associated with tumor delivery of synergistic drug ratios. *Oncology Research Featuring Preclinical and Clinical Cancer Therapeutics* **2006***, 16*, 361-374.

31. Parhi, P.; Mohanty, C.; Sahoo, S. K. Nanotechnology-based combinational drug delivery: an emerging approach for cancer therapy. *Drug Discov. Today* **2012***, 17*, 1044-1052.

32. Chou, T. C. Drug combination studies and their synergy quantification using the Chou-Talalay method. *Cancer Res.* **2010***, 70*, 440-446.

33. Chiang, C.; Yeh, P.; Gao, M.; Chen, C.; Yeh, L.; Feng, W.; Kuo, S.; Hsu, C.; Lu, Y.; Cheng, A. Combinations of mTORC1 inhibitor RAD001 with gemcitabine and paclitaxel for treating non-Hodgkin lymphoma. *Cancer Lett.* **2010***, 298*, 195-203.

34. Lage, H. An overview of cancer multidrug resistance: a still unsolved problem. *Cellular and molecular life sciences* **2008***, 65*, 3145-3167.

35. Robert, J.; Jarry, C. Multidrug resistance reversal agents. *J. Med. Chem.* **2003***, 46*, 4805-4817.

36. Hubensack, M.; Müller, C.; Höcherl, P.; Fellner, S.; Spruss, T.; Bernhardt, G.; Buschauer, A. Effect of the ABCB1 modulators elacridar and tariquidar on the distribution of paclitaxel in nude mice. *J. Cancer Res. Clin. Oncol.* **2008***, 134*, 597-607.

37. Lancet, J. E.; Baer, M. R.; Duran, G. E.; List, A. F.; Fielding, R.; Marcelletti, J. F.; Multani, P. S.; Sikic, B. I. A phase I trial of continuous infusion of the multidrug resistance inhibitor zosuquidar with daunorubicin and cytarabine in acute myeloid leukemia. *Leuk. Res.* **2009***, 33*, 1055-1061.

38. Dasanu, C. A.; Herzog, T. J.; Alexandrescu, D. T. Carboplatin-gemcitabine in the therapy of advanced ovarian cancer: dose reduction consideration. *J. Oncol. Pharm. Pract.* **2010***, 16*, 63-66.

39. Bava, S. V.; Puliappadamba, V. T.; Deepti, A.; Nair, A.; Karunagaran, D.; Anto, R. J. Sensitization of taxol-induced apoptosis by curcumin involves down-regulation of nuclear factor-kappaB and the serine/threonine kinase Akt and is independent of tubulin polymerization. *J. Biol. Chem.* **2005***, 280*, 6301-6308.

40. Chou, T. C. Theoretical basis, experimental design, and computerized simulation of synergism and antagonism in drug combination studies. *Pharmacol. Rev.* **2006***, 58*, 621-681.

41. Ramsay, E. C.; Dos Santos, N.; Dragowska, W. H.; Laskin, J. J.; Bally, M. B. The formulation of lipid-based nanotechnologies for the delivery of fixed dose anticancer drug combinations. *Curr. Drug Deliv.* **2005***, 2*, 341-351.

42. Logman, J. F.; Heeg, B. M.; Botteman, M. F.; Kaura, S.; van Hout, B. A. Economic evaluation of zoledronic acid for the prevention of osteoporotic fractures in postmenopausal women with early-stage breast cancer receiving aromatase inhibitors in the UK. *Ann. Oncol.* **2010***, 21*, 1529-1536.

43. Pauwels, B.; Korst, A. E.; Lardon, F.; Vermorken, J. B. Combined modality therapy of gemcitabine and radiation. *Oncologist* **2005***, 10*, 34-51.

44. Nigro, N. D.; Vaitkevicius, V.; Considine, B. Combined therapy for cancer of the anal canal: a preliminary report. *Diseases of the Colon & Rectum* **1974***, 17*, 354-356.

45. Gulley, J. L.; Arlen, P. M.; Bastian, A.; Morin, S.; Marte, J.; Beetham, P.; Tsang, K. Y.; Yokokawa, J.; Hodge, J. W.; Menard, C.; Camphausen, K.; Coleman, C. N.; Sullivan, F.; Steinberg, S. M.; Schlom, J.; Dahut, W. Combining a recombinant cancer vaccine with standard definitive radiotherapy in patients with localized prostate cancer. *Clin. Cancer Res.* **2005***, 11*, 3353-3362.

46. Greco, F.; Vicent, M. J. Combination therapy: opportunities and challenges for polymer–drug conjugates as anticancer nanomedicines. *Adv. Drug Deliv. Rev.* **2009***, 61*, 1203-1213.

47. Tanabe, M.; Ito, Y.; Tokudome, N.; Sugihara, T.; Miura, H.; Takahashi, S.; Seto, Y.; Iwase, T.; Hatake, K. Possible use of combination chemotherapy with mitomycin C and methotrexate for metastatic breast cancer pretreated with anthracycline and taxanes. *Breast Cancer* **2009***, 16*, 301-306.

48. Arkenau, H. T.; Bermann, A.; Rettig, K.; Strohmeyer, G.; Porschen, R.; Arbeitsgemeinschaft Gastrointestinale Onkologie 5-Fluorouracil plus leucovorin is an effective adjuvant chemotherapy in curatively resected stage III colon cancer: long-term follow-up results of the adjCCA-01 trial. *Ann. Oncol.* **2003***, 14*, 395-399.

49. Berhoune, M.; Banu, E.; Scotte, F.; Prognon, P.; Oudard, S.; Bonan, B. Therapeutic strategy for treatment of metastatic non-small cell lung cancer. *Ann. Pharmacother.* **2008***, 42*, 1640-1652.

50. Bilal, E.; Dutkowski, J.; Guinney, J.; Jang, I. S.; Logsdon, B. A.; Pandey, G.; Sauerwine, B. A.; Shimoni, Y.; Vollan, H. K. M.; Mecham, B. H. Improving breast cancer survival analysis through competition-based multidimensional modeling. *PLoS Comput Biol* **2013***, 9*, e1003047.

51. Cooley, S.; Burns, L. J.; Repka, T.; Miller, J. S. Natural killer cell cytotoxicity of breast cancer targets is enhanced by two distinct mechanisms of antibody-dependent cellular cytotoxicity against LFA-3 and HER2/neu. *Exp. Hematol.* **1999***, 27*, 1533-1541.

52. Gennari, R.; Menard, S.; Fagnoni, F.; Ponchio, L.; Scelsi, M.; Tagliabue, E.; Castiglioni, F.; Villani, L.; Magalotti, C.; Gibelli, N.; Oliviero, B.; Ballardini, B.; Da Prada, G.; Zambelli, A.; Costa, A. Pilot study of the mechanism of action of preoperative trastuzumab in patients with primary operable breast tumors overexpressing HER2. *Clin. Cancer Res.* **2004***, 10*, 5650-5655.

53. Clynes, R. A.; Towers, T. L.; Presta, L. G.; Ravetch, J. V. Inhibitory Fc receptors modulate in vivo cytoxicity against tumor targets. *Nat. Med.* **2000***, 6*, 443-446.

54. Burstein, H. J.; Harris, L. N.; Gelman, R.; Lester, S. C.; Nunes, R. A.; Kaelin, C. M.; Parker, L. M.; Ellisen, L. W.; Kuter, I.; Gadd, M. A.; Christian, R. L.; Kennedy, P. R.; Borges, V. F.; Bunnell, C. A.; Younger, J.; Smith, B. L.; Winer, E. P. Preoperative therapy with trastuzumab and paclitaxel followed by sequential adjuvant

doxorubicin/cyclophosphamide for HER2 overexpressing stage II or III breast cancer: a pilot study. *J. Clin. Oncol.* **2003***, 21*, 46-53.

55. Wenzel, C.; Hussian, D.; Bartsch, R.; Pluschnig, U.; Locker, G. J.; Rudas, M.; Gnant, M. F.; Jakesz, R.; Zielinski, C. C.; Steger, G. G. Preoperative therapy with epidoxorubicin and docetaxel plus trastuzumab in patients with primary breast cancer: a pilot study. *J. Cancer Res. Clin. Oncol.* **2004***, 130*, 400-404.

56. Hurley, J.; Doliny, P.; Reis, I.; Silva, O.; Gomez-Fernandez, C.; Velez, P.; Pauletti, G.; Powell, J. E.; Pegram, M. D.; Slamon, D. J. Docetaxel, cisplatin, and trastuzumab as primary systemic therapy for human epidermal growth factor receptor 2-positive locally advanced breast cancer. *J. Clin. Oncol.* **2006***, 24*, 1831-1838.

57. Buzdar, A. U.; Ibrahim, N. K.; Francis, D.; Booser, D. J.; Thomas, E. S.; Theriault, R. L.; Pusztai, L.; Green, M. C.; Arun, B. K.; Giordano, S. H.; Cristofanilli, M.; Frye, D. K.; Smith, T. L.; Hunt, K. K.; Singletary, S. E.; Sahin, A. A.; Ewer, M. S.; Buchholz, T. A.; Berry, D.; Hortobagyi, G. N. Significantly higher pathologic complete remission rate after neoadjuvant therapy with trastuzumab, paclitaxel, and epirubicin chemotherapy: results of a randomized trial in human epidermal growth factor receptor 2-positive operable breast cancer. *J. Clin. Oncol.* **2005***, 23*, 3676-3685.

58. Remillard, S.; Rebhun, L. I.; Howie, G. A.; Kupchan, S. M. Antimitotic activity of the potent tumor inhibitor maytansine. *Science* **1975***, 189*, 1002-1005.

59. Raja, S. M.; Clubb, R. J.; Bhattacharyya, M.; Dimri, M.; Cheng, H.; Pan, W.; Ortega-Cava, C.; Lakku-Reddi, A.; Naramura, M.; Band, V. A combination of Trastuzumab and 17-AAG induces enhanced ubiquitinylation and lysosomal pathway-dependent ErbB2 degradation and cytotoxicity in ErbB2-overexpressing breast cancer cells. *Cancer biology & therapy* **2008***, 7*, 1630-1640.

60. Wakankar, A. A.; Feeney, M. B.; Rivera, J.; Chen, Y.; Kim, M.; Sharma, V. K.; Wang, Y. J. Physicochemical stability of the antibody− drug conjugate trastuzumab-DM1: changes due to modification and conjugation processes. *Bioconjug. Chem.* **2010***, 21*, 1588-1595.

61. Jumbe, N. L.; Xin, Y.; Leipold, D. D.; Crocker, L.; Dugger, D.; Mai, E.; Sliwkowski, M. X.; Fielder, P. J.; Tibbitts, J. Modeling the efficacy of trastuzumab-DM1, an antibody drug conjugate, in mice. *Journal of pharmacokinetics and pharmacodynamics* **2010***, 37*, 221-242.

62. Junutula, J. R.; Flagella, K. M.; Graham, R. A.; Parsons, K. L.; Ha, E.; Raab, H.; Bhakta, S.; Nguyen, T.; Dugger, D. L.; Li, G.; Mai, E.; Lewis Phillips, G. D.; Hiraragi, H.; Fuji, R. N.; Tibbitts, J.; Vandlen, R.; Spencer, S. D.; Scheller, R. H.; Polakis, P.; Sliwkowski, M. X. Engineered thio-trastuzumab-DM1 conjugate with an improved therapeutic index to target human epidermal growth factor receptor 2-positive breast cancer. *Clin. Cancer Res.* **2010***, 16*, 4769-4778.

63. Nahta, R.; Yuan, L. X.; Zhang, B.; Kobayashi, R.; Esteva, F. J. Insulin-like growth factor-I receptor/human epidermal growth factor receptor 2 heterodimerization contributes to trastuzumab resistance of breast cancer cells. *Cancer Res.* **2005***, 65*, 11118-11128.

64. Ritter, C. A.; Perez-Torres, M.; Rinehart, C.; Guix, M.; Dugger, T.; Engelman, J. A.; Arteaga, C. L. Human Breast Cancer Cells Selected for Resistance to Trastuzumab In vivo Overexpress Epidermal Growth Factor Receptor and ErbB Ligands and Remain Dependent on the ErbB Receptor Network. *Clinical Cancer Research* **2007***, 13*, 4909-4919.

65. Phillips, M. A.; Gran, M. L.; Peppas, N. A. Targeted nanodelivery of drugs and diagnostics. *Nano Today* **2010***, 5*, 143-159.

66. Junttila, T. T.; Li, G.; Parsons, K.; Phillips, G. L.; Sliwkowski, M. X. Trastuzumab-DM1 (T-DM1) retains all the mechanisms of action of trastuzumab and efficiently inhibits growth of lapatinib insensitive breast cancer. *Breast Cancer Res. Treat.* **2011***, 128*, 347-356.

67. Hommelgaard, A. M.; Lerdrup, M.; van Deurs, B. Association with membrane protrusions makes ErbB2 an internalization-resistant receptor. *Mol. Biol. Cell* **2004***, 15*, 1557-1567.

68. Lerdrup, M.; Bruun, S.; Grandal, M. V.; Roepstorff, K.; Kristensen, M. M.; Hommelgaard, A. M.; van Deurs, B. Endocytic down-regulation of ErbB2 is stimulated by cleavage of its C-terminus. *Mol. Biol. Cell* **2007***, 18*, 3656-3666.

69. Lerdrup, M.; Hommelgaard, A. M.; Grandal, M.; van Deurs, B. Geldanamycin stimulates internalization of ErbB2 in a proteasome-dependent way. *J. Cell. Sci.* **2006***, 119*, 85-95.

70. Gianni, L.; Pienkowski, T.; Im, Y.; Roman, L.; Tseng, L.; Liu, M.; Lluch-Hernandez, A.; Semiglazov, V.; Szado, T.; Ross, G. Abstract S3-2: Neoadjuvant Pertuzumab (P) and Trastuzumab (H): Antitumor and Safety Analysis of a Randomized Phase II Study ('NeoSphere'). *Cancer Res.* **2010***, 70*, S3-2-S3-2.

71. Burris, H. A.,3rd; Moore, M. J.; Andersen, J.; Green, M. R.; Rothenberg, M. L.; Modiano, M. R.; Cripps, M. C.; Portenoy, R. K.; Storniolo, A. M.; Tarassoff, P.; Nelson, R.; Dorr, F. A.; Stephens, C. D.; Von Hoff, D. D. Improvements in survival and clinical benefit with gemcitabine as first-line therapy for patients with advanced pancreas cancer: a randomized trial. *J. Clin. Oncol.* **1997***, 15*, 2403-2413.

72. Conroy, T.; Desseigne, F.; Ychou, M.; Bouché, O.; Guimbaud, R.; Bécouarn, Y.; Adenis, A.; Raoul, J.; Gourgou-Bourgade, S.; de la Fouchardière, C. FOLFIRINOX versus gemcitabine for metastatic pancreatic cancer. *N. Engl. J. Med.* **2011***, 364*, 1817-1825.

73. Moore, M. J.; Goldstein, D.; Hamm, J.; Figer, A.; Hecht, J. R.; Gallinger, S.; Au, H. J.; Murawa, P.; Walde, D.; Wolff, R. A.; Campos, D.; Lim, R.; Ding, K.; Clark, G.; Voskoglou-Nomikos, T.; Ptasynski, M.; Parulekar, W.; National Cancer Institute of Canada Clinical Trials Group Erlotinib plus gemcitabine compared with gemcitabine alone in patients with advanced pancreatic cancer: a phase III trial of the National Cancer Institute of Canada Clinical Trials Group. *J. Clin. Oncol.* **2007***, 25*, 1960-1966.

74. Cunningham, D.; Chau, I.; Stocken, D. D.; Valle, J. W.; Smith, D.; Steward, W.; Harper, P. G.; Dunn, J.; Tudur-Smith, C.; West, J.; Falk, S.; Crellin, A.; Adab, F.; Thompson, J.; Leonard, P.; Ostrowski, J.; Eatock, M.; Scheithauer, W.; Herrmann, R.; Neoptolemos, J.

P. Phase III randomized comparison of gemcitabine versus gemcitabine plus capecitabine in patients with advanced pancreatic cancer. *J. Clin. Oncol.* **2009***, 27*, 5513-5518.

75. Sultana, A.; Smith, C. T.; Cunningham, D.; Starling, N.; Tait, D.; Neoptolemos, J.; Ghaneh, P. Systematic review, including meta-analyses, on the management of locally advanced pancreatic cancer using radiation/combined modality therapy. *Br. J. Cancer* **2007***, 96*, 1183-1190.

76. Heinemann, V.; Boeck, S.; Hinke, A.; Labianca, R.; Louvet, C. Meta-analysis of randomized trials: evaluation of benefit from gemcitabine-based combination chemotherapy applied in advanced pancreatic cancer. *BMC Cancer* **2008***, 8*, 1.

77. Von Hoff, D. D.; Ervin, T.; Arena, F. P.; Chiorean, E. G.; Infante, J.; Moore, M.; Seay, T.; Tjulandin, S. A.; Ma, W. W.; Saleh, M. N. Increased survival in pancreatic cancer with nab-paclitaxel plus gemcitabine. *N. Engl. J. Med.* **2013***, 369*, 1691-1703.

78. Ychou, M.; Conroy, T.; Seitz, J. F.; Gourgou, S.; Hua, A.; Mery-Mignard, D.; Kramar, A. An open phase I study assessing the feasibility of the triple combination: oxaliplatin plus irinotecan plus leucovorin/ 5-fluorouracil every 2 weeks in patients with advanced solid tumors. *Ann. Oncol.* **2003***, 14*, 481-489.

79. Bendell, J.; Britton, S.; Green, M.; Willey, J.; Lemke, K.; Marshall, J. In *In Immediate impact of the FOLFIRINOX phase III data reported at the 2010 ASCO Annual Meeting on prescribing plans of American oncology physicians for patients with metastatic pancreas cancer (MPC).* ASCO Annual Meeting Proceedings; 2011; Vol. 29, pp 286.

80. Attard, C. L.; Brown, S.; Alloul, K.; Moore, M. J. Cost-effectiveness of FOLFIRINOX for first-line treatment of metastatic pancreatic cancer. *Current Oncology* **2013***, 21*, 41-51.

81. Eastman, A. Activation of programmed cell death by anticancer agents: cisplatin as a model system. *Cancer Cells* **1990***, 2*, 275-280.

82. Hertel, L.; Kroin, J.; Misner, J.; Tustin, J. Synthesis of 2-deoxy-2, 2-difluoro-D-ribose and 2-deoxy-2, 2'-difluoro-D-ribofuranosyl nucleosides. *J. Org. Chem.* **1988***, 53*, 2406-2409.

83. van Moorsel, C. J.; Pinedo, H. M.; Veerman, G.; Bergman, A. M.; Kuiper, C. M.; Vermorken, J. B.; van der Vijgh, W. J.; Peters, G. J. Mechanisms of synergism between cisplatin and gemcitabine in ovarian and non-small-cell lung cancer cell lines. *Br. J. Cancer* **1999***, 80*, 981-990.

84. Yang, L.; Li, L.; Liu, L.; Keating, M.; Plunkett, W. In *In Gemcitabine suppresses the repair of cisplatin adducts in plasmid DNA by extracts of cisplatin-resistant human colon carcinoma cells;* Proc Am Assoc Cancer Res; 1995; Vol. 36, pp 357.

85. McMahon, M. B.; Bear, M. D.; Kulp, S. K.; Pennell, M. L.; London, C. A. Biological activity of gemcitabine against canine osteosarcoma cell lines in vitro. *Am. J. Vet. Res.* **2010***, 71*, 799-808.

86. Köhler, G.; Milstein, C. Continuous cultures of fused cells secreting antibody of predefined specificity. *Nature* **1975***, 256*, 495-497.

87. Badger, C.; Anasetti, C.; Davis, J.; Bernstein, I. D. Treatment of malignancy with unmodified antibody. *Pathol. Immunopathol. Res.* **1987***, 6*, 419-434.

88. Khazaeli, M.; Conry, R. M.; LoBuglio, A. F. Human immune response to monoclonal antibodies. *Journal of immunotherapy* **1994***, 15*, 42-52.

89. Lee, E.; Kim, D.; Youn, Y.; Oh, K.; Bae, Y. A Virus-Mimetic Nanogel Vehicle. *Angewandte Chemie* **2008***, 120*, 2452-2455.

90. Steplewski, Z.; Lubeck, M. D.; Koprowski, H. Human macrophages armed with murine immunoglobulin G2a antibodies to tumors destroy human cancer cells. *Science* **1983***, 221*, 865-867.

91. Cartron, G.; Dacheux, L.; Salles, G.; Solal-Celigny, P.; Bardos, P.; Colombat, P.; Watier, H. Therapeutic activity of humanized anti-CD20 monoclonal antibody and polymorphism in IgG Fc receptor FcgammaRIIIa gene. *Blood* **2002***, 99*, 754-758.

92. Weng, W. K.; Levy, R. Two immunoglobulin G fragment C receptor polymorphisms independently predict response to rituximab in patients with follicular lymphoma. *J. Clin. Oncol.* **2003***, 21*, 3940-3947.

93. Adams, G. P.; Weiner, L. M. Monoclonal antibody therapy of cancer. *Nat. Biotechnol.* **2005***, 23*, 1147-1157.

94. Sunada, H.; Magun, B. E.; Mendelsohn, J.; MacLeod, C. L. Monoclonal antibody against epidermal growth factor receptor is internalized without stimulating receptor phosphorylation. *Proc. Natl. Acad. Sci. U. S. A.* **1986***, 83*, 3825-3829.

95. Li, W.; Liu, Q.; Liu, L. Amino acid-based zwitterionic polymers: antifouling properties and low cytotoxicity. *Journal of Biomaterials Science, Polymer Edition* **2014***, 25*, 1730-1742.

96. Ricart, A. D.; Tolcher, A. W. Technology insight: cytotoxic drug immunoconjugates for cancer therapy. *Nature clinical practice Oncology* **2007***, 4*, 245-255.

97. Carter, P. J.; Senter, P. D. Antibody-drug conjugates for cancer therapy. *Cancer J.* **2008***, 14*, 154-169.

98. Rohrer, T. New weapons for the oncology arsenal. *Chem.Rundschau* **2008***, 9*, 26-28.

99. Ducry, L.; Stump, B. Antibody− drug conjugates: linking cytotoxic payloads to monoclonal antibodies. *Bioconjug. Chem.* **2009***, 21*, 5-13.

100. Hamblett, K. J.; Senter, P. D.; Chace, D. F.; Sun, M. M.; Lenox, J.; Cerveny, C. G.; Kissler, K. M.; Bernhardt, S. X.; Kopcha, A. K.; Zabinski, R. F.; Meyer, D. L.; Francisco, J. A. Effects of drug loading on the antitumor activity of a monoclonal antibody drug conjugate. *Clin. Cancer Res.* **2004***, 10*, 7063-7070.

101. McDonagh, C. F.; Turcott, E.; Westendorf, L.; Webster, J. B.; Alley, S. C.; Kim, K.; Andreyka, J.; Stone, I.; Hamblett, K. J.; Francisco, J. A.; Carter, P. Engineered antibody-drug conjugates with defined sites and stoichiometries of drug attachment. *Protein Eng. Des. Sel.* **2006***, 19*, 299-307.

102. Borcoman, E.; Le Tourneau, C. Antibody drug conjugates: the future of chemotherapy? *Curr. Opin. Oncol.* **2016***, 28*, 429-436.

103. Soni, K. S.; Desale, S. S.; Bronich, T. K. Nanogels: An overview of properties, biomedical applications and obstacles to clinical translation. *J. Controlled Release* **2015**.

104. Pattni, B. S.; Chupin, V. V.; Torchilin, V. P. New developments in liposomal drug delivery. *Chem. Rev.* **2015***, 115*, 10938-10966.

105. van Rooy, I.; Hennink, W. E.; Storm, G.; Schiffelers, R. M.; Mastrobattista, E. Attaching the phage display-selected GLA peptide to liposomes: factors influencing target binding. *European Journal of Pharmaceutical Sciences* **2012***, 45*, 330-335.

106. Munster, P. N.; Miller, K.; Krop, I. E.; Dhindsa, N.; Niyikiza, C.; Nielsen, U.; Odueyungbo, A.; Rajarethinmam, A.; Campbell, K.; Geretti, E. In *In A Phase I study of MM-302, a HER2-targeted liposomal doxorubicin, in patients with advanced, HER2-positive (HER2) breast cancer;* ASCO Annual Meeting. Chicago, IL, USA; 2012; , pp 1-5.

107. Munster, P.; Krop, I. E.; Miller, K.; Dhindsa, N.; Niyijiza, C.; Nielsen, U.; Odueyungbo, A.; Rajarethinam, A.; Marande, M.; Campbell, K. Abstract P4-12-29: Assessment of safety and activity in an expanded phase 1 study of MM-302, a HER2-targeted liposomal doxorubicin, in patients with advanced HER2-positive (HER2) breast cancer. *Cancer Res.* **2013***, 73*, P4-12-29-P4-12-29.

108. Wickham, T.; Reynolds, J.; Drummond, D.; Kirpotin, D.; Lahdenranta, J.; Leonard, S.; Geretti, E.; Lee, H.; Klinz, S.; Hendriks, B. Abstract P3-14-09: Preclinical Safety and Activity of MM-302, a HER2-Targeted Liposomal Doxorubicin Designed To Have an Improved Safety and Efficacy Profile over Approved Anthracyclines. *Cancer Res.* **2010***, 70*, P3-14-09-P3-14-09.

109. Lukyanov, A. N.; Elbayoumi, T. A.; Chakilam, A. R.; Torchilin, V. P. Tumor-targeted liposomes: doxorubicin-loaded long-circulating liposomes modified with anti-cancer antibody. *J. Controlled Release* **2004***, 100*, 135-144.

110. ElBayoumi, T. A.; Torchilin, V. P. Tumor-targeted nanomedicines: enhanced antitumor efficacy in vivo of doxorubicin-loaded, long-circulating liposomes modified with cancer-specific monoclonal antibody. *Clin. Cancer Res.* **2009***, 15*, 1973-1980.

111. Matsumura, Y.; Gotoh, M.; Muro, K.; Yamada, Y.; Shirao, K.; Shimada, Y.; Okuwa, M.; Matsumoto, S.; Miyata, Y.; Ohkura, H.; Chin, K.; Baba, S.; Yamao, T.; Kannami, A.; Takamatsu, Y.; Ito, K.; Takahashi, K. Phase I and pharmacokinetic study of MCC-465, a doxorubicin (DXR) encapsulated in PEG immunoliposome, in patients with metastatic stomach cancer. *Ann. Oncol.* **2004***, 15*, 517-525.

112. Le Meins, J.; Sandre, O.; Lecommandoux, S. Recent trends in the tuning of polymersomes' membrane properties. *The European Physical Journal E* **2011***, 34*, 1-17.

113. Nahire, R.; Haldar, M. K.; Paul, S.; Ambre, A. H.; Meghnani, V.; Layek, B.; Katti, K. S.; Gange, K. N.; Singh, J.; Sarkar, K. Multifunctional polymersomes for cytosolic delivery of gemcitabine and doxorubicin to cancer cells. *Biomaterials* **2014***, 35*, 6482-6497.

114. Ahmed, F.; Pakunlu, R. I.; Brannan, A.; Bates, F.; Minko, T.; Discher, D. E. Biodegradable polymersomes loaded with both paclitaxel and doxorubicin permeate and shrink tumors, inducing apoptosis in proportion to accumulated drug. *J. Controlled Release* **2006***, 116*, 150-158.

115. Rolland, J. P.; Maynor, B. W.; Euliss, L. E.; Exner, A. E.; Denison, G. M.; DeSimone, J. M. Direct fabrication and harvesting of monodisperse, shape-specific nanobiomaterials. *J. Am. Chem. Soc.* **2005***, 127*, 10096-10100.

116. Kersey, F. R.; Merkel, T. J.; Perry, J. L.; Napier, M. E.; DeSimone, J. M. Effect of aspect ratio and deformability on nanoparticle extravasation through nanopores. *Langmuir* **2012***, 28*, 8773-8781.

117. Ayame, H.; Morimoto, N.; Akiyoshi, K. Self-assembled cationic nanogels for intracellular protein delivery. *Bioconjug. Chem.* **2008***, 19*, 882-890.

118. Raemdonck, K.; Demeester, J.; De Smedt, S. Advanced nanogel engineering for drug delivery. *Soft Matter* **2009***, 5*, 707-715.

119. Qiao, Z.; Zhang, R.; Du, F.; Liang, D.; Li, Z. Multi-responsive nanogels containing motifs of ortho ester, oligo (ethylene glycol) and disulfide linkage as carriers of hydrophobic anti-cancer drugs. *J. Controlled Release* **2011***, 152*, 57-66.

120. Oh, J. K.; Siegwart, D. J.; Lee, H.; Sherwood, G.; Peteanu, L.; Hollinger, J. O.; Kataoka, K.; Matyjaszewski, K. Biodegradable nanogels prepared by atom transfer radical polymerization as potential drug delivery carriers: synthesis, biodegradation, in vitro release, and bioconjugation. *J. Am. Chem. Soc.* **2007***, 129*, 5939-5945.

121. Nochi, T.; Yuki, Y.; Takahashi, H.; Sawada, S.; Mejima, M.; Kohda, T.; Harada, N.; Kong, I. G.; Sato, A.; Kataoka, N. Nanogel antigenic protein-delivery system for adjuvant-free intranasal vaccines. *Nature materials* **2010***, 9*, 572-578.

122. Chacko, R. T.; Ventura, J.; Zhuang, J.; Thayumanavan, S. Polymer nanogels: A versatile nanoscopic drug delivery platform. *Adv. Drug Deliv. Rev.* **2012***, 64*, 836-851.

123. McAllister, K.; Sazani, P.; Adam, M.; Cho, M. J.; Rubinstein, M.; Samulski, R. J.; DeSimone, J. M. Polymeric nanogels produced via inverse microemulsion polymerization as potential gene and antisense delivery agents. *J. Am. Chem. Soc.* **2002***, 124*, 15198-15207.

124. Park, J.; Wrzesinski, S. H.; Stern, E.; Look, M.; Criscione, J.; Ragheb, R.; Jay, S. M.; Demento, S. L.; Agawu, A.; Limon, P. L. Combination delivery of TGF-β inhibitor and IL-2 by nanoscale liposomal polymeric gels enhances tumour immunotherapy. *Nature materials* **2012***, 11*, 895-905.

125. Nishikawa, T.; Akiyoshi, K.; Sunamoto, J. Supramolecular assembly between nanoparticles of hydrophobized polysaccharide and soluble protein complexation between the self-aggregate of cholesterol-bearing pullulan and. alpha.-chymotrypsin. *Macromolecules* **1994***, 27*, 7654-7659.

126. Akiyoshi, K.; Kobayashi, S.; Shichibe, S.; Mix, D.; Baudys, M.; Kim, S. W.; Sunamoto, J. Self-assembled hydrogel nanoparticle of cholesterol-bearing pullulan as a carrier of

protein drugs: complexation and stabilization of insulin. *J. Controlled Release* **1998***, 54*, 313-320.

127. Ganguly, K.; Chaturvedi, K.; More, U. A.; Nadagouda, M. N.; Aminabhavi, T. M. Polysaccharide-based micro/nanohydrogels for delivering macromolecular therapeutics. *J. Controlled Release* **2014***, 193*, 162-173.

128. Nagarajan, R.; Ganesh, K. Block copolymer self-assembly in selective solvents: Spherical micelles with segregated cores. *J. Chem. Phys.* **1989***, 90*, 5843-5856.

129. Allen, T. M. Ligand-targeted therapeutics in anticancer therapy. *Nature Reviews Cancer* **2002***, 2*, 750-763.

130. Kabanov, A. V.; Nazarova, I. R.; Astafieva, I. V.; Batrakova, E. V.; Alakhov, V. Y.; Yaroslavov, A. A.; Kabanov, V. A. Micelle formation and solubilization of fluorescent probes in poly (oxyethylene-b-oxypropylene-b-oxyethylene) solutions. *Macromolecules* **1995***, 28*, 2303-2314.

131. Kim, J. O.; Nukolova, N. V.; Oberoi, H. S.; Kabanov, A. V.; Bronich, T. K. Block Ionomer Complex Micelles with Cross-Linked Cores for Drug Delivery. *Polym. Sci. Ser. A. Chem. Phys.* **2009***, 51*, 708-718.

132. Kwon, G. S.; Okano, T. Polymeric micelles as new drug carriers. *Adv. Drug Deliv. Rev.* **1996***, 21*, 107-116.

133. Lu, G.; Jiang, X.; Li, Y.; Lv, X.; Huang, X. Synthesis and self-assembly of PMBTFVB-g-PNIPAM fluorine-containing amphiphilic graft copolymer. *RSC Advances* **2015***, 5*, 74947-74952.

134. Tian, M.; Qin, A.; Ramireddy, C.; Webber, S. E.; Munk, P.; Tuzar, Z.; Prochazka, K. Hybridization of block copolymer micelles. *Langmuir* **1993***, 9*, 1741-1748.

135. Prochazka, K.; Kiserow, D.; Ramireddy, C.; Tuzar, Z.; Munk, P.; Webber, S. Time-resolved fluorescence studies of the chain dynamics of naphthalene-labeled polystyrene-block-poly (methacrylic acid) micelles in aqueous media. *Macromolecules* **1992***, 25*, 454-460.

136. Teng, Y.; Morrison, M.; Munk, P.; Webber, S.; Procházka, K. Release kinetics studies of aromatic molecules into water from block polymer micelles. *Macromolecules* **1998***, 31*, 3578-3587.

137. Pacovska, M.; Prochazka, K.; Tuzar, Z.; Munk, P. Formation of block copolymer micelles: a sedimentation study. *Polymer* **1993***, 34*, 4585-4588.

138. Halperin, A. Polymeric micelles: a star model. *Macromolecules* **1987***, 20*, 2943-2946.

139. Cammas, S.; Suzuki, K.; Sone, C.; Sakurai, Y.; Kataoka, K.; Okano, T. Thermo-responsive polymer nanoparticles with a core-shell micelle structure as site-specific drug carriers. *J. Controlled Release* **1997***, 48*, 157-164.

140. Duncan, R. Polymer conjugates as anticancer nanomedicines. *Nature Reviews Cancer* **2006***, 6*, 688-701.

141. Shin, H.; Alani, A. W.; Cho, H.; Bae, Y.; Kolesar, J. M.; Kwon, G. S. A 3-in-1 polymeric micelle nanocontainer for poorly water-soluble drugs. *Molecular pharmaceutics* **2011***, 8*, 1257-1265.

142. Wang, X.; Niu, D.; Li, P.; Wu, Q.; Bo, X.; Liu, B.; Bao, S.; Su, T.; Xu, H.; Wang, Q. A Dual-Enzyme Loaded Multifunctional Hybrid Nanogel System for Pathological Responsive Ultrasound Imaging and T2-Weighted Magnetic Resonance Imaging. *ACS nano* **2015**.

143. Han, Y.; He, Z.; Schulz, A.; Bronich, T. K.; Jordan, R.; Luxenhofer, R.; Kabanov, A. V. Synergistic combinations of multiple chemotherapeutic agents in high capacity poly (2-oxazoline) micelles. *Molecular pharmaceutics* **2012***, 9*, 2302-2313.

144. Cho, K. R.; Shih Ie, M. Ovarian cancer. *Annu Rev Pathol* **2009***, 4*, 287-313.

145. Owens III, D. E.; Peppas, N. A. Opsonization, biodistribution, and pharmacokinetics of polymeric nanoparticles. *Int. J. Pharm.* **2006***, 307*, 93-102.

146. Jeon, S. I.; Lee, J. H.; Andrade, J. D.; De Gennes, P. G. Protein-surface interactions in the presence of polyethylene oxide. I. Simplified theory. *J. Colloid Interface Sci.* **1991***, 142*, 149-158.

147. Mitragotri, S.; Lahann, J. Physical approaches to biomaterial design. *Nature materials* **2009***, 8*, 15-23.

148. Jokerst, J. V.; Lobovkina, T.; Zare, R. N.; Gambhir, S. S. Nanoparticle PEGylation for imaging and therapy. *Nanomedicine* **2011***, 6*, 715-728.

149. Peracchia, M. T.; Fattal, E.; Desmaële, D.; Besnard, M.; Noël, J. P.; Gomis, J. M.; Appel, M.; D'Angelo, J.; Couvreur, P. Stealth(®) PEGylated polycyanoacrylate nanoparticles for intravenous administration and splenic targeting. *J. Controlled Release* **1999***, 60*, 121-128.

150. Moghimi, S. M.; Hunter, A. C.; Murray, J. C. Long-circulating and target-specific nanoparticles: theory to practice. *Pharmacol. Rev.* **2001***, 53*, 283-318.

151. Hendrickson, G. R.; Lyon, L. A. Microgel translocation through pores under confinement. *Angewandte Chemie International Edition* **2010***, 49*, 2193-2197.

152. Banquy, X.; Suarez, F.; Argaw, A.; Rabanel, J.; Grutter, P.; Bouchard, J.; Hildgen, P.; Giasson, S. Effect of mechanical properties of hydrogel nanoparticles on macrophage cell uptake. *Soft Matter* **2009***, 5*, 3984-3991.

153. Anselmo, A. C.; Zhang, M.; Kumar, S.; Vogus, D. R.; Menegatti, S.; Helgeson, M. E.; Mitragotri, S. Elasticity of Nanoparticles Influences Their Blood Circulation, Phagocytosis, Endocytosis, and Targeting. *ACS nano* **2015***, 9*, 3169-3177.

154. Zhang, X.; Malhotra, S.; Molina, M.; Haag, R. Micro-and nanogels with labile crosslinks–from synthesis to biomedical applications. *Chem. Soc. Rev.* **2015***, 44*, 1948-1973.

155. Maeda, H.; Bharate, G. Y.; Daruwalla, J. Polymeric drugs for efficient tumor-targeted drug delivery based on EPR-effect. *European Journal of Pharmaceutics and Biopharmaceutics* **2009***, 71*, 409-419.

156. Maeda, H. The enhanced permeability and retention (EPR) effect in tumor vasculature: The key role of tumor-selective macromolecular drug targeting. *Advances in Enzyme Regulation* **2001***, 41*, 189-207.

157. Danhier, F.; Feron, O.; Préat, V. To exploit the tumor microenvironment: passive and active tumor targeting of nanocarriers for anti-cancer drug delivery. *J. Controlled Release* **2010***, 148*, 135-146.

158. Kamaly, N.; Xiao, Z.; Valencia, P. M.; Radovic-Moreno, A. F.; Farokhzad, O. C. Targeted polymeric therapeutic nanoparticles: design, development and clinical translation. *Chem. Soc. Rev.* **2012***, 41*, 2971-3010.

159. Fang, J.; Nakamura, H.; Maeda, H. The EPR effect: Unique features of tumor blood vessels for drug delivery, factors involved, and limitations and augmentation of the effect. *Adv. Drug Deliv. Rev.* **2011***, 63*, 136-151.

160. Nuhn, L.; Braun, L.; Overhoff, I.; Kelsch, A.; Schaeffel, D.; Koynov, K.; Zentel, R. Degradable Cationic Nanohydrogel Particles for Stimuli-Responsive Release of siRNA. *Macromolecular rapid communications* **2014***, 35*, 2057-2064.

161. Averick, S. E.; Paredes, E.; Irastorza, A.; Shrivats, A. R.; Srinivasan, A.; Siegwart, D. J.; Magenau, A. J.; Cho, H. Y.; Hsu, E.; Averick, A. A. Preparation of cationic nanogels for nucleic acid delivery. *Biomacromolecules* **2012***, 13*, 3445-3449.

CHAPTER 2

Trastuzumab-Conjugated Polypeptide-Based Carrier System for Combination Therapy in Breast Cancer

2.1 Introduction

Polypeptides have an inherent property to assemble into supramolecular structures in solution. The formation of supramolecular structures is a controlled and organized process that depends by and large on the nature of the polypeptide and conditions of the solvent it is exposed to. Formation of amphiphilic copolymers based on such polypeptides can allow for tailoring the assembly process to a predefined nanoscale supramolecular structure, which can then be used as drug delivery vehicles [1-4]. The overall process of self-assembly of such amphiphilic copolymers can then be regarded as a complex phenomenon of structural organization that is governed by the nature of constituent hydrophilic and hydrophobic blocks, their relative lengths, as well as properties of the solvent-phobic block that is the driving force for self-assembly [5,6]. The inherent biocompatibility and biodegradability of polypeptides is of additional advantage for their biological applications. For the purpose of the current study, amphiphilic block copolymer with following composition was chosen: polyethylene glycol (PEG) as the hydrophilic, stealth imparting block and polyleucine (PLeu) as the hydrophobic part and the initiator of micelle formation in aqueous environment [7,8]. The variables explored in the current study were altering the ratio of lengths of constituent blocks as well as chirality of PLeu block and the temperature of solvent used for preparation of micelles via the film rehydration method. The impact of all these variables on the thermodynamic stability as well as type of secondary structures formed and the influence of these attributes on the ability of the

micelles to encapsulate a combination of hydrophobic drugs into their core are also described.

The primary purpose of designing this micellar carrier was for combination therapy of ErbB2 positive breast cancer. The receptor tyrosine kinase, ErbB2 is a viable target in 20-25 % breast cancer patients due to its overexpression. Its degradation is associated with slower progression of the disease and increased survival times [9,10]. While the monoclonal antibody Trastuzumab (Herceptin™) is the first line therapy in such patients, monotherapy with Trastuzumab has shown little benefit and therefore must be given with chemotherapeutic agents. Such combinations also help in delaying the development of resistance to Trastuzumab, since multiple cellular pathways can be targeted simultaneously. ErbB2 is a client protein of heat shock protein 90 and 17-N-allylamino-17-demethoxygeldanamycin (17-AAG) is a potent inhibitor of HSP90. Previous work in our lab has demonstrated strong synergy of action between 17-AAG and a model cytotoxic agent doxorubicin [11,12]. In order to further improve the efficacy of the therapy, our goal was to replace doxorubicin with the more potent, clinically relevant agent paclitaxel (PTX) [13], which has been shown to have strong synergistic antitumor effect with 17-AAG in ErbB2-driven breast cancers [14,15]. Since synergy of such therapy is often sequence and dose ratio specific, co-delivery of the drugs via the same vehicle is desirable as well as beneficial [16]. Dual drug-loaded micelles thus prepared could load 17-AAG and PTX in a ratio 2:1 by weight. The formulation showed a high level of synergy on BT-474 cells that express a high amount of ErbB2 while the synergy was negligible in ErbB2low MCF-7 cells. The strong synergy also observed when the formulation was tested in an orthotopic breast cancer mouse model developed using ErbB2 overexpressing BT-474 cells, and an arrest in the growth of tumors in animals treated with dual drug-loaded micelles was observed, while both 17-AAG and PTX were used at sub therapeutic doses of 10 mg and

5 mg equivalents per kg body weight. The lower doses also helped avoid toxicity associated with the therapy. We also show the importance of simultaneously delivering the two drugs via a single carrier system as opposed to cocktail of individual drug-loaded micelles administered at equivalent doses, which has a better therapeutic outcome than the cocktail therapy. These combination drug-loaded micelles were developed as a platform for chemotherapy with Trast. The triple therapeutic system of Trast with combination drug-loaded micelles containing 17-AAG and PTX exhibited an even stronger anticancer effect, with complete regression of tumors at the end of treatment, which reached a palpable size again after day 45 with much slower progression than other treatment controls.

2.2 Materials and methods

Materials

PEG-*b*-PLeu block copolymers with different number of leucine units (7 and 20) were synthesized as described below. α-Amino-ω-methoxy poly(ethylene glycol) (mPEG-NH_2, M_w = 10,000 g mol^{-1}, M_w / M_n = 1.05) and FMOC-NH-PEG--NH_2, M_w = 10,000 g mol^{-1} were purchased from JenKem Technology (TX, USA) and mPEG-NH_2, M_w = 5,000 g mol^{-1}. L-leucine and D,L-leucine (Leu), 1,2-ethylenediamine, 1-(3-dimethylaminopropyl)-3-ethylcarbodiimide hydrochloride (EDC), paclitaxel, and other chemicals were purchased from Sigma-Aldrich (St Louis, MO) and were used without further purification. Trastuzumab was obtained from UNMC pharmacy. Fetal bovine serum (FBS), DMEM and RPMI 1640 medium, penicillin, streptomycin, Trypsin–ethylenediaminetetraacetic acid (EDTA) (0.5% trypsin, 5.3 mM EDTA tetra-sodium) and other chemicals were purchased from Invitrogen (Carlsbad, CA, USA). MTT reagent (3-(4,5-Dimethylthiazol-2-yl)-2,5-diphenyltetrazolium bromide) was purchased from Research Products International

(Prospect, IL). Cyanine3 (Cy3) carboxylic acid was purchased from Lumiprobe life science solutions. All other chemicals were of reagent grade and used without further purification.

Methods

N-carboxyanhydride (NCA) of Leu

D,L or L-Leu (0.015 mol) and anhydrous tetrahydrofuran (THF) were added into a dried glass reactor in inert (nitrogen) atmosphere to form a suspension. Triphosgen (0.017 mol) was likewise separately dissolved in fresh anhydrous THF and injected drop wise into reaction mixture. Nitrogen was bubbled through the mixture during synthesis. The mixture was heated at about 55^{o}C with constant stirring till it became transparent. The product was precipitated by addition of 5 times excess of n-hexane and then stored at -20^{o}C overnight in order to allow complete precipitation of D,L or L–N-carboxyanhydride (Leu-NCA). The obtained product was purified further by repeated precipitation with n-hexane, dried under vacuum for 24 h and characterized by proton nuclear magnetic resonance (^{1}H-NMR) and Gel Permeation Chromatography.

PEG-b-PLeu block copolymer

Monoaminomethoxypoly(ethylene glycol) (mPEG-NH_2) (0.03 mmol) was dissolved under stirring in 25 mL of anhydrous dimethylformamide (DMF) in nitrogen atmosphere at 30^{o}C. Leu-NCA (0.75 mmol, the feed molar ratio of mPEG-NH_2 to Leu-NCA was 1: 25) dissolved in 5 mL of anhydrous DMF was added dropwise and the solution was stirred for 5 days. The aliquot of the reaction mixture was precipitated using excess of diethyl ether, dried under vacuum, and the composition of PEG-PBGlu diblock copolymer was determined by ^{1}H-NMR from the peak intensity ratios of the methylene protons of PEG and the methyl protons of the isopropyl groups of Leu (500 MHz in DMSO-d_6, 80 ^{0}C : ^{1}H NMR [δ = 3.53 (-C**H2**- C**H2**- of PEG), 1.43 – 1.72 {-C**H2**- C**H**-(CH3)2}, 0.8 – 0.97 {CH2- CH-(C**H3**)2} for

Leu. The product (PEG-*b*-Leu) was precipitated by diethyl ether, purified by repeated precipitation in diethyl ether and dried under vacuum. By varying the feed molar ratio of mPEG-NH_2 to Leu-NCA (1:12 and 1:25), copolymers with targeted compositions PEG-*b*-PLeu(10) and PEG-*b*-PLeu(20) were synthesized. Self-assembly behavior of PEG-*b*-PLeu copolymers was examined using pyrene as a hydrophobic fluorescence probe [17]. The biodegradability of the copolymer was studied upon incubation with Cathepsin B as reported previously [18]. For conjugation with mAb, polymer was synthesized using FMOC-NH-PEG--NH_2 as the initiator as described above. When the polymerization reaction was complete, 10% v/v piperidine in DMF for 1 h was used to deprotect FMOC. The polymer was precipitated and washed with diethyl ether, redissolved in DMF and reacted with 4 eq of succinic anhydride (SA) overnight. The polymer was purified by reprecipitation and washing with ether, dissolved in 70% ethanol in water and subjected to exhaustive dialysis against deionized water, followed by lyophilization. For the synthesis of Cy3 labeled polymer, Cy3 carboxylic acid was conjugated to polymer prior to deprotection of FMOC in DMF and processed as above.

Preparation of polymeric micelles

Micelles were prepared by film rehydration method. PEG-*b*-PLeu copolymer was dissolved in acetonitrile (1mg/mL) followed by evaporation of the organic solvent under reduced pressure to form a thin film. The film was then rehydrated using hot water (60 ^{0}C) and the solution was stirred for additional 1h at 60 ^{0}C and then cooled gradually to room temperature.

Physicochemical and biophysical methods of characterization

The ^{1}H NMR spectra for the monomer and copolymers were acquired in DMSO-d_6 at 25 °C and 80 °C respectively using a Bruker Avance III HD NMR spectrometer (500 MHz).

Effective hydrodynamic diameters (D_{eff}) of micelles were determined by dynamic light scattering (DLS) using a Zetasizer Nano ZS (Malvern Instruments Ltd., Malvern, UK). All measurements were performed in automatic mode at 25°C. Software provided by the manufacturer was used to calculate the size, polydispersity indices (PDI), and ζ-potential of micelles. All measurements were performed at least in triplicate to calculate mean values ± SD. The CD spectra were recorded by using an Aviv circular dichroism spectrometer (model 202SF, Aviv Associates Inc., Lakewood, NJ). The spectra were measured at 25 °C using a 1 cm path length cell over a wavelength range from 190 to 260 nm in deionized water. Data were collected at 1 nm intervals with a scan rate of 15 nm/min. All spectra were acquired in triplicate and averaged. The spectrum of an appropriate control sample was then subtracted from each of the sample spectra. The final spectral data were converted to mean molar ellipticities. The polymer concentrations were 0.02 mM.

Differential Scanning Calorimetry was used to measure the heat capacity of melting transition with a VP-DSC (Microcal, Northampton, MA), using a temperature ramping rate of 0.5 ^{0}C/min and polypeptide concentration of 0.167 mM. Standard thermodynamic profiles were determined using the following equations: $\Delta G_T = \Delta H_m (1 - T/T_m)$ and $\Delta G = \Delta H - T\Delta S$, where T = 298 K. ΔG_T is the free energy at temperature T, ΔH_m is the calorimetric enthalpy at transition temperature T_m and ΔS is the unfolding entropy.

Molecular weight of micelles was determined using Agilent 1260 Infinity LC system equipped with a miniDAWN TREOS multi-angle light scattering (MALS) detector and a Optilab T-rEX refractive index detector (Wyatt Technology, Santa Barbara, CA) operated in an offline batch mode at a flow rate of 0.5 mL/min using DI water as the mobile phase. All analysis was carried out using the software Astra 6.1 (Wyatt Technology), and the dn/dc value of PEG (0.162 mL/g) was used for calculations.

Drug loading, conjugation of mAb and drug release

17-AAG and/or PTX-loaded micelles were prepared by film rehydration method. Briefly, polymer and either or both drugs (drug/polymer ratio – 0.8:1) were dissolved in acetonitrile and the solvent was evaporated to form a thin film. This film was rehydrated with hot water (60 ^{0}C) and the solution was stirred for additional 1h at 60 ^{0}C and then cooled gradually to room temperature. Precipitates of unloaded drugs were removed by centrifugation. Drug content was determined by high-performance liquid chromatography (HPLC) analysis under isocratic conditions using an Agilent 1200 HPLC system a diode array detector set at 227 nm (PTX) and 334 nm (17-AAG). A Nucleosil C18 column was used as stationary phase (250 mm $\times$ 4.6 mm), and mobile phase comprised of acetonitrile/water mixture (55/45, v/v) at a flow rate of 1 mL/min.

Drug-loaded micelles were prepared from SA-modified polymer in the same manner. The terminal carboxylic acid was activated by EDC (1.5 molar excess) and Trast was added to activated micelles and allowed to react for 2 hours, followed by purification to remove unconjugated mAb by SEC. Amount of mAb present in the mAb-micelles conjugate was measured by Bradford method using blank micelles as control.

Drug release from the micelles was examined in PBS (pH 7.4) by dialysis method using a membrane with 3,500 Da cutoff. The concentrations of PTX and 17-AAG released were determined by HPLC and expressed as a percentage of the total PTX or 17-AAG available *vs.* time.

Cell culture, cellular association and cytotoxicity assay

BT-474 and MCF-7 cell lines were obtained from the American Type Culture Collection (ATCC) and cultured as described previously [11,12]. Cells were harvested with trypsin-EDTA (Life Technologies) after 80% confluence. Cells seeded in 96-well plates (5,000 cells/well)

24 h prior the experiment were exposed to various doses (0-100 ng/mL on 17-AAG or PTX basis) of 17-AAG alone, polymeric micelles alone, 17-AAG-loaded micelles, PTX-loaded micelles and (17-AAG+PTX)-loaded micelles for 72 h at 37 °C. Cytotoxicity of drug-loaded *cl*-micelles was assessed by a standard MTT assay [19] and the IC_{50} values were calculated using GraphPad Prism software. Combination index (CI) analysis based on Chou and Talalay method [20] was performed using CompuSyn software for 17-AAG and PTX combinations, determining synergistic, additive, or antagonistic cytotoxic effects against the breast cancer cells. Values of CI < 1 demonstrate synergism while CI = 1 and CI > 1 values represent additive and antagonistic effects of drug combination, respectively. For flow cytometry, cells (50,000 per well) were grown in a 24-well plate 24 hours prior the start of the experiment and exposed to Cy3-labeled Trast- or IgG-micelles (25 or 50 µg protein per mg polymer) at 37 °C, for 1 or 2 h, washed 3 times with PBS, trypsinized, centrifuged (1200 rpm, 3 min) and resuspended in PBS. The % gated cells were analyzed using Becton Dickinson FACStarPlus flow cytometer and FACSDiva software (Version 8.0, Becton Dickinson, San Jose, CA). At least 5000 events were acquired in linear mode, gated to exclude debris and dead cells, and visualized in logarithmic mode.

Animal studies

Animal model was developed as previously reported (PPGA, trast). All studies were performed in strict accordance with the guidelines of University of Nebraska Medical Center Institutional Animal Care and Use Committee (IACUC). 4-6 weeks old female athymic NCr-nu/nu mice (Taconic Biosciences, NY) implanted with 17-β-Estradiol pellets (0.72mg/pellet; 60 day release; Innovative Research of America, Sarasota, Fl) were implanted subcutaneously on the lateral side of the neck of the mice three days prior to the injection of the tumor cells. 10^7 BT-474 cells (an ErbB2 overexpressing human breast cancer cell line) reconstituted in 50% Matrigel (BD Biosciences, California) in media were

injected directly into the mammary fat pad. The animals were randomized into treatment groups (n=10) when tumor size reached 100-200 mm^3. Drug amount was calculated based on the average animal body weight. Treatments were administered by tail vein injection, comprising of various treatments as indicated in each specific section of results at the same drug ratio at a dose of 10 mg/kg 17-AAG and 5 mg/kg PTX and 6.5 mg/kg Trast. Free PTX or free 17-AAG + PTX were formulated using Cremophor-EL: propylene glycol: ethanol (2:3:5 by volume) mixture for injections as a component of the free drug combination. Tumor dimensions were measured using electronic calipers and tumor volume was calculated using the formula $V = 0.5 \times L \times W^2$ where L: longer dimension and W: shorter dimension. Animals were sacrificed when tumor volume was close to 2000 mm^3, greatest tumor dimension was close to 20 mm or tumor became necrotic or animal exhibited body weight loss of 20%.

Apoptosis and proliferation

Tumors from mice that received different treatments were excised on day 13 (2-3 mice per group). The tumors were dissected and fixed in 10% neutral buffered formalin. Then, the tissues were processed routinely into paraffin, sectioned at a thickness of 4 μm. Proliferating and apoptotic cells were detected using an antibody against Ki-67 and caspase-3, respectively. Visualization was done by incubation with DAB+ (brown, for Ki-67) and Permanent red (for caspase-3) (DAKO) for 2 min. After being rinsed with distilled water, the sections were counterstained with hematoxylin. For quantification of Ki-67 and caspase-3 expression, the area of positive cells was determined (Image J) in 3 random high power fields (10X magnification) and divided by the total area of cells for each field of slice.

Sample preparation and drug content measurement in tissue.

Tissue samples harvested from animals sacrificed were frozen and stored at -80 ^{0}C until further use. Known weights of thawed tissues were homogenized with 3 volumes of HPLC grade water using TissueLyser (Qiagen). Calibration curves were built by spiking tissue samples from control animals to achieve the final concentration of 5 – 2000 ng/mL. Docetaxel was used as an internal standard at a final concentration of 500 ng/mL. Homogenates were vortexed for 30 sec, left for 5 mins, then extracted using excess (1 mL) of ice-cold acetonitrile, vortexed for 3 min and put on a shaker for additional 15 mins. All samples were then centrifuged at 16,000 x g for 10 mins and the clear supernatant was separated into clean vials and evaporated to dryness followed by reconstitution with 100 µL of 70% acetonitrile in water (HPLC grade). These samples were run on LC-MS/MS system using a Nucleosil C18 column (250 mm×4.6 mm) and a mobile phase of 70% acetonitrile in water was applied under isocratic conditions at a flow rate of 0.5 mL/min. A LC-MS/MS system equipped with triple quadrupole (QTRAP® 6500, Sciex) coupled to HPLC system (Nexera X2, Shimadzu) was used in multiple reaction monitoring (MRM) mode as follows; m/z 853.995 $\longrightarrow$286 for PTX, 584.07 $\longrightarrow$541 for 17-AAG and

808.08 $\longrightarrow$ 527 for docetaxel.

Blood chemistry and histopathology

Blood from the sacrificed animals was collected in heparin tubes and analyzed for blood cell count and liver and kidney function markers (VetScan Comprehensive Diagnostic Profile) using Vetscan VS (Abaxis). Fixed tissues were processed, sectioned, inserted into tissue cassettes, dehydrated in 70% ethanol overnight, and paraffin embedded (UNMC Tissue Sciences Facility, Omaha, NE). Serial 5 µm sections were stained with either hematoxylin or eosin (H&E) or by immunohistochemistry (IHC). For histopathological diagnosis, H&E-stained slides were examined by light microscopy and photomicrographs were taken using a Nikon camera mounted on a Nikon Eclipse 600 microscope (both

Nikon Instruments, Melville, NY) with Adobe Elements 3.0 software (Adobe Systems, San Jose, CA).

Statistical analysis

Statistical comparisons except animal studies were carried out using Student t-test. For the antitumor study and toxicity studies, group means for tumor volume and body weights were evaluated using repeated measures analysis of variance with the Bonferroni posttest. Survival was estimated using Kaplan–Meier analysis and compared using log-rank test. *P* values less than 0.05 were considered significant. Analysis of variance with Bonferroni test and Kaplan–Meier analysis with log-rank test were performed using GraphPad Prism 5 (GraphPad Software, Inc.).

2.3 Results

Synthesis of biodegradable block copolymer PEG-b-PLeu

The primary objective of this study was to optimize carrier system for hydrophobic drugs used in cancer therapy that can be used as a safer substitute to toxic cosolvent currently used in clinical practice for such agents. To this end, we chose polypeptide based copolymers made from polyethylene glycol and leucine as the hydrophobic block to develop micellar carriers for combination of hydrophobic drugs 17-AAG and PTX. The block copolymers were synthesized by living ring opening polymerization using amino-terminated PEG as a macro initiator to polymerize Leu-NCA (Fig. 6). The length of polyleucine block was controlled by feed ratio of PEG to Leu-NCA, using a 20% excess by weight of Leu-NCA than the targeted block length. Structure of the final copolymer was confirmed by ^{1}H-NMR (Fig. 7) and polydispersity by Gel Permeation Chromatography (Fig. 8). The polymer had 228 units of ethylene glycol and 20 units of (D,L)-Leucine. Breast

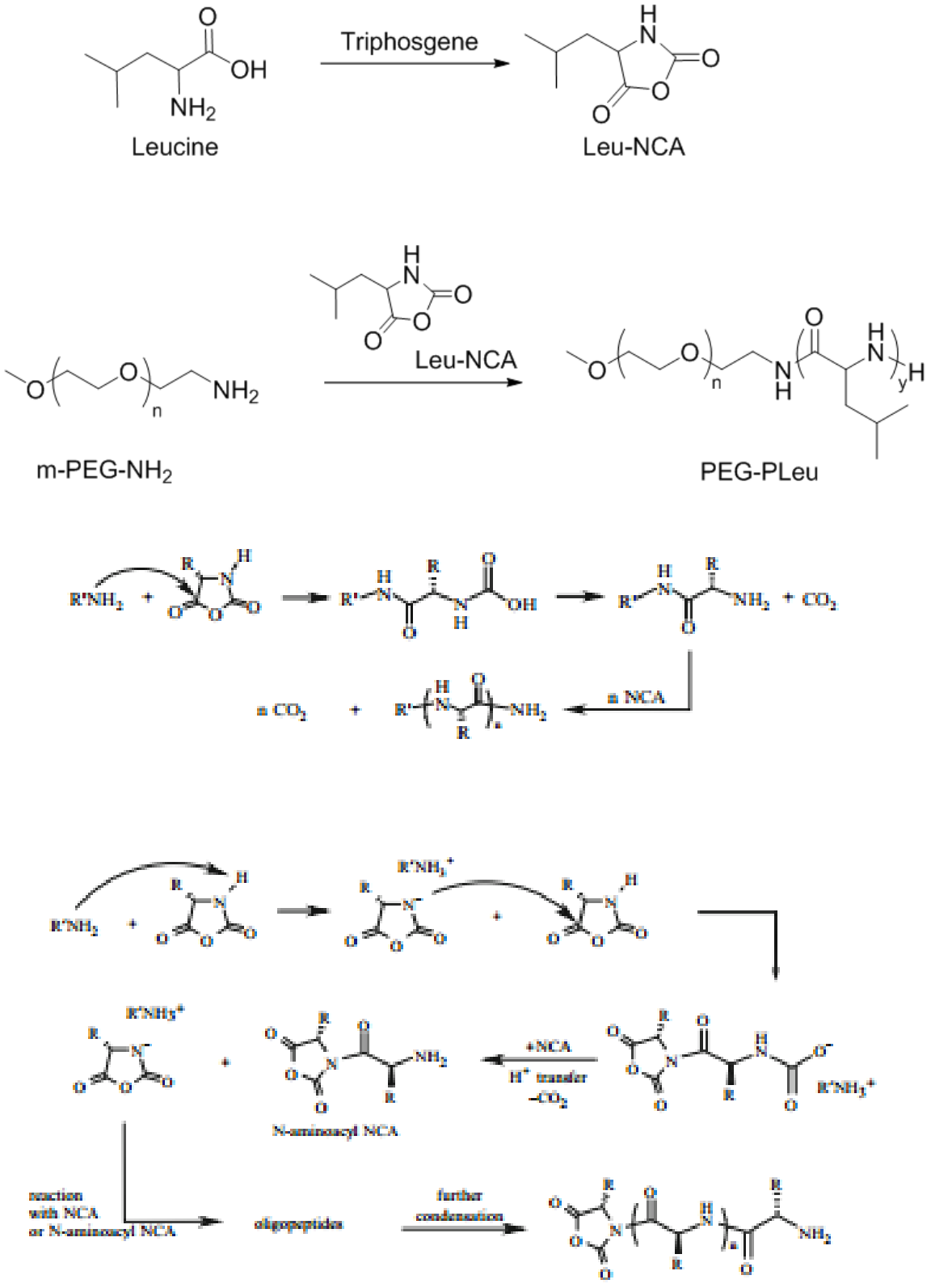

Figure 6. Scheme for the synthesis and mechanism of PEG-b-PLeu polymer via ring-opening NCA-based polymerization.

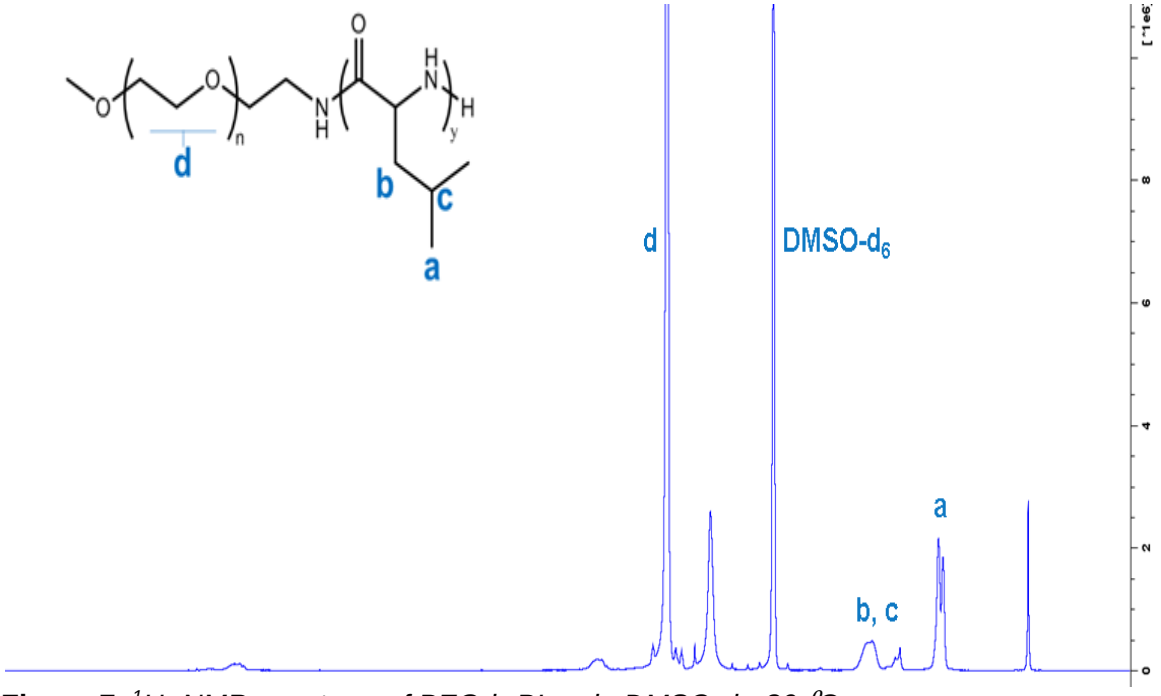

Figure 7. *^{1}H- NMR spectrum of PEG-b-PLeu in DMSO-d_6, 80 ^{0}C*

Characteristic peaks include: δ = 3.53 (-CH2- CH2- of PEG), 1.43 – 1.72 {-CH2- CH-(CH3)2}, 0.8 – 0.97 {CH2- CH-(CH3)2} for Leu. Repeating units of Leu were calculated from the -CH_3- proton signal (5.06ppm) of two terminal methyl groups of Leu and the -CH_2CH_2- proton signal (3.45ppm) of PEG chain

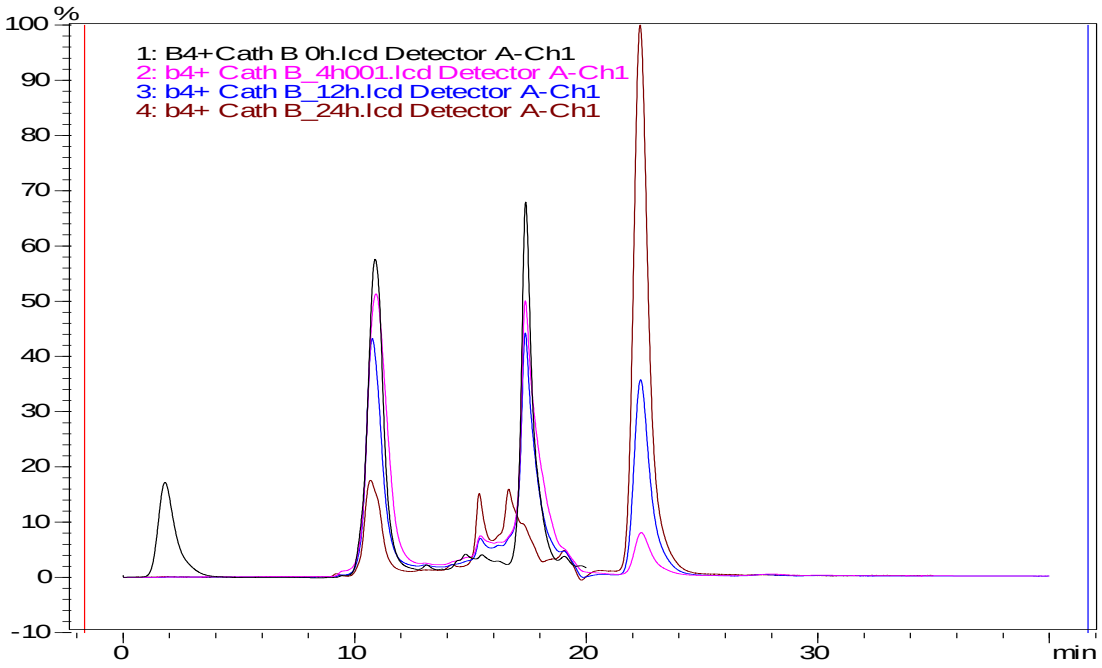

Figure 8. Degradation of PEG_{228}-$PLeu_{20}$ upon incubation with Cathepsin B at 37 °C, pH 5.5, as studied by Gel Permeation Chromatography at 0 (black), 4 (pink), 12 (blue) and 24 hours (brown) using UV detector at 280 nm.

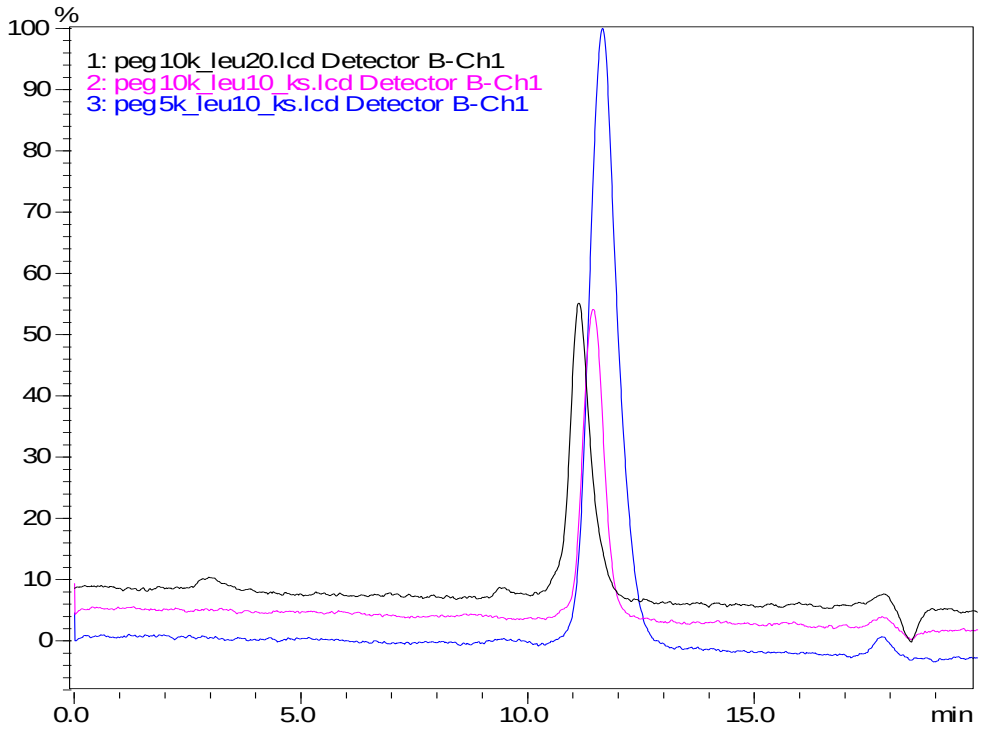

Figure 9. Gel Permeation chromatogram for PEG-b-PLeu synthesized using 228 units PEG and Leucine 10 units (magenta) or 20 units (black) or PEG (MW: 5000) and 10 units of Leucine (blue). Polymers were detected using UV absorbance at 280 nm.

cancer cells are known to express an excess of Cathepsin B in the lysosomes. It is a cysteine protease that can potentially degrade polypeptides [12,18,21,22]. We studied the degradation profile of the polymer in presence of cathepsin B using size exclusion chromatography (Fig 8). The intensity of the polymer peak diminished over time while that of the peaks corresponding to low molecular weight fragments showed a corresponding increase, proving that the polymer can be easily degraded by proteases like cathepsin B.

Optimization of hydrophilic and hydrophobic block lengths of PEG-PLeu

It is a well-demonstrated fact that the lengths of both hydrophilic and hydrophobic blocks play a crucial role in the self-assembly behavior of amphiphilic copolymers and that a certain length of the hydrophilic block is needed to provide optimal coverage of the hydrophobic block [23-26]. Diblock copolymers with different lengths of the hydrophilic PEG block and hydrophobic PLeu block were synthesized as described in the previous section. The length of polyleucine block was controlled by feed ratio of PEG to Leu-NCA (1:25 and 1:15). The polymers were characterized by ^{1}H-NMR and Gel Permeation Chromatography (Fig. 9) and results are summarized in Table 3. Micelles were prepared from all the polymers using the film rehydration technique [27,28]. Two different conditions were chosen for rehydration: room temperature (RT) and elevated temperature of 60 ^{0}C, which is safely below the lower critical solution temperature of PEG in water [29]. Physicochemical characteristics of the micelles prepared under both conditions are listed in Table 4. Only the polymer PEG_{228}-*b*-P(D,L)-Leu_{20} showed a temperature-dependent change in self-assembly behavior that was reflected in nearly 3-fold reduction of the hydrodynamic diameter of the micelles prepared by film rehydration at elevated temperature of 60 ^{0}C. However, the same trend was not observed when the block

Polymer	Feed molar ratio (mmol)		Repeating units ratio*		M_w* (g/mol)	PD#
	PEG	Leu-NCA	PEG	PLeu		
PEG_{228}-*b*-P(D,L)-Leu_{20}	0.02	0.5	228	20	12,263	1.03
PEG_{228}-*b*-P(D,L)-Leu_{10}	0.02	0.3	228	10	11,132	1.03
PEG_{114}-*b*-P(D,L)-Leu_{10}	0.02	0.3	114	12	6,358	1.06

Table 3. Characterization of PEG-*b*-Pleu block copolymers.
* Calculated from ^{1}H-NMR spectra; #Calculated from Gel Permeation Chromatography.

Sample	D_{eff} (nm)		PdI	
	RT	60 ^{0}C	RT	60 ^{0}C
PEG_{228}-*b*-P(D,L)-Leu_{10}/m	112	158	0.22	0.29
PEG_{228}-*b*-P(D,L)-Leu_{20}/m	142	58	0.26	0.12
PEG_{114}-*b*-P(D,L)-Leu_{10}/m	141	107	0.27	0.28

Table 4. Physicochemical characteristics of micelles prepared by film rehydration with water at either room temperature (RT) or 60 ^{0}C. Hydrodynamic diameter (D_{eff}) and Polydispersity Index (PdI) were measured by Dynamic Light Scattering.

lengths of PEG and PLeu were reduced to half while keeping the same weight ratio of the two blocks for the polymer PEG_{114}-*b*-P(D,L)-Leu_{10}. The shorter length of PEG was not able to stabilize the assemblies, probably due to the high hydrophobicity of the polyleucine block, and our observations show that higher molecular weight PEG was essential for the formation of small-sized micelles. In the opposite scenario, with the polymer PEG_{228}-*b*-P(D,L)-Leu_{10}, the length of the hydrophobic PLeu block was probably insufficient to drive proper assembly of the resultant micelles and showed no temperature-dependent change in self-assembly. In fact, when the critical micelle concentration (CMC) of 2 polymers with constant PEG length and variable polyleucine length was compared, we observed that increasing the PLeu block length from 10 units to 20 units brought down the CMC of respective PEG_{228}-*b*-P(D,L)-Leu copolymers from 1000 mg/L to a mere 15.6 mg/L. Similar evidence has been reported previously in the literature [30,31]. Thus, in conclusion, both the lengths of the composite blocks as well as the thermal activation provided by rehydration with water at elevated temperature (60 ^{0}C) were necessary for the formation of relatively small-sized micelles, making PEG_{228}-*b*-P(D,L)-Leu_{20} give the most favorable micellar assemblies.

Effect of rehydration temperature on aggregation number of micelles

To investigate further the effect of rehydration temperature on self-assembly of PEG_{228}-*b*-P(D,L)-Leu_{20}, we determined the aggregation number of micelles prepared from PEG_{228}-*b*-P(D,L)-Leu_{20} by film rehydration at RT and 60 ^{0}C. The results are summarized in Table 5. Measurement of molecular weight of the formed micelles by static light scattering technique revealed an order of magnitude of

Sample	D_{eff} (nm)	PdI	M_w	M_n	M_w/M_n	N_{agg}
PEG_{228}-*b*-P(D,L)-Leu_{20}/m - 60 ^{0}C	58	0.12	23,58,000	32,70,000	1.39	267
PEG_{228}-*b*-P(D,L)-Leu_{20}/m - RT	142	0.26	4,60,20,000	3,25,30,000	1.42	2,653

Table 5. Characterization of PEG(10K)-b-PLeu20 micelles prepared by film rehydration at room temperature (RT) or 60 ^{0}C. Deff and PdI were measured by Dynamic Light Scattering. Mw and Mn were obtained from Static Light Scattering measurement of the respective micelles. N_{agg} was calculated as N_{agg} = (M_n of micelles)/(M_n of polymer)

difference in Mw and Mn as well as the aggregation number (N_{agg}). Higher aggregation number lead to a higher hydrodynamic size of the micelles rehydrated at RT. No significant changes were observed in the hydrodynamic diameter as well as PdI of these micelles once formed, when subjected to heating at a rate of 0.5 ^{0}C on the DLS, from 10 – 65 ^{0}C (Fig. S5). This suggests that the polymer chains once assembled into micelles have a tight packing of the core with does not change upon subsequent heating. Collectively, the data suggests that higher temperature helps in better assembly of the polymer chains. The higher temperature can increase the mobility of the hydrophobic leucine chains and the enhanced flexibility can result in closer packing of the polymer chains. After gradual cooling of the micellar dispersion, the structure is locked in place, and subsequent heating does not result in any dramatic changes in the hydrodynamic size as well as the PdI of these micelles (Fig. 11).

Optimization of the nature of PLeu block

It has been shown before that blocks of enantiomerically pure form of leucine can assemble into closely packed secondary structures [32]. This can have a profound effect on the manner of assembly of the polymer as well as the physicochemical characteristics of the resultant micelles such as hydrodynamic diameter and drug loading capacity and is therefore an important parameter of optimization of amino acid based polymers. Having optimized the lengths of the constitutive blocks as well as the film rehydration temperature, the next step was to compare the effect of nature of hydrophobic block on the properties of micelles. To this end, a control polymer with P(L)-Leu as the hydrophobic block and similar block length as its

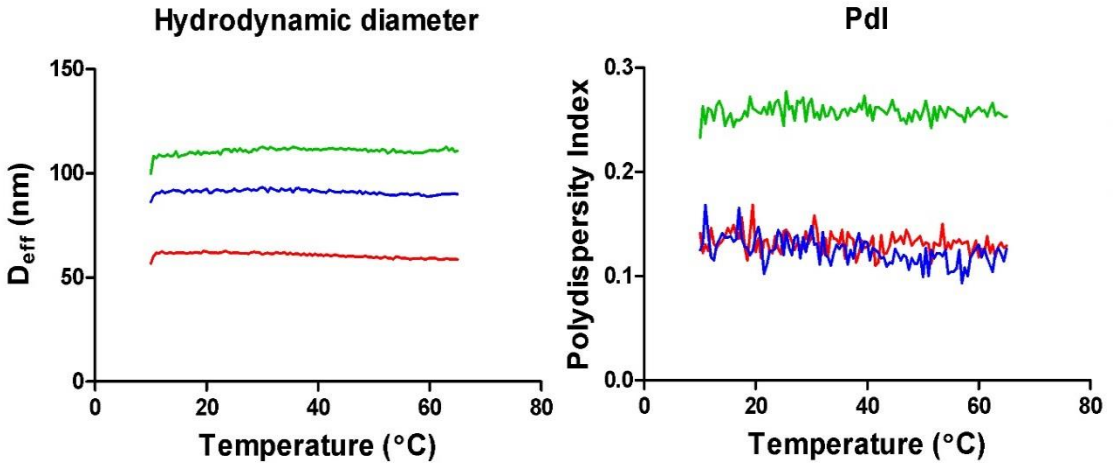

Figure 10. Changes in (A) hydrodynamic diameter (D_{eff}) and PdI as a function of temperature as measured by dynamic light scattering for PEG-P(D,L)-Leu/m - 60 ^{0}C (red), PEG-P(D,L)-Leu/m - RT (green) and PEG-P(L)-Leu/m - 60 ^{0}C (blue). All samples were heated starting from 10 ^{0} – 65 ^{0}C and measurements were recorded after every 0.5 ^{0}C change.

racemic counterpart (20 units of Leu) was synthesized via ring opening polymerization. Micelles were prepared from PEG_{228}-*b*-P(L)-Leu_{20} via film rehydration at 60 ^{0}C had a narrow PdI of 0.14 ± 0.03 and hydrodynamic size of 82 ± 2 nm, which was slightly larger than that of PEG_{228}-*b*-P(D,L)-Leu_{20}/m (58 ± 1) prepared in a similar manner. Both types of micelles were further characterized for their thermodynamic stability, secondary structure and loading capacities for encapsulation of the hydrophobic drugs, 17-AAG and PTX.

Thermodynamic stability of micelles

Thermal stability evaluation of preformed micelles by differential scanning calorimetry (DSC) revealed quite different thermodynamic profiles for PEG-P(D,L)-Leu/m and PEG-P(L)-Leu/m, despite both micelles being prepared in the same manner. DSC thermograms showed a much sharper transition of melting for PEG-P(D,L)-Leu/m as compared to PEG-P(L)-Leu/m and also a higher calorimetric enthalpy (ΔH) and Gibbs free energy (ΔG_T) of the meting transition. This resulted in an entropy value that was half of PEG-P(L)-Leu/m post melting (Table 6). Data shown in Fig.11 indicates that all of the melting transitions occur within individual micelles, since heating preformed micelles to 65 ^{0}C practically did not change the hydrodynamic size or the PdI of these micelles. Overall, the thermodynamic parameters were indicative of a more cooperative melting transition for PEG-P(D,L)-Leu/m and mimicked the classic two-state model, with the values of calorimetric enthalpy (ΔH) and van't hoff enthalpy (ΔH_v) being very close [33,34]. As opposed to this, thermodynamic parameters for PEG-P(L)-Leu/m were indicative of a more disorganized transition with intermediate states and resembled more to

Sample	ΔH (cal)	T (K)	Tm (K)	ΔG_T cal mol^{-1}	ΔH_v cal mol^{-1}	ΔS cal $mol^{-1}K^{-1}$
PEG-P(D,L)-Leu/m - 60 ^{0}C	20,333	298.2	317 ± 0.3	1,209	19,867	-72.25
PEG-P(L)-Leu/m - 60 ^{0}C	9,534		320.3 ± 0.2	660.3	29,800	-34.19
PEG-P(D,L)-Leu/m - RT	12,967		321.4 ± 0.7	940.7	29,767	-46.65

Table 6. Thermodynamic parameters as caculated from the DSC thermograms for micelles prepared from PEG-P(D,L)-Leu/m by film rehydration at room temperature (RT) or 60 ^{0}C or PEG-P(L)-Leu/m at 60 ^{0}C.

the characteristics of PEG-P(D,L)-Leu/m prepared by film rehydration at RT, indicating that using elevated temperature does not cause any changes in the conformation of the P(L)-Leu core unlike the P(D,L)-Leu core. As a further confirmation of the high temperature requirement, micelles were also prepared from polymer with poly-D,L-Leu block by rehydration and subsequent heating at 40 ^{0}C, and the size and PdI were 114 nm and 0.29 respectively. This further supported our initial hypothesis of rehydration at an elevated temperature that helps in better interaction between the hydrophobic PLeu segments of the polymer and yields closely packed structures with relatively small hydrodynamic diameter.

Secondary structure

CD spectrum of preformed micelles from PEG-P(L)-Leu/m showed an α – helical secondary structure whereas micelles prepared from PEG-P(D,L)-Leu exhibited a random coil behavior in solution (Fig. 12B). When the CD spectrum was recorded for both types of micelles at an elevated temperature of 60 ^{0}C, no changes were observed. This is in line with the DLS data that showed no changes in hydrodynamic size and PdI of preformed micelles upon heating (Fig. 11). This indicated that, once formed, the core of the micelles retained their secondary structure. Also, for PEG-P(L)-Leu/m, this served to show the tightly organized core structure and probable rigidity of conformation that prevented close alignment of the polymer chains and lead to the formation of micelles with a larger hydrodynamic diameter than PEG-P(D,L)-Leu/m (Table 5). No significant changes in secondary structure were observed for micelles prepared from either polymer when measured at different temperatures.

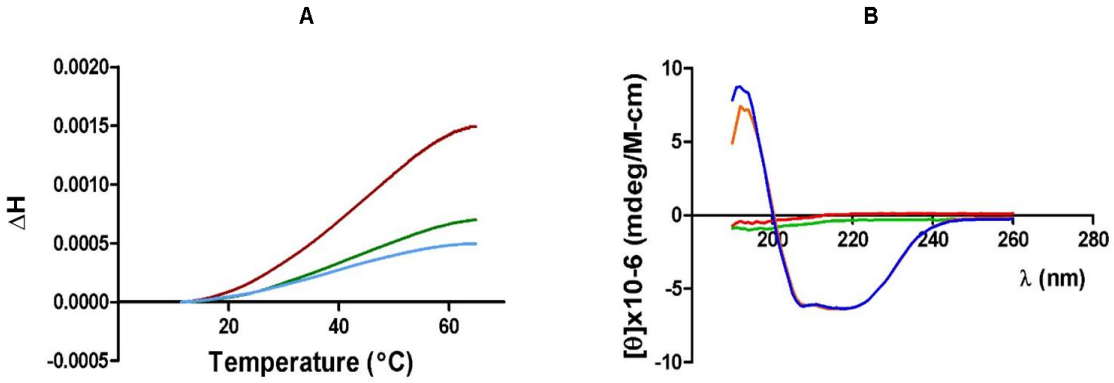

Figure 11. (A) Changes in enthalpy as a function of temperature as measured after every 0.5 ^{o}C change in temperature by Differential Scanning Calorimetry for PEG-P(D,L)-Leu/m - 60 ^{0}C (red), PEG-P(D,L)-Leu/m - RT (green) and PEG-P(L)-Leu/m - 60 ^{0}C (blue). (B) Changes in secondary structure as measured by circular dichroism spectroscopy at different temperatures; micelles were prepared by film rehydration at 60 ^{0}C from PEG-P(L)-Leu and measured at 60 ^{0}C (orange) or RT (blue) and from PEG-P(D,L)-Leu, measured at 60 ^{0}C (red) or RT (green). No significant changes in secondary structure were observed for micelles prepared from either polymer when measured at different temperatures.

Loading and release profile of hydrophobic drugs

Drug loading into the micelles was carried out using the same method of film rehydration used for preparing empty micelles. For drug loading, the film consisted of polymer plus either or both 17-AAG and PTX and rehydration led to micelle formation and simultaneous encapsulation of the drugs into the hydrophobic core of the micelles. The elevated temperature used for rehydration not only leads to increased kinetic mobility of the polymer chains in the core but also facilitates its interaction with the hydrophobic drugs and helps in their incorporation into the micelles. In case of drug-loaded PEG-P(D,L)-Leu/m, it was observed that there was no compromise in the loading capacity when the number of drugs increased from one to two (Table 7). Infact, the loading capacity of 17-AAG was nearly doubled when it was co-loaded with PTX as has been reported with other systems incorporating hydrophobic drugs in the literature, probably due to the presence of one hydrophobic drug creating a favorable environment for the incorporation of the other [35]. Moreover, the micelles showed an intrinsic preference for 17-AAG, and 17-AAG loading was always higher than that of PTX, even when the initial feeding ratio of drug to polymer was kept same for both the drugs. The increased hydrophobization of the micellar core after solubilization of both 17-AAG and PTX led to a slight reduction of the hydrodynamic diameter (from 58 nm for empty micelles to 47 nm for 17-AAG + PTX/m). In spite of incorporation of almost 10% by weight of hydrophobic drugs, the resultant micelles showed no increase in polydispersity index and remained stable in solution for up to 2 months without signs of aggregation. On the other hand, all of the above attributes were absent for drug-loaded micelles prepared from PEG-P(L)-Leu. The loading capacities for individual as well as both drugs loaded simultaneously remained much lower than corresponding micelles prepared from PEG-P(D,L)-Leu and hydrodynamic diameters remained consistently higher. This was further evidence in support of the hypothesis that

Polymer	Sample	D_{eff} (nm)	Polydispersity Index (PdI)	Loading capacity (%w/w)
PEG-P(D,L)-Leu	**Empty micelles**	**58 ± 1**	**0.15 ± 0.01**	**-**
	17-AAG/m	**57 ± 2**	**0.17 ± 0.03**	**4**
	PTX/m	**52 ± 1**	**0.11 ± 0.02**	**3**
	(17-AAG + PTX)/m	**47 ± 1**	**0.15 ± 0.02**	**3 (PTX) 6.6 (17-AAG)**
PEG-P(L)-Leu	Empty micelles	92 ± 2	0.14 ± 0.03	-
	17-AAG/m	85 ± 1	0.18 ± 0.05	2.25
	PTX/m	83 ± 2	0.18 ± 0.01	0.75
	(17-AAG + PTX)/m	80 ± 2	0.16 ± 0.01	0.95 (PTX) 2.6 (17-AAG)

Table 7. Physicochemical characteristics of drug-loaded micelles after loading of drug(s). Deff and PdI were measured by Dynamic Light Scattering. Drug concentrations were determined by RP-HPLC.

P(L)-Leu core is rigid and does not show higher flexibility at elevated temperature. The same kinetic rigidity probably prevents adequate interaction between the hydrophobic drugs and the core and results in lower loading capacities for the drugs. In conclusion, micelles prepared from PEG-P(D,L)-Leu served to be the best carriers for hydrophobic drugs.

The release profile was studied at physiological pH (in PBS) for micelles loaded with one or two drugs. The release profiles were nearly the same in both cases and for both the drugs (Fig.13). Release profiles were not affected due to the presence of the other drug. Practically all of the encapsulated drug was released within 24 hours.

In vitro cytotoxicity of the drug-loaded micelles

In vitro cytotoxicity of the free drugs and drug-loaded micelles was tested on two breast cancer cell lines with differential expression of ErbB2, BT-474 (ErbB2 high) and MCF-7 (ErbB2 low). IC_{50} values are summarized in Table 8. PTX is a known microtubule stabilizer and is the standard chemotherapeutic agent used in ErbB2+ breast cancer in combination with trastuzumab therapy [36]. Herein we studied the synergy of PTX and 17-AAG, which is a heat shock protein 90 (HSP90) inhibitor. Among other functions, HSP90 acts as a chaperone protein for ErbB2 and inhibition of HSP90 leads to enhanced lysosomal degradation of ErbB2 [11]. Indeed, in the ErbB2 overexpressing cell line BT-474 we observed a 1000-fold reduction in the IC_{50} value of PTX when administered in combination with 17-AAG, at a dose ratio of 17-AAG: PTX of 2:1 w/w for 72 hours. Combination index analysis at IC_{50} using the Chou and Talalay method [20] showed a strong synergy between the two drugs, both in the form of free drugs (CI = 0.088) and combination in micelles (CI = 0.083). When both drugs were administered in the form of a cocktail of single drug-

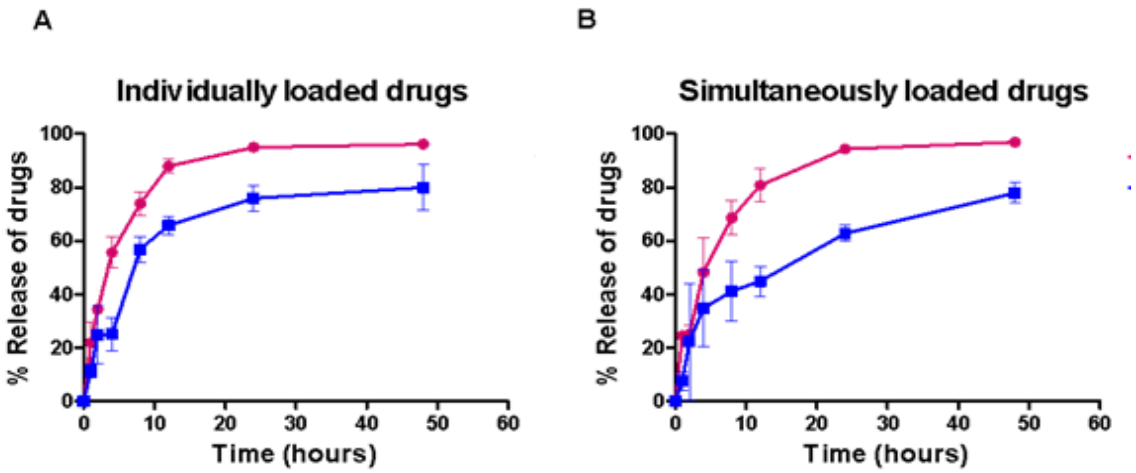

Figure 12. Release profile of 17-AAG (●) and PTX (■) when loaded individually **(A)** or simultaneously **(B)** in the micelles**.**

Sample	IC_{50} (nM)	
	BT-474	**MCF-7**
17-AAG	8 ± 0.4	84.5 ± 1.2
PTX	14.05 ± 0.3	28.4 ± 0.6
*17-AAG + PTX	0.043 ± 0.012 (CI = 0.088)	62 ± 0.6 (CI = 0.79)
17-AAG/m	16 ± 1.3	116.4 ± 1
PTX/m	31 ± 1	45.3 ± 0.8
*(17-AAG+PTX)/m	0.12 ± 0.03 (CI = 0.083)	91.5 ± 0.72 (CI = 0.86)
17-AAG/m + PTX/m	0.18 ± 0.12 (CI = 0.097)	94 ± 1 (CI = 0.88)

Table 8. IC_{50} values for free drugs and micellar formulations on cell line expressing high ErbB-2 (BT-474) and low ErbB-2 (MCF-7)
*calculated with respect to 17-AAG. CI – combination index, calculated at IC_{50}.
Ratio of 17-AAG to PTX was c.a. 2:1 w/w.

loaded micelles at equivalent doses, the synergy of action was still retained and the effect was the same as that seen in case of combination of dual drug-loaded micelles. When the same formulations were applied to ErbB2 low MCF-7 cells, the synergy of action was quite low, and the CI value was closer to 1, which is indicative of a mere additive effect.

Antitumor activity of single vs dual drug-loaded micelles

Antitumor efficacy of the drug-loaded micelles was studied in orthotopic model of ErbB2-driven breast cancer. 4-week old female athymic nude mice were implanted with BT-474 cells directly into the fat pad to induce tumor formation according to previously reported procedures [11,12]. When the tumors reached an average size of 60 – 100 mm^3, the animals were randomly divided into groups of 10 and treated with either 2 drug-loaded (17-AAG+PTX)/micelles or cocktail of single drug loaded 17-AAG/micelles + PTX/micelles or free PTX or 5% dextrose as control. Treatments were administered in a total volume of 100 µL every 4^{th} day for a total of 4 injections. The doses of 17-AAG and PTX used were 10mg/kg and 5mg/kg, which are sub therapeutic doses for each agent (therapeutic i.v. doses of 17-AAG and PTX used are 40 and 20 mg/kg body weight, respectively). As shown in Fig. 14, only 2-drug regimens were effective in suppressing tumor growth. Free PTX showed very little antitumor effect, which is an expected outcome for the sub-therapeutic dose used. The strong synergy of the 2-drug regimen seen *in vitro* was also seen *in vivo,* and both combination loaded (17-AAG + PTX)/m as well as cocktail of single drug-loaded (17-AAG)/m + (PTX)/m showed significant inhibition of tumor growth as compared to control or free PTX groups. Of great interest, however, was the difference in activity of the (17-AAG + PTX)/m vs cocktail of single drug-loaded micelles at the same dose ratio; tumor suppression in animals treated with (17-AAG+PTX)/m was significantly better than those treated with mixture of 17-AAG/micelles + PTX/micelles (P<0.05). This can be attributed to the altered pharmacokinetics of the mixture of micelles, which leads

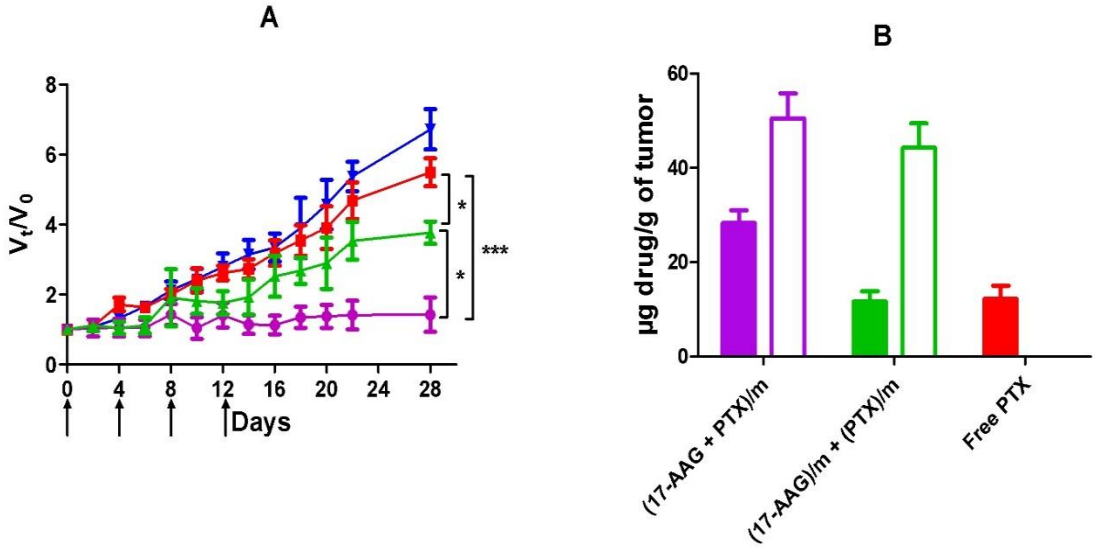

Figure 13. *In vivo* antitumor efficacy of (17-AAG+PTX)/micelles in BT-474 human breast cancer xenograft-bearing female nude mice. **(A)** Relative changes in tumor volume measured following intravenous administration of (17-AAG+PTX)/micelles (●) or free PTX (■) or 17-AAG/micelles + PTX/micelles (▲) or 5% dextrose (▼) at 10 mg 17-AAG or 5 mg PTX equivalents/kg body weight. Drug formulations were injected in100 µL 4 times at 4-day intervals. Values indicated are means ± SEM (n = 7). **(B)** Drug content in tumor tissue in various treatment groups collected on day 13. Solid bars represent PTX and empty bars represent 17-AAG. Data are represented as mean ± SD (n=3). Tumor volume is normalized with respect to tumor volume at day 0. * P<0.05, ** P<0.01, *** P<0.001.

Organ	Ratio (17-AAG:PTX)	
	(17-AAG + PTX)/m	(17-AAG)/m + (PTX)/m
Tumor	1.8 ± 0.2	4 ± 0.5
Liver	1.8 ± 0.2	4 ± 0.5
Spleen	1.7 ± 0.3	3.5 ± 0.1
Kidney	1.8 ± 0.1	4.1 ± 0.4

Table 9. Weight ratio of 17-AAG: PTX in different organs of mice sacrificed on day 14, as measured by LC-MS/MS (n = 3).

to an altered ratio of the drugs reaching the tumor. Analysis of drug content in the tumors of animals (n = 3) sacrificed on day 13 revealed that the ratio of 17-AAG to PTX was 1.8 ± 0.2 (Fig. 14 and Table 9), which is relatively close to the initially administered drug ratio of 2:1 by weight. However, in the groupreceiving cocktail of (17-AAG)/m + (PTX)/m, this ratio was found to be 4 ± 0.5. When BT-474 cells were treated with ratio of 4:1 *in vitro*, it was found that there was only 10-fold reduction in the IC_{50} of PTX in combination as opposed to the 1000-fold reduction seen when the cells were treated with drugs in the ratio of 2:1 and this was also reflected in the CI value changing from 0.088 to 0.47 (Tables 8 and 10). This further reinforce the importance of spatio-temporal synchronization of delivery of the drugs at a defined ratio to retain synergy of action, as was reported in our previous work [37].

Efficacy of therapy

The efficacy of anticancer therapy was judged by two major parameters: impact on survival as well as changes in the population of apoptotic vs proliferating cells in tumors at the mechanistic level. Dual drug-loaded (17-AAG+PTX)/m outperformed the cocktail therapy with (17-AAG)/m + (PTX)/m in all subsequent analysis. Animals treated with (17-AAG+PTX)/m had the longest survival times, with only 2 out of 7 animals reaching the point of termination in span of 85 days (Fig. 15A). On the other hand, median survival for animals treated with cocktail of (17-AAG)/m + (PTX)/m (48 days) was only slightly better than free PTX group (42 days) or the untreated control (40 days).

Excised tumor tissue sections were stained for apoptotic and proliferation markers (cleaved caspase 3 and Ki67) and the results are summarized in Fig. 15B and 15C. The number of proliferating cells were significantly lower in the tumors of animals treated with (17-AAG+PTX)/m as compared with cocktail of (17-AAG)/m + (PTX)/m (*P<0.05*) or free PTX (*P<0.01*). This could explain the continued inhibition in tumor growth seen in animals

Sample	*IC_{50} (ng/mL)
Free 17-AAG + PTX	0.72 ± 0.15 (CI = 0.47)

Table 10. IC_{50} values for free drugs on cell line expressing high ErbB-2 (BT-474). *calculated with respect to 17-AAG. CI – combination index, calculated at IC_{50}. Ratio of 17-AAG to PTX was c.a. 4:1 w/w.

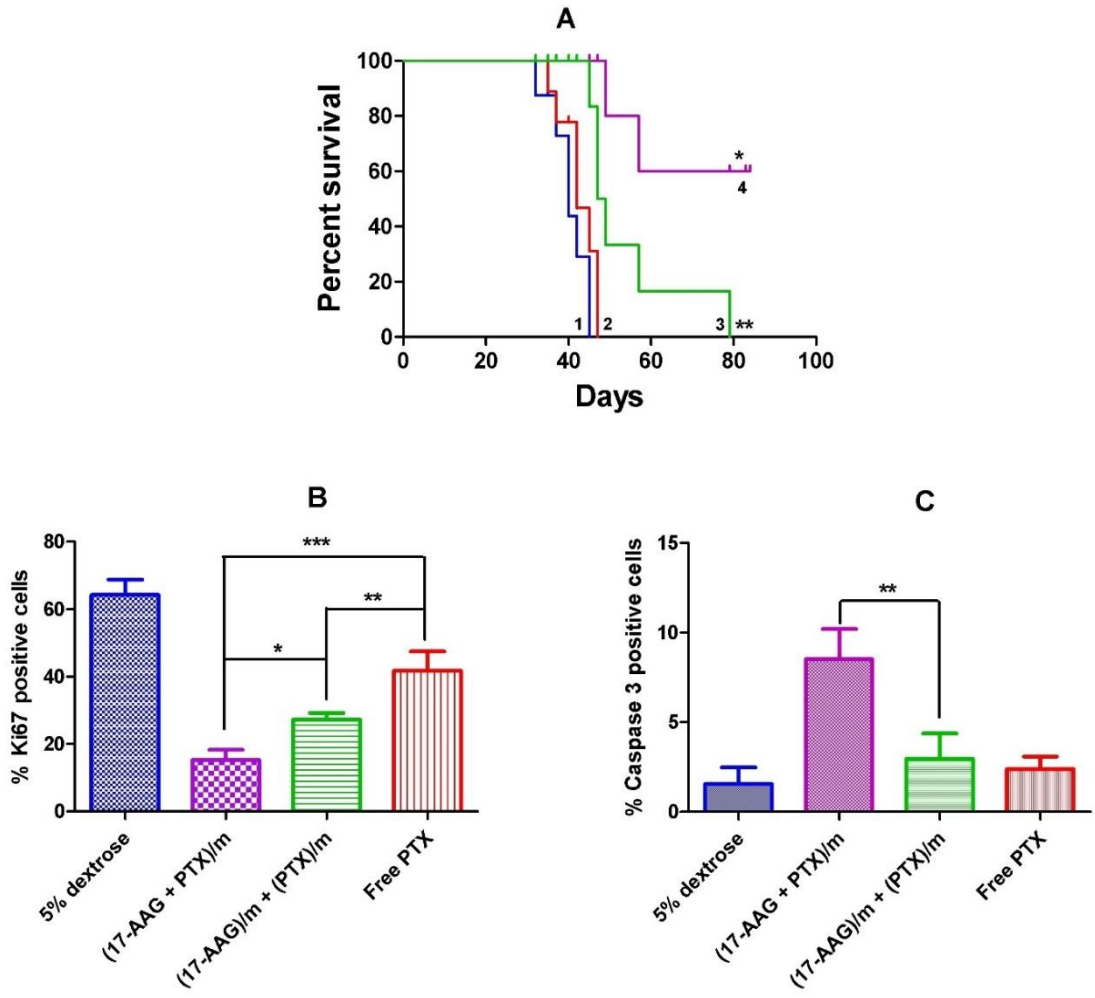

Figure 14. (A) Kaplan–Meier analysis of overall survival in 5% dextrose group (1) or free PTX group (2) or 17-AAG/micelles + PTX/micelles group (3) or (17-AAG+PTX)/micelles group (4). Ki-67-caspase-3 apoptosis assay. Quantification of **(B)** Ki67 positive and **(C)** caspase-3 positive cells in tumor tissue from mice from various groups. Data are presented as mean ± SD (n = 3 random microscopic fields for each tumor slice).

treated with (17-AAG+PTX)/m even after 2 weeks of stopping the treatment, while the tumors of animals treated with cocktail of (17-AAG)/m + (PTX)/m showed a relatively faster rate of progression. Overall, the evidence suggested a strong synergy of anticancer action of the combination of 17-AAG and PTX in a ratio-specific manner.

Toxicity profile

Having proven the efficacy of the combination therapy, it was also of concern to look at the toxicity profile of the treatment. Blood collected from 3 animals sacrificed from each treatment group on day 13 was tested for changes in the clinical parameters for hepatic, renal and hemopoietic functions. The results are summarized in Table 11. No significant changes were observed in any of the markers, which could be attributed to the low dose of both agents used. This was of utmost importance for tolerability of the therapy, since hepatotoxicity is a dose-limiting side effect of 17-AAG. Safety of the treatment was further confirmed at the microscopic level by examination of the H&E stained sections of tissues by a pathologist. No changes in the morphology of the organs at the tissue level were observed (Fig. 17), except extramedullary hematopoiesis, which was observed in spleens of control as well as treated animals and therefore was of no additional health concern. Moreover, no changes were noted in the weights of vital organs excised on day 13. Another sign of acute toxicity common to most anticancer agents is to the hemopoietic system. However, none of the animals showed significant changes in the counts of RBCs, WBCs or platelets when whole blood taken from animals on day 13 was analyzed. The only sign of side effect was loss in body weight of animals treated with free PTX, which is a common effect seen due to the toxic cosolvent Cremophor EL ® used for solubilization of PTX. Body weights of animals treated with all micellar formulations remained normal throughout the duration of the study.

	ALP (IU/L)	ALT (IU/L)	BUN (mg/dL)	RBC (*10^{12}/l)	WBC (*10^{9}/l)	PLT (*10^{9}/l)
Saline	198 ± 15	53 ± 3	16 ± 0.7	9.4 ± 0.5	1.9 ± 0.6	46 ± 8
PTX	229 ± 34	62 ± 6	15 ± 2.3	9.2 ± 0.4	2.4 ± 0.4	61 ± 11
(17-AAG + PTX)/m	179 ± 18	61 ± 2	15 ± 3	8.5 ± 1.3	1.6 ± 0.9	54 ± 12
(17-AAG)/m + (PTX)/m	186 ± 22	61 ± 8	17 ± 1.7	9.2 ± 0.1	1.4 ± 0.6	33 ± 9

Table 11. Clinical chemistry parameters and hematocrit of blood samples collected from animals sacrificed on day 13 across all treatment groups. Data are represented as mean ± SD (n = 3).

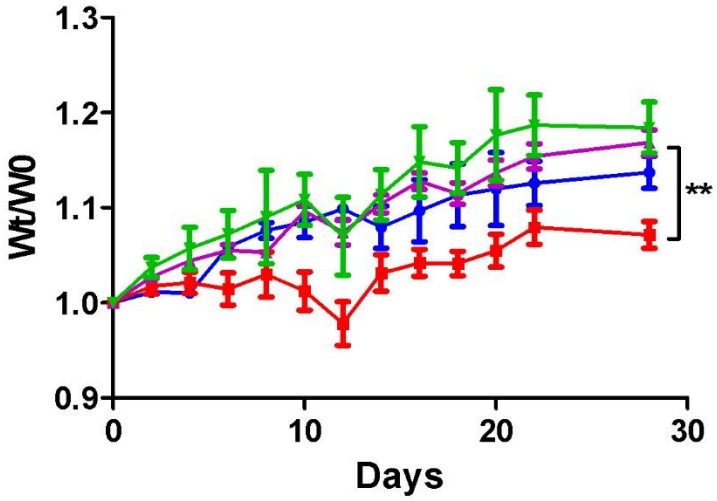

Figure 15. Relative changes in body weight measured during the course of treatment with (17-AAG+PTX)/micelles (●) or free PTX (■) or 17-AAG/micelles + PTX/micelles (▲) or 5% dextrose (▼) at 10 mg 17-AAG or 5 mg PTX equivalents/kg body weight. Values indicated are means ± SEM (n = 7). Body weights are normalized with respect to body weight at day 0. ** *P*<0.01.

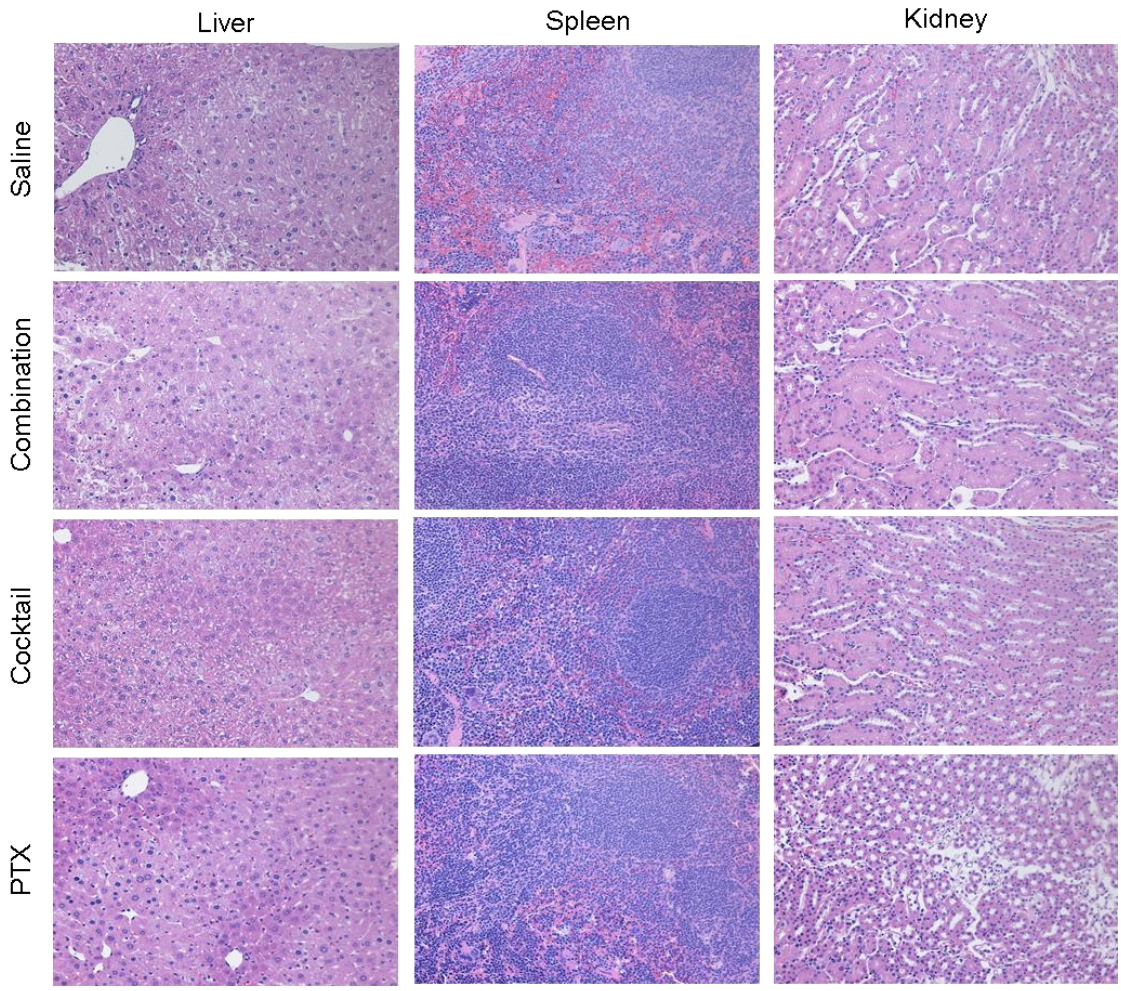

Figure 16. Representative H & E stained sections of liver, spleen and kidney of animals across different treatment groups. No significant changes in morphology of the organs were seen as compared to control animals.

Synthesis, purification and characterization of Trastuzumab-conjugated micelles

The polymer PEG_{228}-b-P(L)-Leu_{20} was modified to allow for the conjugation of a targeting ligand on the surface. Fmoc-NH-PEG-NH_2 was now used as a macroinitiator to polymerize (D,L)-Leu-NCA. The modification scheme is described in Fig. 18. Post polymerization, Fmoc was removed by piperidine and this deprotection was confirmed by absence of Fmoc signals in the resultant ^1H-NMR spectrum (Fig. 19). The free amines were then conjugated with succinic anhydride to yield free carboxylic acid residues at both ends of the polymer and the characteristic peaks were observed in the ^1H-NMR spectrum (Fig. 19). Drug-loaded micelles were prepared by film rehydration technique as described above and EDC coupling reaction was used to conjugate free amino group on the side chain of lysine residues on Trastuzumab to the activated carboxyl groups on the free terminus of PEG corona of the micelles. Unconjugated Trastuzumab was separated from Trast-micelle conjugates using size exclusion chromatography (Fig. 20). The mean hydrodynamic diameters and polydispersity indices of different micelles are described in Table 12. The size of drug-loaded micelles increased by around 20 – 25 nm post conjugation of either Trast or IgG, while the polydispersity indices still remained low (< 0.2). Post surface modification with either IgG or Trast .The loading capacities for 17-AAG and PTX, alone or in combination also remained relatively the same as that described in the previous section (Table 12).

Cellular association and cytotxicity

Binding activity of Trastuzumab after its conjugation to micelles was studied using flow cytometry. Trastuzumab was conjugated to Cy3-labeled micelles at two different surface densities – 25 and 50 µg/mg of the polymer and purified as described above. Control samples consisted of IgG-conjugated micelles at similar surface densities. It was observed that the uptake of Cy-3 labeled Trast-micelles in BT-474 cells (ErbB2 overexpressing cells)

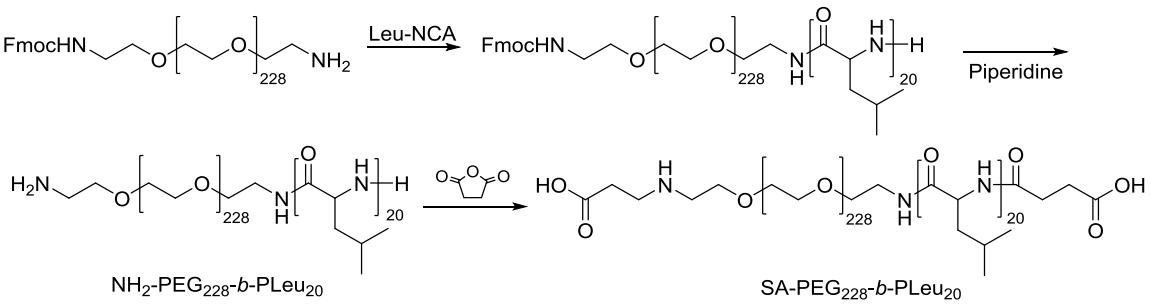

Figure 17. Scheme for synthesis of SA-conjugated PEG_{228}-*b*-$PLeu_{20}$

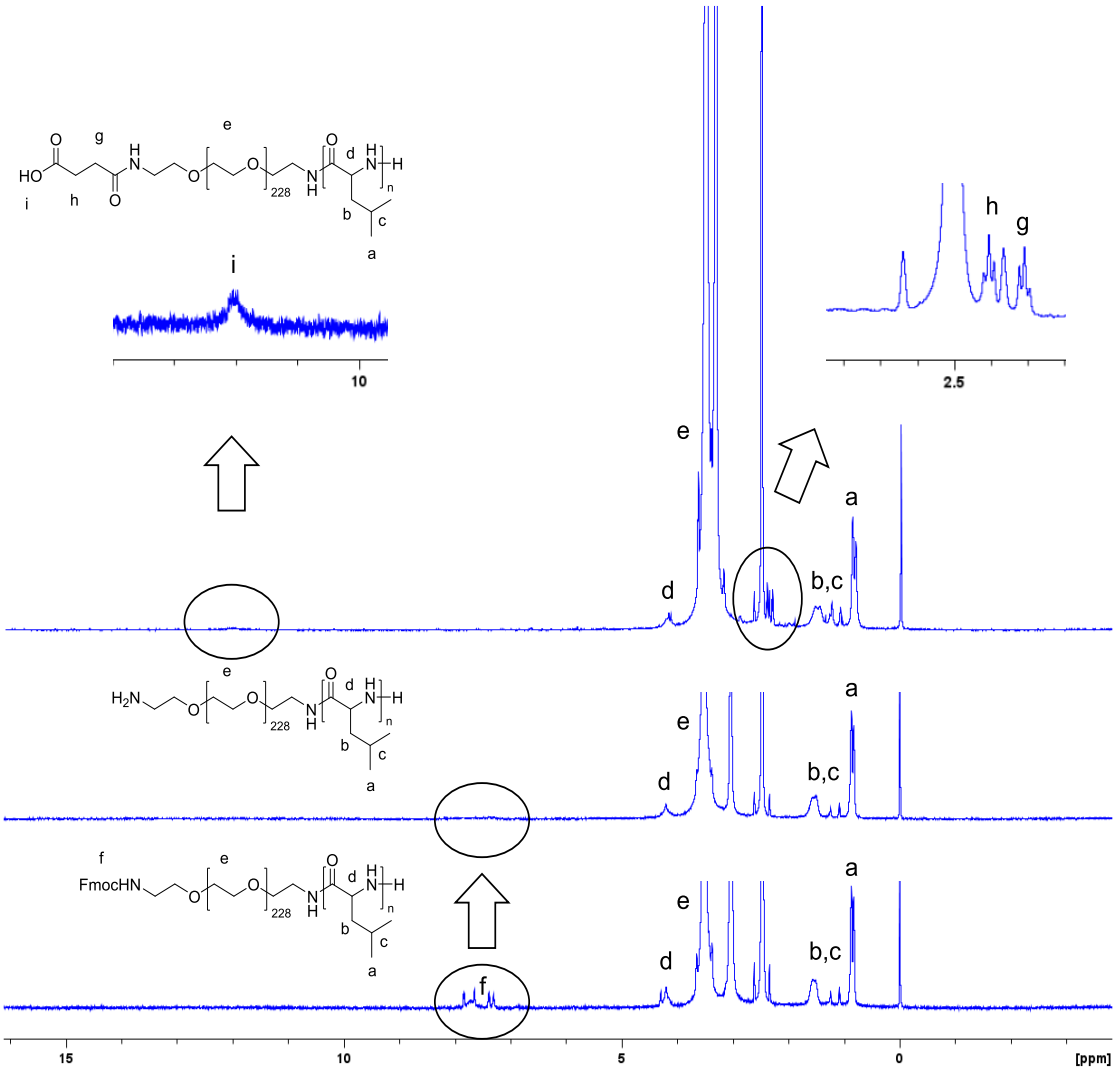

Figure 18. *^{1}H*- NMR spectrum of PEG-*b*-PLeu in DMSO-d_6, 80 ^{0}C through various steps of modification.

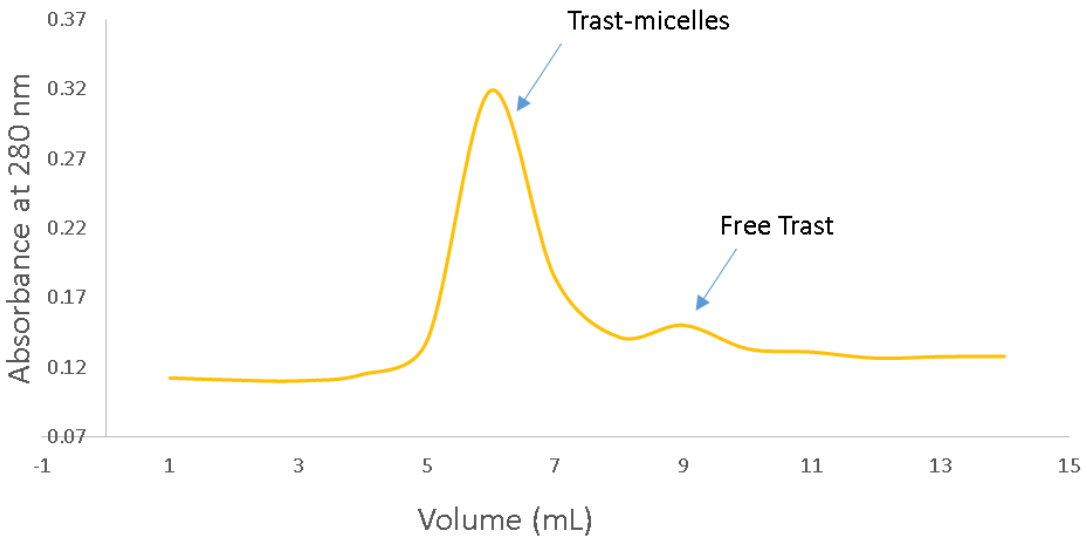

Figure 19. Size exclusion chromatogram for purification of Trast-micelles

Sample	D_{eff} (nm)	PDI	ζ-potential (mV)	Loading Capacity (% w/w)
IgG-(17-AAG+PTX)/m	70 ± 2	0.10 ± 0.01	2.09 ± 0.25	PTX: 3
Trast-(17-AAG+PTX)/m	73 ± 3	0.18 ± 0.02	1.8 ± 0.1	17-AAG: 6.5
Trast-(PTX)/m	69 ± 2	0.19 ± 0.02	1.83 ± 0.08	2.8
Trast-(17-AAG)/m	75 ± 3	0.18 ± 0.01	1.7 ± 0.07	6.2

Table 12. Characterization of antibody conjugated micelles

was significantly higher than the corresponding control IgG-micelles. The uptake of IgG-micelles, irrespective of the surface density of IgG, remained practically the same over time (Fig. 21). On the other hand, Trast-micelles showed increased uptake by BT-474 cells in a time-dependent manner, over a period of 2 hours, indicating that Trastuzumab retained its binding affinity to ErbB2 receptor even after conjugation to micelles and that a surface density as low as 25 µg Trast per mg polymer was sufficient to enhance the uptake of micelle in BT-474 cells (Fig. 21).

The cytotoxic activity of various formulations was tested on both high and low ErbB2 expressing cell lines, BT-474 and MCF-7 respectively. Presence of Trast led to a 4-fold reduction in the IC_{50} value of the 17-AAG – PTX combination (from 0.08 ± 0.020 to 0.02 ± 0.015, Table 13). The cocktail of Trast-(17-AAG)/m + Trast-(PTX)/m was similar to that of Trast-(17-AAG + PTX)/m, since the overall doses of all 3 therapeutic agents, viz, Trast, 17-AAG and PTX was the same in both treatment groups. To maintain the same dose of Trast, the surface density of Trast used for cocktail was 25 µg per mg polymer for both individual drug-loaded micelles, so that their admixture resulted in the same amount of Trast as in Trast-(17-AAG + PTX)/m, which had a surface density of 50 µg Trast per mg polymer. However, no obvious contribution from Trast was observed in the cytotoxic activity of combination of 17-AAG and PTX in the ErbB2 low MCF-7 cells, indicating that Trast had both a therapeutic as well as targeting effect that was mediated specifically via its target ErbB2 receptor.

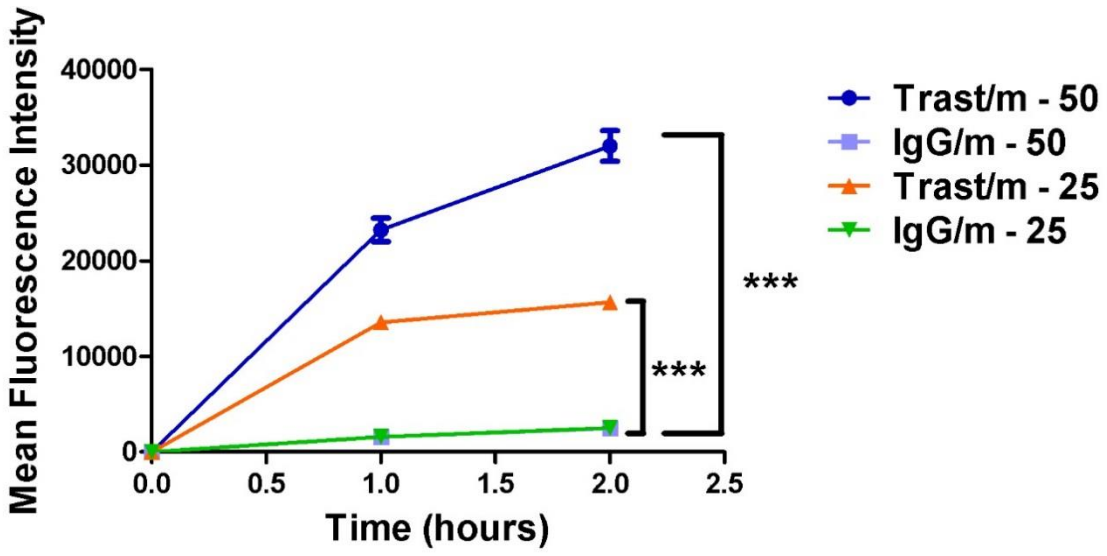

Figure 20. Cellular association of Cyanine3-labeled Trast/m and IgG/m at two different surface densities – 50 and 25 µg protein per mg polymer. Cells were treated with Trast/m or IgG/m at 0.5mg/mL polymer. *** $P < 0.001$. Data are represented as mean ± SD.

Sample	IC_{50} (nM)	
	BT-474	**MCF-7**
IgG-(17-AAG + PTX)/m	0.14 ± 0.03	97 ± 6
Trast-(17-AAG + PTX)/m	0.03 ± 0.025	85 ± 8.5
Trast-(17-AAG) + Trast-(PTX)/m	0.05 ± 0.03	102.4 ± 11

Table 13. IC_{50} values for micellar formulations on cell line expressing high ErbB-2 (BT-474) and low ErbB-2 (MCF-7), calculated with respect to 17-AAG. Ratio of 17-AAG to PTX was c.a. 2:1 w/w.

Antitumor activity of Trast-conjugated drug-loaded micelles

The orthotopic BT-474 xenograft mouse model as described in the previous section was used to test the efficacy of Trast-conjugated drug-loaded micelles. Animals were administered a total of 4 injections, once every 4th day intravenously via the tail vein. The treatment consisted of the vehicle, 5% dextrose or Trast/m or free 17-AAG + PTX in Cremophor or IgG-(17-AAG + PTX)/m or Trast-(17-AAG + PTX)/m or Trast-(17-AAG)/m + Trast-(PTX)/m at equivalent doses of 6.5 mg Trast, 10 mg 17-AAG and 5 mg PTX per kg body weight. Data are representative of 6 animals in each group and curves terminated when single animal in the group reached the point of sacrifice. Micellar combination therapy with Trast was able to significantly retard tumor growth with respect to control animals or animals treated with free drugs. Therapy with Trast alone was also effective in retarding tumor growth as compared to vehicle, as the dose of Trast used was within the therapeutic window. On the other hand, free 17-AAG and PTX formulated in Cremophor had negligible effect on retardation of tumor growth (Fig. 22A), and the progression as well as survival (Fig. 22B) remained similar to control animals. Combination loaded IgG-(17-AAG + PTX)/m were slightly better than cocktail of Trast-(17-AAG)/m + Trast-(PTX)/m in terms of tumor progression (not statistically significant) while the survival was significantly better than the latter group ($P<0.05$). However, the best therapeutic outcomes were seen in animals treated with combination drug-loaded Trast-(17-AAG + PTX)/m that outperformed IgG-(17-AAG + PTX)/m in terms of tumor progression ($P<0.001$) and survival ($P<0.01$). Tumors regressed at the end of the treatment in this group and reached palpable size only after day 45 since the start of the treatment. No animal died from the group treated with Trast-(17-AAG + PTX)/m till day 92, whereas the second best response was observed in animals treated with IgG-(17-AAG + PTX)/m, with a median survival of 90 days. The median survival times for each treatment group are listed in Table 14.

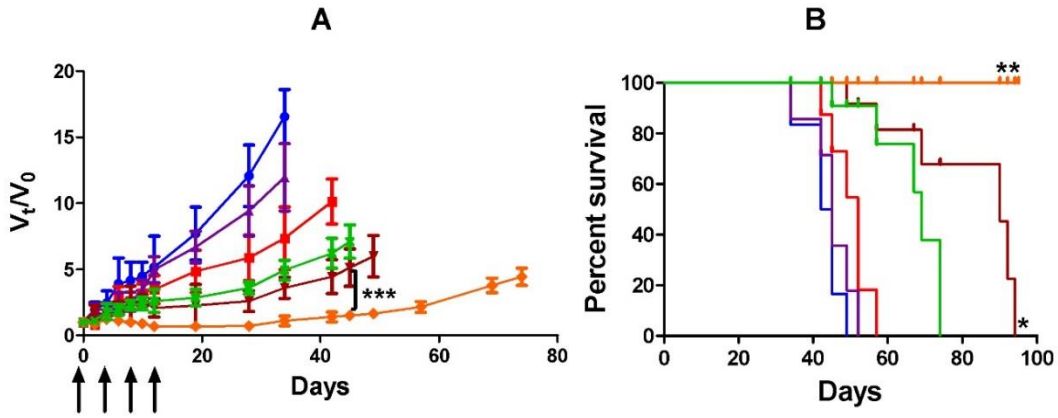

Figure 21. In vivo antitumor efficacy of (17-AAG+PTX)/micelles in BT-474 human breast cancer xenograft-bearing female nude mice. **(A)** Relative changes in tumor volume measured following intravenous administration of 5% dextrose (●) or free 17-AAG + PTX (▲) or Trast/m (■) or Trast-(17-AAG)/m + Trast-(PTX)/m (**x**) or IgG-(17-AAG + PTX)/m (▼) or Trast-(17-AAG + PTX)/m (♦) at 10 mg 17-AAG or 5 mg PTX equivalents/kg body weight. Drug formulations were injected in100 µL 4 times at 4-day intervals. Values indicated are means ± SEM (n = 6). **(B)** Kaplan–Meier analysis of overall survival in 5% dextrose group (1) or free 17-AAG + PTX group (2) Trast/m group (3) or Trast-(17-AAG)/m + Trast-(PTX)/m group (4) or IgG-(17-AAG + PTX)/m (5) or Trast-(17-AAG + PTX)/m (6).

Treatment group	Median Survival (days)	p-values (vs. 5% dextrose control)	% survival at censoring date (92 days)
5% dextrose	43.5	-	0
Trast/m	52	0.0151	0
Free 17-AAG + PTX	45	0.3156	0
IgG-(17-AAG+PTX)/m	90	<0.0001	22.6
Trast-(17-AAG+PTX)/m	NE	<0.0001	100
Trast-(17-AAG)/m + Trast-(PTX)/m	69	<0.0001	0

Table 14. Median survival (days) and p-values of different treatment regimens with respect to 5% dextrose. NE – Estimate not reached.

Drug content in tumor and vital organs post treatment

Animals were sacrificed (3 each) from treatment groups post 24 and 72 hours of the last injection (day 13 and 15 of treatment) and the drug content was measured using an LC-MS/MS method as described before. This provided insight into total drug accumulation immediately at the end of the treatment (24 h after last injection) as well as the clearance after 72 fours. Results are summarized in Fig. 23. In animals treated with Trast-(17-AAG + PTX)/m, tumors were practically nonexistent and thus no tumor drug content data from this group could be obtained. In general, administration of both 17-AAG and PTX encapsulated in micelles lead to significantly higher accumulation ($P<0.001$) as compared to free drugs. While the initial dose ratio for 17-AAG: PTX was 2:1 in all the cases, the ratio in which these drugs accumulated into the tumor tissue varied widely (Table 15). For free drugs, the ratio was random and variable in all the three animals tested (1.93 ± 0.53). The same trend was observed in animals treated with Trast-(17-AAG)/m + Trast-(PTX)/m with a ratio of 1.57 ± 0.5 while in animals treated with IgG-(17-AAG + PTX)/m, where both the drugs were co-loaded in the same carrier, the ratio was 1.79 ± 0.19. This value was found to be much closer to the initial dose ratio of 2:1 and proves the importance of synchronized delivery via the same carrier for two drugs that helps in achieving the desired ratio of two drugs into the tumor. Both the drugs were washed out from the tumor across all treatment groups over time. However, the overall levels of the drug 72 h post last injection were still higher in animals treated with micellar formulations, which explains the higher therapeutic efficacy in terms of retardation of tumor growth that was seen in these groups as compared to free drugs. The accumulation of micellar formulations in organs of the MPS system remained higher than free drugs and the accumulation was similar within different micellar formulations. The ratio of accumulation in different organs is summarized in table 15.

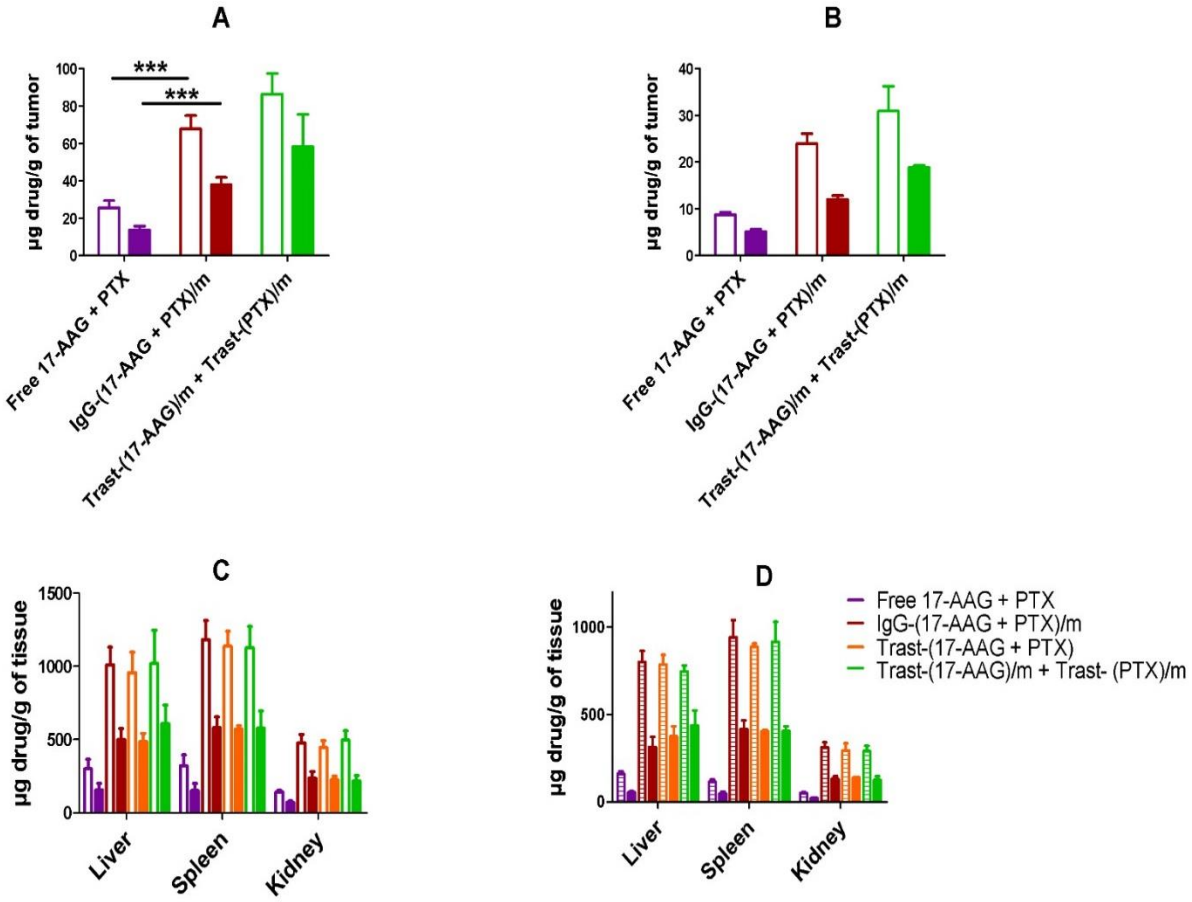

Figure 22. Tissue distribution of 17-AAG and PTX in different treatment groups as determined LC-MS/MS. Mice were sacrificed and tumor, liver, spleen and kidney were harvested 24 h (day 13, fig. **A** and **C**) or 72 h after last injection (day 15 of the treatment, fig. **B** and **D**). Values indicated are mean ± SD (n = 3).

Organ	Time (hours)	Free drugs	Ratio (17-AAG:PTX) w/w		
			IgG-(17-AAG + PTX)/m	Trast-(17-AAG + PTX)/m	Trast-(17-AAG)/m + Trast-(PTX)/m
Tumor	24	1.93 ± 0.53	1.79 ± 0.19	-	1.57 ± 0.5
	72	1.74 ± 0.28	2 ± 0.31	-	1.64 ± 0.32
Liver	24	1.96 ± 0.19	2.03 ± 0.08	1.97 ± 0.07	1.75 ± 0.7
	72	3 ± 0.61	2.58 ± 0.28	2.11 ± 0.18	1.73 ± 0.26
Spleen	24	2.2 ± 0.4	2.03 ± 0.02	1.98 ± 0.13	2.03 ± 0.64
	72	2.46 ± 0.36	2.27 ± 0.05	2.2 ± 0.05	2.25 ± 0.14
Kidney	24	2.02 ± 0.17	2.05 ± 0.23	1.9 ± 0.07	2.38 ± 0.72
	72	2.35 ± 0.12	2.38 ± 0.52	2.08 ± 0.3	2.32 ± 0.16

Table 15. Weight ratio of 17-AAG: PTX in different organs of mice sacrificed 24 h and 72 h after the last injection (day 13 and 15 of treatment respectively), as measured by LC-MS/MS (n = 3).

Toxicity profile

As reported above for the previous animal experiment, 3 animals were sacrificed on day 13 from each treatment group and was analyzed for changes in clinical markers indicative of hepatic, renal and hemopoietic systems. The results are summarized in Table 8. Changes in levels of ALP and ALT were seen only in the case of animals treated with Trast-(17-AAG)/m + Trast-(PTX)/m and H&E stained sections of livers of 2 out of 3 animals showed signs of chronic inflammation. However, other parameters remained normal for this group. All of the other micellar formulations were found to be very well tolerated with no signs of acute toxicity, both in clinical markers (Table 16) and in morphological examination. As opposed to previous study, no weight loss was seen in the animals receiving free drugs formulated in Cremophor. This can be attributed to better solubility of both drugs (5.2 mg 17-AAG and 2.6 mg PTX per mL) as opposed to 4 mg/mL of PTX alone) which reduced the total amount of cosolvent administered per mouse.

2.4 Discussion

Combination therapy has become the mainstay of cancer treatment, given the aggressive nature of the disease and development of resistance to monotherapy. While it is expected that delivering two drugs at their maximum tolerated dose (MTD) would result in a greater therapeutic response, often times this is not the case. Examples abound in the literature where drugs have been found to have a beneficial effect only at certain dose ratios. When used in unfavorable ratios, the effect can be antagonistic, or simply put, the total effect is less than that of individual drugs. Moreover, when two drugs are administered systemically even at their synergistic ratio, the actual ratio presented to the tumor can vary drastically due to differences in their pharmacokinetic parameters like circulation half-life and clearance [38]. However, when such drugs are administered co-encapsulated in a single nanocarrier system, the probability of maintaining the same ratio till they actually reach

	ALP (IU/L)	ALT (IU/L)	BUN (mg/dL)	RBC (*10^{12}/l)	WBC (*10^{9}/l)	PLT (*10^{9}/l)
Saline	195 ± 11	63 ± 6	16	8.02 ± 0.3	1.5 ± 0.7	66 ± 6
Free drugs	188 ± 13	72 ± 15	17 ± 1	7.5 ± 0.5	1.8 ± 0.1	65 ± 15
Trast/m	188 ± 25	64 ± 8	16 ± 3	8.1 ± 0.3	1.9 ± 1.2	63 ± 11
IgG-(17-AAG + PTX)/m	180 ± 26	62 ± 9	15 ± 3	8 ± 0.2	1.5 ± 0.8	61 ± 11
Trast-(17-AAG + PTX)/m	184 ± 15	66 ± 8	17 ± 1	7.8 ± 0.3	1.6 ± 0.1	59 ± 3
Trast-(17-AAG)/m + Trast-(PTX)/m	224 ± 14*	87 ± 7*	13 ± 1	8.3 ± 0.1	2.1 ± 0.4	51 ± 4

Table 16. Clinical chemistry parameters and hematocrit of blood samples collected from animals sacrificed on day 13 across all treatment groups. Data are represented as mean ± SD (n = 3). * *P <0.05*

the tumor increases tremendously. One of the primary reasons for administration of higher doses or higher frequency of administration is the fast clearance of the small molecule drugs. Encapsulation into nanocarriers imparts them macromolecular characteristics. Put together, all of these advantages justify the development of nanocarriers tailored to meet the demands of ratiometric delivery. Of equal importance with enhanced therapeutic efficacy is the avoidance of toxicity. Although encapsulation of cytotoxic agents into nanocarriers has shown to reduce the toxicities associated with free drugs, herein we take advantage of the high level of synergy to use the therapeutic agents at doses much lower than their MTDs that drastically reduces the overall clearance burden on the body for these drugs and the synergy of action ensures that the net effect remains much higher than the sum of individual effects to maintain the desired therapeutic effect.

Breast cancer is no exception to the combination therapy approach. The present study is focused on ErbB2+ breast cancer, a specific subtype with a prevalence of 20-25 percent of all breast cancer cases diagnosed and ErbB2 is well-researched important oncogene responsible for progression of the disease [9,10]. Trastuzumab, a monoclonal antibody that interferes with ErbB2 signaling, remains the mainstay of therapy in clinical practice since its approval by the FDA in 1998. However, it is always administered in combination with a cytotoxic agent like paclitaxel [36]. Paclitaxel being a highly hydrophobic molecule needs toxic cosolvents like Cremophor EL for administration, and consequent side effects like severe anaphylactoid hypersensitivity reactions, neuropathy and aggregation of erythrocytes are well-documented [39]. The goal of the present study was to develop a nanocarrier to also eliminate the need for such cosolvents. A third agent, 17-AAG, which is a model heat shock protein 90 (HSP 90) was also used. 17-AAG has been shown to have synergistic anticancer effects with Trast [40] as well as other cytotoxic agents like paclitaxel [14,15].

A polypeptide based polymer platform, PEG-PLeu was adopted as the biodegradable construction material for micelles. Leucine was chosen as the hydrophobic block to drive micellization of the polymer chains. The technique of living ring opening polymerization was adopted for the synthesis polyleucine block from the reactive amino terminus of PEG. This technique yielded polymers with relatively narrow polydispersity (Table 3) [41], which in turn lead to the formation of more uniform micelles thereof. In general, the advantage of using polypeptide-based polymers is their tendency to form secondary structures, which leads to additional stabilization of the resultant micellar assemblies, over and above the hydrophobic interactions. Moreover, tweaking the secondary structure by using different enantiomeric forms of the amino acids can offer leverage to optimize the polymer's self-assembly for desired attributes like better stability and drug holding capacity. However, micellization is a complex process governed by other parameters like lengths of the constituent blocks as well as the method employed to make micelles. The effect of all these variables was investigated in the present study to find the optimal conditions for preparation of micelles. PEG-PLeu polymers with different lengths of PEG and PLeu blocks were synthesized and micelles were prepared by the film rehydration technique at either room temperature or elevated temperature (60 ^{0}C). It is a well-documented fact that alteration of the solution conditions can change the way polymers self-assemble [1]. High temperature of water used for rehydration can lead to thermal activation of the rigid hydrophobic polyleucine block, melting it or making it more pliable, leading to a better chance of self-assembly than at room temperature [42]. When the system is cooled to room temperature, the solubility of polyleucine block decreases gradually and results in freezing of the structure of the formed micellar aggregates with small size and relatively narrow size distribution. While this temerature-dependent alteration in micellar size, molecular weight and aggregation number was observed for PEG_{228}-*b*-P(D,L)-Leu_{20} (Table 4 and 5), alteration in the lengths of constituent blocks negated this effect. This is in conjunction

with other studies of amphiphilic diblock copolymers, wherein the authors have noted that length of both hydrophilic block and hydrophobic blocks are equally important in the formation of uniform micellar aggregates [25,26]. When the PEG corona is not long enough to stabilize the hydrophobic part, there is an increase in the aggregation number that eventually leads to increase in the size of the resultant micelles. In this case, even using higher temperatures wasn't enough to yield smaller micelles. The thermodynamic stability of micelles prepared from polymer with P(D,L)-Leu vs P(L)-Leu block was also different, along with differences in size and drug loading capacity. Partially, this could be explained by looking at the secondary structures of preformed micelles using CD spectroscopy (Fig 12B). The polymer with enantiomerically pure P(L)-Leu block showed an α – helical structure, the intensity of which did not change even upon heating to 60 ^{0}C. This rigidity in assembly might serve to explain the limited capacity to hold drugs that was exhibited by micelles formed from this polymer as opposed to the micelles prepared from polymer with P(D.L)-Leu that showed a random coil structure.

PEG_{228}-*b*-P(D,L)-Leu_{20} micelles also showed a higher loading capacity for 17-AAG and PTX together (~10% w/w) as opposed to individual drugs (3 – 4% w/w). This has been reported on other drug carrier systems in literature [35,43], wherein the presence of multiple hydrophobic drugs in the same core did not compromise on the loading capacity of individual agents, in spite of them occupying the same space. These micelles showed a preference for 17-AAG over PTX, and this caused the drugs to be loaded in the ratio 2:1 by weight. The increased hydrophobicity due to the presence of two drugs also lead to a slight decrease in the size of micelles (Table 7). Since the drugs were physically entrapped into the core, the release profiles of 17-AAG and PTX were quite similar, with most of the drug being released in the first 24 hours. This release pattern is favorable as previous

studies have demonstrated that 17-AAG and PTX in combination have the highest synergy of action when administered at the same time [15].

The cytotoxic activity of free drugs and their micellar formulations revealed a strong synergy of action between 17-AAG and PTX only on the cell line over-expressing ErbB2 (BT-474), whereas in ErbB2-low MCF-7 cells, the cytotoxic effect was additive (Table 5). The effect of combination drug-loaded (17-AAG + PTX)/m and cocktail of (17-AAG)/m + (PTX)/m remained practically the same. This similarity can be attributed to the fact that both drugs have a similar type of interaction with the hydrophobic core of the micelles and therefore a similar release pattern, making the availability of drugs in static, *in vitro* conditions similar for both (17-AAG + PTX)/m and cocktail of (17-AAG)/m + (PTX)/m of micelles. Conjugation of Trast to the drug-loaded micelles further increased the potency of the overall formulation and IC_{50} value (calculated with respect to 17-AAG) decreased fivefold (from 0.14 ± 0.03 to 0.03 ± 0.025, Table 7).

Based on the strong synergy and drastic reduction in the IC_{50} value observed *in vitro*, doses of 17-AAG and PTX selected for testing of the formulation *in vivo* were in the sub therapeutic range (10 mg and 5 mg equivalents per kg body weight). As a result, neither PTX alone nor 17-AAG + PTX showed anticancer activity in the free form (Fig 3A and 7). As opposed to that, formulations of combination drug-loaded micelles (either (17-AAG + PTX)/m or IgG-(17-AAG + PTX)/m) were quite effective in retarding tumor progression as compared to control untreated animals. This was also reflected in the increased median survival (90 days) of these animals (Fig 4A and 7). Investigation of the amount of drugs accumulated into these tumors revealed significantly higher levels of both drugs in case of animals that received micellar formulations as opposed to free drugs (Fig. 3B and 8A). While combination drug-loaded micelles were able to maintain the initial intended ratio of 2:1 of 17-AAG: PTX (Table S2 and S6), the ratio in which free drugs accumulated was

more random (Table S2). This finding illustrates the utility of micellar drug carriers in delivering the desired ratio of drug combinations to target tissues, along with increasing total drug accumulation as compared to free drugs due to the well-known enhanced permeation and retention effect [37,44]. Trast/m without 17-AAG and PTX also had some therapeutic activity, and served as further proof in support of the *in vitro* cell binding assay that conjugation of Trast to micelles retained its activity *in vivo* (Fig 6 and 7). However, the best therapeutic effect was seen in animals treated with Trast-(17-AAG + PTX)/m, wherein no palpable tumor was present at the end of treatment (day 13), and reached a palpable size after day 45 since start of the treatment. Consequently, this group had the best survival outcome, wherein all six animals were alive till the last day of survival monitoring (day 92). This shows that all the three components, Trast, 17-AAG and PTX have a strong synergy of action, and that Trast has both a therapeutic as well as targeting effect which would have potentially resulted in highest accumulation of drugs in the tumor that lead to complete tumor regression by the end of the treatment. Combination loading of 17-AAG and PTX has also played a crucial role in this effect, as was evident from the lower therapeutic response when animals were treated with cocktail of Trast-(17-AAG)/m + Trast-(PTX)/m, which had all the therapeutic elements at equivalent doses. However, accumulation ratios of 17-AAG and PTX were much more skewed in this group (Fig 8A and Table S6), indicating that the ratio-specific synergy of action might have been mitigated due to the randomness of delivery of the drug cargo. As a result, tumor progression in animals treated with cocktail of Trast-(17-AAG)/m + Trast-(PTX)/m was similar to animals treated with IgG-(17-AAG + PTX)/m and the median survival was 69 days. This same trend of combination drug-loaded micelles performing better than cocktail of single drug-loaded micelles was also observed in non-targeted formulations (Fig 3), further reinforcing the importance of synchronized delivery of drugs to the tumor. This was also reflected in a significant difference between the number of proliferating and apoptotic

cells (Fig 4B), and both trends were in favor of combination delivery. These observations are in line with other examples in the literature wherein ratiometric delivery via the same carrier was found to be beneficial over cocktail of single drug-loaded systems [45].

Accumulation of 17-AAG and PTX in vital organs was also determined (Fig 8). As seen with all nanocarriers, drug accumulation in organs of the MPS system (liver and spleen) was higher than free drugs. However, both drugs continued to be washed out slowly as per the data obtained 72 h after the last injection. This trend was found to be similar across all treatment groups, irrespective of the presence of Trast or IgG on the micellar surface. Also, the acute toxicity profile observed in targeted and non-targeted micellar formulation groups (Table 6 and 8) remained favorable, with the exception of Trast-(17-AAG)/m + Trast-(PTX)/m, wherein the livers of 2 out of 3 animals showed signs of chronic inflammation upon microscopic examination of H & E stained sections. This was consistent with the elevated levels of serum APL and ALT levels in these animals as compared to other groups. However, hematocrit of blood samples across all treatment groups remained normal and no other vital organs like the spleen, kidney or heart showed signs of toxicity, indicating that the therapy was well-tolerated.

2.5 Conclusion

The present study demonstrates the importance of biophysical characteristics of core-forming polyleucine block for the preparation of stable micelles that can load hydrophobic drugs. The self-assembly behavior of the block copolymer PEG-PLeu was dictated not only by the lengths of both constitutive blocks but also the conditions of preparing these micelles. Thin film rehydration at elevated temperature of 60 ^{0}C lead to the formation of relatively small sized micelles with a low polydispersity index. The nature of polyleucine block was also an important parameter for consideration; racemic poly(D,L)-Leu block had a smaller hydrodynamic diameter and much higher capacity for encapsulation of

hydrophobic drugs as compared to the enantiomeric ally pure poly(L)-Leu block. PEG-P(D,L)-Leu micelles were able to encapsulate both 17-AAG and PTX in a weight ratio of 2:1. This ratio showed a high level of synergy of cytotoxic action on ErbB2 overexpressing breast cancer cell line BT-474. When tested in an in vivo orthotopic mouse model of breast cancer, combination delivery via the same carrier had superior anticancer effect as compared to cocktail of individual drug-loaded micelles administered at the same drug ratio. Most importantly, marked antitumor effect was seen at a sub therapeutic doses of both 17-AAG and PTX, which lead to much better tolerability of the therapy and lack of signs of acute toxicity. This combination drug-loaded micellar carrier when conjugated with Trast showed complete retardation of tumor growth for prolonged period of time, without any signs of acute toxicity, which translated into the longest survival time amongst all treatment groups.

2.6 References

1. Choucair, A.; Eisenberg, A. Control of amphiphilic block copolymer morphologies using solution conditions. *The European Physical Journal E* **2003***, 10*, 37-44.

2. Carlsen, A.; Lecommandoux, S. Self-assembly of polypeptide-based block copolymer amphiphiles. *Current Opinion in Colloid & Interface Science* **2009***, 14*, 329-339.

3. Rodriguez-Hernandez, J.; Chécot, F.; Gnanou, Y.; Lecommandoux, S. Toward 'smart'nano-objects by self-assembly of block copolymers in solution. *Progress in Polymer Science* **2005***, 30*, 691-724.

4. Harada, A.; Kataoka, K. Supramolecular assemblies of block copolymers in aqueous media as nanocontainers relevant to biological applications. *Progress in polymer science* **2006***, 31*, 949-982.

5. Dionzou, M.; Morère, A.; Roux, C.; Lonetti, B.; Marty, J.; Mingotaud, C.; Joseph, P.; Goudounèche, D.; Payré, B.; Léonetti, M. Comparison of methods for the fabrication and the characterization of polymer self-assemblies: what are the important parameters? *Soft matter* **2016***, 12*, 2166-2176.

6. Allen, C.; Maysinger, D.; Eisenberg, A. Nano-engineering block copolymer aggregates for drug delivery. *Colloids and Surfaces B: Biointerfaces* **1999***, 16*, 3-27.

7. Hanson, J. A.; Li, Z.; Deming, T. J. Nonionic block copolypeptide micelles containing a hydrophobic rac-leucine core. *Macromolecules* **2010***, 43*, 6268-6269.

8. Ding, J.; Li, C.; Zhang, Y.; Xu, W.; Wang, J.; Chen, X. Chirality-mediated polypeptide micelles for regulated drug delivery. *Acta biomaterialia* **2015***, 11*, 346-355.

9. Hendriks, B. S.; Klinz, S. G.; Reynolds, J. G.; Espelin, C. W.; Gaddy, D. F.; Wickham, T. J. Impact of tumor HER2/ERBB2 expression level on HER2-targeted liposomal doxorubicin-mediated drug delivery: multiple low-affinity interactions lead to a threshold effect. *Mol. Cancer. Ther.* **2013***, 12*, 1816-1828.

10. Inoue, S.; Ding, H.; Portilla-Arias, J.; Hu, J.; Konda, B.; Fujita, M.; Espinoza, A.; Suhane, S.; Riley, M.; Gates, M.; Patil, R.; Penichet, M. L.; Ljubimov, A. V.; Black, K. L.; Holler, E.; Ljubimova, J. Y. Polymalic acid-based nanobiopolymer provides efficient systemic breast cancer treatment by inhibiting both HER2/neu receptor synthesis and activity. *Cancer Res.* **2011***, 71*, 1454-1464.

11. Raja, S. M.; Desale, S. S.; Mohapatra, B.; Luan, H.; Soni, K.; Zhang, J.; Storck, M. A.; Feng, D.; Bielecki, T. A.; Band, V.; Cohen, S. M.; Bronich, T. K.; Band, H. Marked enhancement of lysosomal targeting and efficacy of ErbB2-targeted drug delivery by HSP90 inhibition. *Oncotarget* **2016***, 7*, 10522-10535.

12. Desale, S. S.; Raja, S. M.; Kim, J. O.; Mohapatra, B.; Soni, K. S.; Luan, H.; Williams, S. H.; Bielecki, T. A.; Feng, D.; Storck, M. Polypeptide-based nanogels co-encapsulating a synergistic combination of doxorubicin with 17-AAG show potent anti-tumor activity in ErbB2-driven breast cancer models. *J. Controlled Release* **2015***, 208*, 59-66.

13. Hudis, C. A. Trastuzumab—mechanism of action and use in clinical practice. *N. Engl. J. Med.* **2007***, 357*, 39-51.

14. Munster, P. N.; Basso, A.; Solit, D.; Norton, L.; Rosen, N. Modulation of Hsp90 function by ansamycins sensitizes breast cancer cells to chemotherapy-induced apoptosis in an RB- and schedule-dependent manner. See: E. A. Sausville, Combining cytotoxics and 17-allylamino, 17-demethoxygeldanamycin: sequence and tumor biology matters, Clin. Cancer Res., 7: 2155-2158, 2001. *Clin. Cancer Res.* **2001***, 7*, 2228-2236.

15. Solit, D. B.; Basso, A. D.; Olshen, A. B.; Scher, H. I.; Rosen, N. Inhibition of heat shock protein 90 function down-regulates Akt kinase and sensitizes tumors to Taxol. *Cancer Res.* **2003***, 63*, 2139-2144.

16. Desale, S. S.; Soni, K. S.; Romanova, S.; Cohen, S. M.; Bronich, T. K. Targeted delivery of platinum-taxane combination therapy in ovarian cancer. *J. Controlled Release* **2015**.

17. Ananthapadmanabhan, K.; Goddard, E.; Turro, N.; Kuo, P. Fluorescence probes for critical micelle concentration. *Langmuir* **1985***, 1*, 352-355.

18. Kim, J. O.; Nukolova, N. V.; Oberoi, H. S.; Kabanov, A. V.; Bronich, T. K. Block Ionomer Complex Micelles with Cross-Linked Cores for Drug Delivery. *Polym. Sci. Ser. A. Chem. Phys.* **2009***, 51*, 708-718.

19. Ferrari, M.; Fornasiero, M. C.; Isetta, A. M. MTT colorimetric assay for testing macrophage cytotoxic activity in vitro. *J. Immunol. Methods* **1990***, 131*, 165-172.

20. Chou, T. C. Drug combination studies and their synergy quantification using the Chou-Talalay method. *Cancer Res.* **2010***, 70*, 440-446.

21. Otto, H.; Schirmeister, T. Cysteine proteases and their inhibitors. *Chem. Rev.* **1997***, 97*, 133-172.

22. Hashimoto, Y.; Kakegawa, H.; Narita, Y.; Hachiya, Y.; Hayakawa, T.; Kos, J.; Turk, V.; Katunuma, N. Significance of cathepsin B accumulation in synovial fluid of rheumatoid arthritis. *Biochem. Biophys. Res. Commun.* **2001***, 283*, 334-339.

23. Gref, R.; Minamitake, Y.; Peracchia, M. T.; Trubetskoy, V.; Torchilin, V.; Langer, R. Biodegradable long-circulating polymeric nanospheres. *Science* **1994***, 263*, 1600-1603.

24. Riley, T.; Govender, T.; Stolnik, S.; Xiong, C.; Garnett, M.; Illum, L.; Davis, S. Colloidal stability and drug incorporation aspects of micellar-like PLA–PEG nanoparticles. *Colloids and surfaces B: Biointerfaces* **1999***, 16*, 147-159.

25. Sezgin, Z.; Yüksel, N.; Baykara, T. Preparation and characterization of polymeric micelles for solubilization of poorly soluble anticancer drugs. *European journal of pharmaceutics and biopharmaceutics* **2006***, 64*, 261-268.

26. Wei, Z.; Hao, J.; Yuan, S.; Li, Y.; Juan, W.; Sha, X.; Fang, X. Paclitaxel-loaded Pluronic P123/F127 mixed polymeric micelles: formulation, optimization and in vitro characterization. *Int. J. Pharm.* **2009***, 376*, 176-185.

27. Burt, H. M.; Zhang, X.; Toleikis, P.; Embree, L.; Hunter, W. L. Development of copolymers of poly (D, L-lactide) and methoxypolyethylene glycol as micellar carriers of paclitaxel. *Colloids and Surfaces B: Biointerfaces* **1999***, 16*, 161-171.

28. Letchford, K.; Burt, H. A review of the formation and classification of amphiphilic block copolymer nanoparticulate structures: micelles, nanospheres, nanocapsules and polymersomes. *European journal of pharmaceutics and biopharmaceutics* **2007***, 65*, 259-269.

29. Saeki, S.; Kuwahara, N.; Nakata, M.; Kaneko, M. Upper and lower critical solution temperatures in poly (ethylene glycol) solutions. *Polymer* **1976***, 17*, 685-689.

30. Kim, S. Y.; Shin, I. G.; Lee, Y. M.; Cho, C. S.; Sung, Y. K. Methoxy poly(ethylene glycol) and epsilon-caprolactone amphiphilic block copolymeric micelle containing indomethacin. II. Micelle formation and drug release behaviours. *J. Control. Release* **1998***, 51*, 13-22.

31. Jeong, Y.; Cheon, J.; Kim, S.; Nah, J.; Lee, Y.; Sung, Y.; Akaike, T.; Cho, C. Clonazepam release from core-shell type nanoparticles in vitro. *J. Controlled Release* **1998***, 51*, 169-178.

32. Breedveld, V.; Nowak, A. P.; Sato, J.; Deming, T. J.; Pine, D. J. Rheology of block copolypeptide solutions: hydrogels with tunable properties. *Macromolecules* **2004***, 37*, 3943-3953.

33. Demarest, S. J.; Frasca, V. Differential Scanning Calorimetry in the Biopharmaceutical Sciences. *Biophysical Characterization of Proteins in Developing Biopharmaceuticals* **2014**, 287-306.

34. Marky, L. A.; Breslauer, K. J. Calculating thermodynamic data for transitions of any molecularity from equilibrium melting curves. *Biopolymers* **1987***, 26*, 1601-1620.

35. Shin, H.; Alani, A. W.; Cho, H.; Bae, Y.; Kolesar, J. M.; Kwon, G. S. A 3-in-1 polymeric micelle nanocontainer for poorly water-soluble drugs. *Molecular pharmaceutics* **2011***, 8*, 1257-1265.

36. Tolaney, S. M.; Barry, W. T.; Dang, C. T.; Yardley, D. A.; Moy, B.; Marcom, P. K.; Albain, K. S.; Rugo, H. S.; Ellis, M.; Shapira, I. Adjuvant paclitaxel and trastuzumab for node-negative, HER2-positive breast cancer. *N. Engl. J. Med.* **2015***, 372*, 134-141.

37. Desale, S. S.; Soni, K. S.; Romanova, S.; Cohen, S. M.; Bronich, T. K. Targeted delivery of platinum-taxane combination therapy in ovarian cancer. *J. Controlled Release* **2015***, 220*, 651-659.

38. Mayer, L. D.; Janoff, A. S. Optimizing combination chemotherapy by controlling drug ratios. *Mol. Interv.* **2007***, 7*, 216-223.

39. Gelderblom, H.; Verweij, J.; Nooter, K.; Sparreboom, A. Cremophor EL: the drawbacks and advantages of vehicle selection for drug formulation. *Eur. J. Cancer* **2001***, 37*, 1590-1598.

40. Modi, S.; Stopeck, A.; Linden, H.; Solit, D.; Chandarlapaty, S.; Rosen, N.; D'Andrea, G.; Dickler, M.; Moynahan, M. E.; Sugarman, S.; Ma, W.; Patil, S.; Norton, L.; Hannah, A. L.; Hudis, C. HSP90 inhibition is effective in breast cancer: a phase II trial of tanespimycin (17-AAG) plus trastuzumab in patients with HER2-positive metastatic breast cancer progressing on trastuzumab. *Clin. Cancer Res.* **2011***, 17*, 5132-5139.

41. Deming, T. J. Living polymerization of α-amino acid-N-carboxyanhydrides. *Journal of Polymer Science Part A: Polymer Chemistry* **2000***, 38*, 3011-3018.

42. Rajagopal, K.; Mahmud, A.; Christian, D. A.; Pajerowski, J. D.; Brown, A. E.; Loverde, S. M.; Discher, D. E. Curvature-coupled hydration of semicrystalline polymer amphiphiles yields flexible worm micelles but favors rigid vesicles: polycaprolactone-based block copolymers. *Macromolecules* **2010***, 43*, 9736-9746.

43. Shin, H.; Alani, A. W.; Rao, D. A.; Rockich, N. C.; Kwon, G. S. Multi-drug loaded polymeric micelles for simultaneous delivery of poorly soluble anticancer drugs. *J. Controlled Release* **2009***, 140*, 294-300.

44. Maeda, H.; Wu, J.; Sawa, T.; Matsumura, Y.; Hori, K. Tumor vascular permeability and the EPR effect in macromolecular therapeutics: a review. *J. Controlled Release* **2000***, 65*, 271-284.

45. Goldman, A.; Kulkarni, A.; Kohandel, M.; Pandey, P.; Rao, P.; Natarajan, S. K.; Sabbisetti, V.; Sengupta, S. Rationally Designed 2-in-1 Nanoparticles Can Overcome Adaptive Resistance in Cancer. *ACS nano* **2016**

CHAPTER 3

Sequential delivery of drugs in pancreatic cancer – a nanoformulation approach

3.1 Introduction

Pancreatic cancer (PC) is one of the most lethal malignancies, due to aggressive tumorigenicity, early metastasis and development of drug resistance to standard care chemotherapy. Since its approval in 1997, Gemcitabine (Gem) has been the first-line treatment for advanced disease. However, there is no standard second-line therapy after Gem failure. FOLFIRINOX, a combination of four agents, folinic acid, fluorouracil, irinotecan and oxaliplatin was approved by the FDA in 2010 [1]. The rationale for this combination was based on these drugs having a different mechanism of action, and, more importantly, non-overlapping toxicities [2]. In cases that could tolerate FOLFIRINOX, an overall improvement in the survival times as well as quality of life was noted [3]. However, even the toxicities are non-overlapping, the cumulative toxicity profile for FOLFIRINOX can become the dose limiting factor. In the first trial itself, 50.8% of the patients needed dose adjustment. The common toxicities observed with FOLFIRINOX include Febrile neutropenia, Thrombocytopenic bleeding, ≥ grade 3 platelets, Grade 2 persistent neurotoxicity, Grade 3 persistent neurotoxicity or Grade 4 neurotoxicity and many more non-hematological toxicities. Most of the toxicities are severe enough to require discontinuation of the treatment or switching to lower doses or alternative agents. The combination of Gem with Cisplatin (CDDP) has been explored in clinical trials for metastatic disease. As a part of FOLFIRINOX, platinum compounds showed significant efficacy. The combination of Gem with Cisplatin (CDDP) has also been explored in clinical trials for metastatic disease. Cisplatin acts by damaging the DNA. It is known to first get converted into the aqua form within the cell, which happens by the replacement of the

labile chloro groups with water molecules. This active form is then able to form covalently linked adducts with the DNA. This initial assault then goes on to activate a series of signaling pathways that ultimately lead to apoptosis and cell death [4]. The DNA adducts thus formed can cause distortion of the DNA and subsequent recognition by various cellular proteins. This leads to problems in DNA synthesis and replication and is reported to cause a prolonged G2 cell-cycle phase arrest. However, the exact mechanism of activation of the apoptotic pathways remains unclear. On the other hand, gemcitabine is a deoxycytidine analog [5,6]. Its mechanism of activation involves conversion into its triphosphate form, which can then be incorporated into the DNA as a false nucleotide. Usually, one more deoxynucleotide can be incorporated into the DNA before the synthesis stops. Another minor mechanism of action of gemcitabine is its ability to inhibit ribonucleotide reductase, which plays a key role in the repair mechanism of the DNA. Many studies report the benefit of administration of gemcitabine prior to that of cisplatin; the reason cited for this is the increase in the formation of Pt-DNA adducts when the DNA had already been damaged and exposed due to the incorporation of deoxycytidine or active gemcitabine [6]. The gemcitabine in turn inhibits the repair of the formed Pt-DNA adducts as well as reduces the efficacy of nucleotide excision repair by its ability to inhibit the action of ribonucleotide reductase [7,8]. On the other hand, when Pt compounds are administered prior to gemcitabine, the formed Pt-DNA adducts can no longer allow for the incorporation of gemcitabine and that leaves no scope for gemcitabine to act. Our preliminary in vitro studies with the free drugs on T3M4 Simple Cells (*COSMC* deleted cells) showed that synergy of the combination is schedule-dependent, and Gem administration followed by CDDP showed the most potent cytotoxic activity. However, this combination proved to be only marginally effective in actual practice due to combined increased toxicity of both the agents. We have shown that encapsulation of CDDP in polymeric nanogels with cross-linked ionic cores enhanced its tumor accumulation and

improved its safety profile. Additionally, sustained release profile of CDDP from nanogels allows for the administration of free Gem and CDDP loaded nanogels in a single injection while still retaining schedule-dependent synergy of the combination. Pancreatic ductal adenocarcinoma cells are known to express truncated O-glycans (Tn and STn antigens) and it was shown that decorating the nanogels with an antibody directed against this antigen further enhanced their uptake by tumor cells while reducing off-target accumulation in an in vivo pancreatic cancer model.

3.2 Materials and methods

Materials

PEG-*b*-PMA di-block copolymer (Mw/Mn = 1.45) was purchased from Polymer Source Inc., Canada. The block lengths were 170 and 180 repeating units for PEG and PMA, respectively. Maleimide-PEG-amine (Mal-PEG-NH_2, MW 7500) was purchased from JenKem Technology, USA. Calcium chloride, Ethylenediamine, 1-(3 dimethylaminopropyl)- 3-ethylcarbodiimide hydrochloride (EDC) Ethylenediaminetetraacetic acid (EDTA), 2-Iminothiolane hydrochloride, were obtained from Sigma-Aldrich (St Louis, MO). Gemcitabine hydrochloride and CDDP were also purchased from Sigma-Aldrich (St Louis, MO). Serum (FBS) (dialyzed and heat-inactivated), Dulbecco's Modified Eagle's Medium (DMEM), RPMI-1640 medium and LysotrackerTM (green) were purchased from Invitrogen Inc. (Carlsbad, CA). MTT reagent (3-(4,5-Dimethylthiazol-2-yl)-2,5-diphenyltetrazolium bromide) was purchased from Research Products International (Prospect, IL). All other chemicals were of reagent grade and used without further purification.

Preparation of NGs

Polymeric nanogels were synthesized as described previously [9,10]. Briefly, PEG-*b*-PMA chains were condensed into complexes using Ca^{2+} ions as a template (molar ratio of $[Ca^{2+}]/[COO^{-}]$ = 1.3) and crosslinked with 1,2 ethylene diamine using EDC chemistry. ([EDC]/[1,2-ethylenediamine] = 2; [COOH]/[EDC] = 5). Unreacted impurities were removed by exhaustive dialysis first against 0.5% aqueous ammonia in the presence of 100 mM EDTA followed by double distilled water.

CDDP loading and antibody conjugation to NGs

CDDP loading was carried out as reported previously [11]. Aqueous solution of CDDP (1mg/mL) was added to the aqueous dispersion of crosslinked NGs (molar ratio of CDDP:$[COO^{-}]$ was 0.5) at pH 9 and incubated at 37 ^{0}C for 48h. Unbound CDDP was removed by repeated ultrafiltration (MWCO 30,000, Millipore) at 3000 rpm for 15 min. Antibody (TKH-2 or non-specific IgG) was thiolated using Traut's reagent [12,13]. Antibody in phosphate buffer, pH 8, 10 mM EDTA was allowed to react with 15-fold molar excess of 2-iminothiolane (Traut's reagent) for 1 h. Thiolated antibody was purified using Zeba™ Spin desalting column previously equilibrated with phosphate buffer, pH 7, 10 mM EDTA as per manufacturer's protocol. Mal-PEG-NH_2 (10 eq) was then added to thiolated antibody and allowed to react for 2h. Unreacted PEG was removed with repeated ultrafiltration (MWCO 30,000, Millipore). The PEGylated antibody was added to dispersion of core carboxylate-activated CDDP-loaded NGs (EDC, 1.5 eq of Mal-PEG-NH_2) and allowed to react for 2h. Unconjugated antibody was purified by size exclusion chromatography using Sepharose CL-6B column (Sigma Aldrich), yielding a mixture of unmodified and antibody-conjugated NGs [14]. Protein content of this mixture was determined by microBCA assay kit (Thermo Scientific) using BSA as standard as per the manufacturer's protocol.

Determination of NG particle size and zeta-potential

Intensity-averaged hydrodynamic diameter (D_{eff}) and zeta potential of NGs were measured using Malvern Zetasizer (Malvern Instruments Ltd.) at 25 ^{0}C, using the automatic mode. Each sample was measured atleast in triplicate and software provided by the manufacturer was used to calculate size, polydispersity and zeta-potential. Values are reported as mean ± SD.

Cell culture conditions

T3M4 COSMC KO cells were grown in DMEM media supplemented with 10% FBS and transfection with F-Luc-GFP Lentivirus (Capital Biosciences,Rockville, MD) was carried out as per manufacturer's instructions.

Flow cytometry and CDDP uptake in cells

Cells (100,000 cells/well) grown in DMEM media in 24-well plates for 24 h were exposed to Cy3-labeled TKH-2 - NG or IgG-NG (~ 65 µg protein/mg of polymer) at 37 °C for up to 2 h, washed three times with PBS, trypsinized, centrifuged (1500 rpm, 5 min) and resuspended in PBS (pH 7.4). The % gated cells were analyzed using Becton Dickinson FACStarPlus flow cytometer and FACSDiva software (Version 8.0, Becton Dickinson, San Jose, CA). At least 5000 events were acquired in linear mode, gated to exclude debris and dead cells, and visualized in logarithmic mode.

In vitro cytotoxic activity

T3M4 COSMC KO or T3M4 WT cells were seeded in 96-well plates (5000 cells/well) 24 h before the experiment and treated with either free Gem or free CDDP or Gem + CDDP or Gem, 24 h + CDDP, 24 h or CDDP, 24h + Gem, 24 h or CDDP-NG or Gem + TKH-2 – NG/CDDP or Gem + IgG – NG/CDDP at equivalent doses of CDDP (0 – 10 µg/mL or Gem 0 – 10 ng/mL) for total of 48 h in DMEM at 37 ^{0}C followed by washing with PBS and maintaining in DMEM with 10% FBS for additional 24 h. Cytotoxicity was determined by

standard colorimetric MTT assay [15] and the IC_{50} values were calculated using GraphPad Prism Software. Ratio of CDDP to Gem was c.a. 1140:1 (mol/mol) or 1000:1 w/w.

Animals and bioluminescence imaging

All animal studies were conducted in accordance with the protocol approved by the University of Nebraska Medical Center Institutional Animal Care and Use Committee. Four-week old female nude mice (athymic nude-nu) were obtained from Charles River Laboratories and housed in AAALAC accredited facility. Food and reverse osmosis water were available ad libitum throughout the study. Animals were quarantined for a week prior to the commencement of studies. Imaging was conducted with the in vivo imaging system IVIS-200 (Xenogen Corporation, Alameda, CA). Whole-body Imaging was performed as reported previously [16]. Briefly, animals were anaesthetized with isoflurane (Henry Schein, Dublin, OH) prior to imaging. IP injection with D-luciferin (Perkin-Elmer, Waltham, MA) at the dose of 150 mg/kg (reconstituted in sterile PBS) was used to generate bioluminescence signal. Total bioluminescence signal in the regions of interest (ROIs) drawn around the whole abdomen region was quantified using Living Image software (version 2.50; Xenogen) and expressed as photons/s/cm^2/sr.

Animal studies

Pancreatic tumor model was generated by injection of T3M4/Luc cells (~2.5×10^5 cells) directly into the pancreas. After development of tumors (14 days after injection) animals were randomized (6 treatment groups, n = 10) and treated with 5% dextrose (control) or IgG – NG/CDDP or TKH-2 – NG/CDDP or Free Gem or combination of Gem + IgG – NG/CDDP or Gem + TKH-2 – NG/CDDP at an equivalent dose of 4 mg/kg CDDP, or 20 mg/kg Gem. A total of 4 injections were administered via tail vein every 4^{th} day. Animal bodyweight and tumor progression, as assessed by BLI, were monitored every fourth day.

All images were acquired using identical BLI system settings. All animals were sacrificed on day 15 of the commencement of the treatment. Organs and whole blood were collected for analysis and peritoneal cavities were checked for the presence of metastasis.

Sample preparation and Pt content measurement in tissues

Known weights of thawed tissues collected from sacrificed animals (tumor, kidney, spleen, liver and lung, 3 mice per group) were decomposed by wet-ashing in screwcapped vials with six volumes of concentrated nitric acid, by heating overnight at 65 °C with constant stirring. An iridium internal standard was added prior to digestion. Total platinum concentrations were determined by ICP-MS using iridium correction. Calibration range for the assay was platinum 2–100 ng/mL with extrapolation to platinum 1000 ng/mL. Necessary dilutions were made when the platinum concentration exceeded the calibration range. Assay sensitivity was 0.8 ng of Pt/mL, with inter- and intraday assay variability not exceeding 5%.

Blood chemistry and histopathology

Blood from the sacrificed animals was collected in heparin tubes and analyzed for levels of markers for hepatic and renal function using Vetscan VS (Abaxis). Fixed tissues were processed, sectioned, inserted into tissue cassettes, dehydrated in 70% ethanol overnight, and paraffin embedded (UNMC Tissue Sciences Facility, Omaha, NE).

Statistical analysis

Statistical comparisons for in vitro studies were carried out using Students t-test. In animal studies, group means BL signal intensity and body weights were analyzed using one-way analysis of variance [17]. Survival was estimated using Kaplan–Meier analysis and compared using log-rank test. P values less than 0.05 were considered significant.

Analysis of variance and Kaplan–Meier analysis tests were performed using GraphPad Prism 5 (GraphPad Software, Inc.).

3.3 Results and discussion

Schedule-dependent cytotoxicity of Gem and CDDP combination

Gem is the first line therapy for pancreatic cancer since its approval by the FDA in 1996. However, development of resistance is a common phenomenon and combination therapy is often the alternative. As seen with most combinations, the synergy of action often depends on the sequence of administration of the drugs. This is attributed to the different mechanisms of actions of the drugs under consideration. Thus, the schedule dependent cytotoxic activity of Gem-CDDP combination in the form of free drugs was studied. As shown in Table 17 below, the combination was found to be synergistic only when cells were exposed to Gem followed by CDDP, with the CI value for this regimen being <1 (CI = 0.17). When the CDDP administration was followed by Gem, the effect of the combination was antagonistic as the CI value exceeded 1 (CI = 1.98) while co-administration of Gem and CDDP provided a mere additive effect with CI ~1. These results indicate that a formulation approach involving immediate availability for Gem while delayed availability for CDDP would help retain the schedule-dependent synergy of action of Gem – CDDP combination. To achieve this, CDDP was formulated in nanogels with a sustained release profile with targeting antibody conjugated on the surface of nanogels to improve probability of delivery of CDDP to tumor tissue [18]. Gem would be administered as a free drug, making it available immediately for uptake upon intravenous administration.

Preparation and characterization of CDDP-loaded, antibody-conjugated NGs

PEO-*b*-PMA complexes were made by the condensation of polyion chains of the polymer using Ca^{+2} ions as a template for condensation. Crosslinking of the polymer chains using

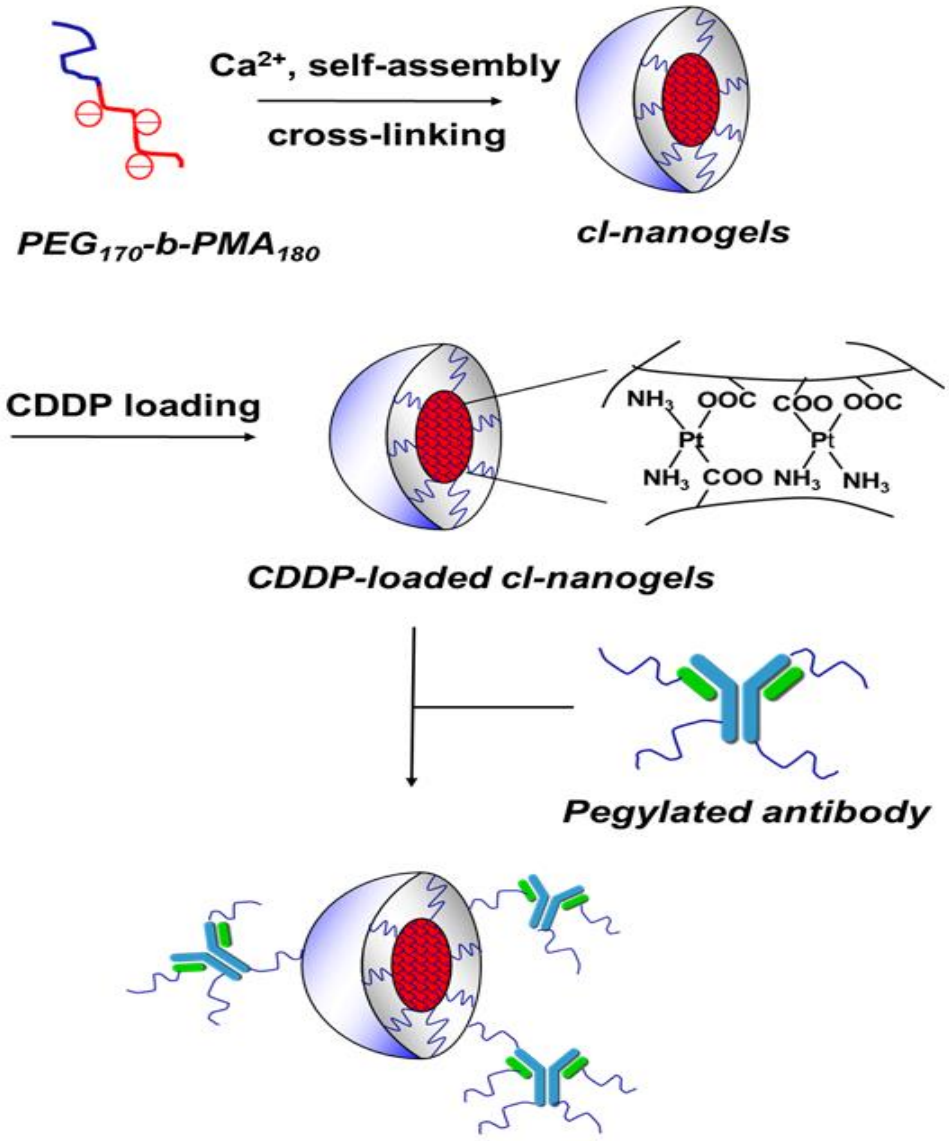

Figure 23 Scheme for the preparation of antibody-nanogel conjugates

Treatment schedule	IC_{50} (with respect to CDDP, µg/ml)
CDDP,24h,Gem, 24h	1.69 ± 0.052 (CI = 1.98)
Gem,24h,CDDP, 24h	0.028 ± 0.004 (CI = 0.17)
CDDP-Gem co-administration	1.51 ± 0.15 (CI = 0.95)
CDDP	1.18 ± 0.14
[a]Gem	0.48 ± 0.03 (ng/mL)
Oxaliplatin	2.7 ± 0.33

Table 17. Comparison of IC_{50} values for different sequences of administration of Gem and CDDP as per MTT assay. T3M4 COSMC KO cells were treated for a total of 48 h. [a]IC_{50} of Gem is expressed in ng/mL.

Sample (pH 7.4)	D_{eff} (nm)	PdI	Zeta potential (mV)
cl-NG	114 ± 2	0.09 ± 0.02	-25 ± 1.8
CDDP/NG	93 ± 1	0.1 ± 0.02	-14 ± 1.3
TKH-2 – NG/CDDP	135 ± 2	0.15 ± 0.02	-9.6 ± 1
IgG – NG/CDDP	137 ± 1	0.14 ± 0.01	-10.7 ± 2.1

Table 18. Physicochemical characteristics of drug-loaded NGs

ethylene diamine lead to the formation of NGs that had a mean particle size of 114 nm. Loading of CDDP occurs through co-ordinate bond formation between Pt and COO^- ions and lead to a reduction in size (D_{eff} = 93 nm) and increase in ζ-potential (from -25 -14 mV). The loading capacity for hydrophilic drugs such as CDDP is very high (~30 % w/w) [19,20]. For conjugation, antibodies (either TKH-2 or IgG) were first thiolated using Traut's reagent and PEGylated using maleimide-PEG-NH_2. The free amine of PEG spacer was then used to conjugate the antibody to core carboxylate groups of CDDP-loaded NGs (fig.23). Such conjugation strategy is non-specific for the site as well as number of PEG spacers conjugated per antibody molecule. The resultant mixture of antibody-conjugated and non-modified NGs was separated from free antibody by size exclusion chromatography using a Sepharose CL-6B column. Conjugation of either TKH-2 or IgG lead to a slight increase in the size (~ 140 nm). The physicochemical parameters are summarized in Table 18. Protein content was ~65 µg/mg polymer for both antibody-decorated NGs, as determined by microBCA assay.

3.1. Cellular interaction of antibody-conjugated NGs

In order to test whether the conjugation process lead to loss of binding affinity, antibodies (TKH-2 or IgG) were conjugated to FITC-labeled NGs as described above and the cellular association of the NGs was estimated using flow cytometry. Both T3M4 COSMC KO (receptor positive) and T3M4 WT (receptor negative) cells were treated with FITC-labeled TKH-2 – NG or IgG – NG. As shown in Figure 24A and Figure 25, the uptake of TKH-2 – NG is significantly higher ($P < 0.01$) than IgG – NG in T3M4 cells while the uptake for both types of NGs remains practically the same in T3M4 WT cells (Figure 24B). Also, the percentage of parent gated cells positive for TKH-2 – NGs is much higher ($P<0.05$) when T3M4 COSMC KO cells are treated with TKH-2 – NGs vs T3M4 WT cells (Figure 24C). A similar trend in the cellular content of Pt was also seen when the cells were treated with.

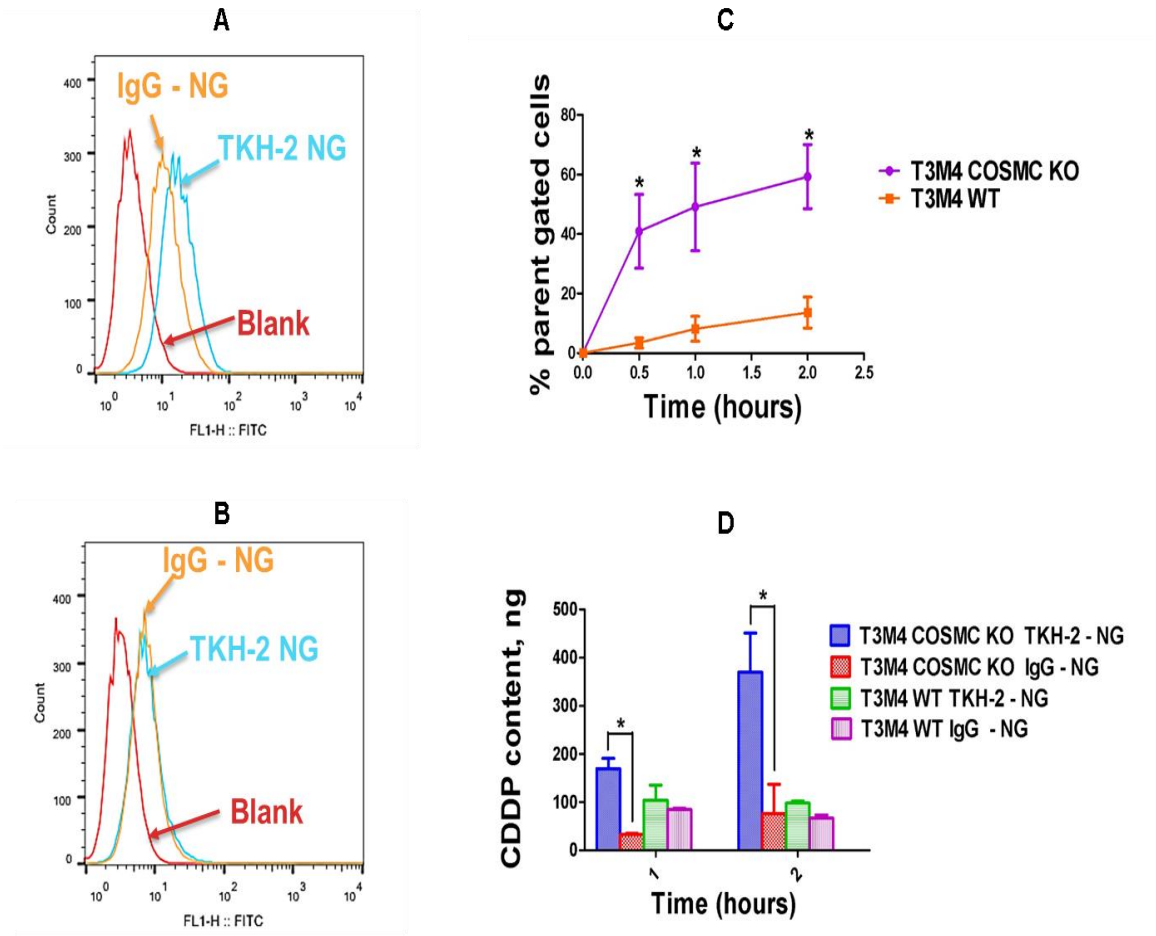

Figure 24. Cellular association of FITC-labeled TKH-2 – NG and IgG – NG on A) T3M4 COSMC KO cells and B) T3M4 WT cells. C) Percentage of parent gated cells as a function of time when T3M4 COSMC KO cells and T3M4 WT cells were treated with FITC-labeled TKH-2 NGs. Cells were treated with 0.5 mg/mL polymer in media. Protein content was 65 µg/mg polymer. *$P < 0.05$. Data are mean ± SD (n = 3).

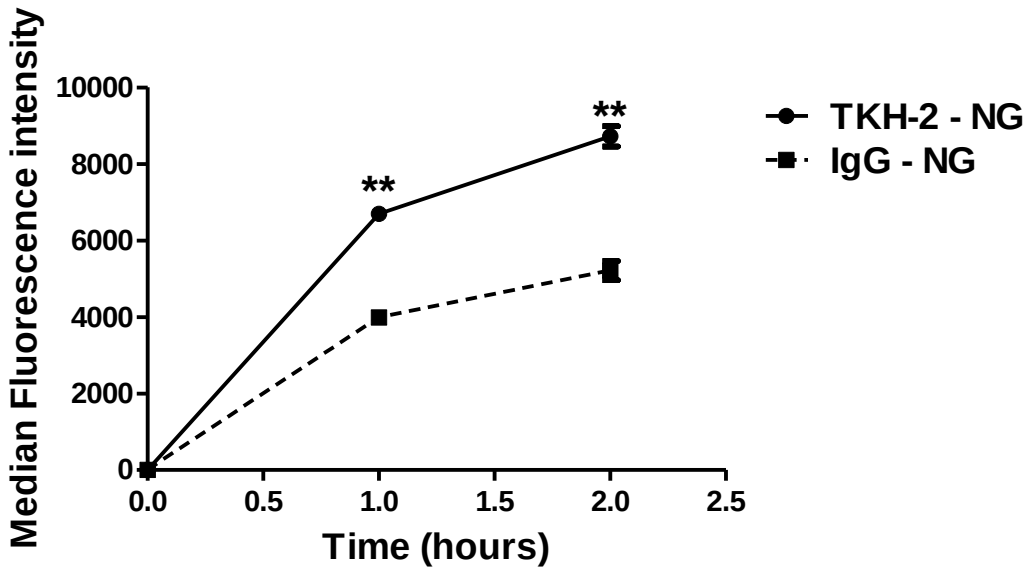

Figure 25. Time dependent cellular association of TKH-2 NG vs IgG – NGs in T3M4 COSMC KO cells.

CDDP-loaded TKH-2 – NG or IgG – NG (Figure 24D). After 1 or 2 h treatment, the cells were washed and lysed and the lysates were checked for Pt content by ICP-MS. Pt content was significantly higher in T3M4 COSMC KO cells treated with TKH-2 – NG as compared with IgG – NG (*P<0.05*), while both the treatments showed similar Pt levels in case of T3M4 WT cells

In vitro cytotoxic activity of formulation

Cells (T3M4 COSMC KO and WT) were treated with Gem + TKH-2 – NG/CDDP or Gem + IgG – NG/CDDP or free Gem, 24h + CDDP, 24h or free Gem or free CDDP or NG/CDDP or Gem + CDDP co-administration. As seen with many targeted delivery systems [16], the uptake of targeted and nontargeted NGs can become practically the same. The same effect is expected to be the cause for no significant difference in the IC_{50} values of cells when treated with targeted (TKH-2 – NG) vs nontargeted NGs (IgG – NG). This trend was also seen across the receptor negative WT cells. To mimic the sequence in which Gem and CDDP were made available to the cells, free Gem was applied to the cells for 24 h and CDDP was added to Gem-containing media for the next 24 h at the same final CDDP concentration as the formulation. This sequence-dependent application of Gem and CDDP resulted in an IC_{50} value that was approx. 5-fold lower than values seen when cells were treated with the formulation, which is observed when transitioning from free CDDP to CDDP loaded into NGs [16,21].

Antitumor activity in orthotopic pancreatic cancer model

The efficacy of the formulation was tested on an orthotopic pancreatic cancer mouse model. Mice were injected with T3M4 COSMC KO/Luc cells directly into the pancreas. Tumors were detectable from day 9 by BLI and treatment was started from day 14 post inoculation of cells. Animals were treated IV via the tail vein every 4^{th} day for a total of 4

Treatment schedule	IC_{50} (w.r.t CDDP, µg/mL)	
	T3M4 COSMC KO	**T3M4 WT**
Gem + TKH-2 – NG/CDDP	0.13 ± 0.014	0.14 ± 0.003
Gem + IgG – NG/CDDP	0.15 ± 0.007	0.16 ± 0.006
Gem, 24h + CDDP, 24h	0.03 ± 0.003	0.035 ± 0.002
[a] Gem	0.5 ± 0.03	0.8 ± 0.03
Free CDDP	1.22 ± 0.15	1.55 ± 0.04
NG/CDDP	6.45 ± 0.30	7.77 ± 0.23
Gem + CDDP co-administration	1.2 ± 0.08	1.49 ± 0.19

Table 19. IC_{50} values of targeted and nontargeted formulation on T3M4 COSMC KO (receptor positive) and T3M4 WT (receptor negative) cell lines as per MTT assay.

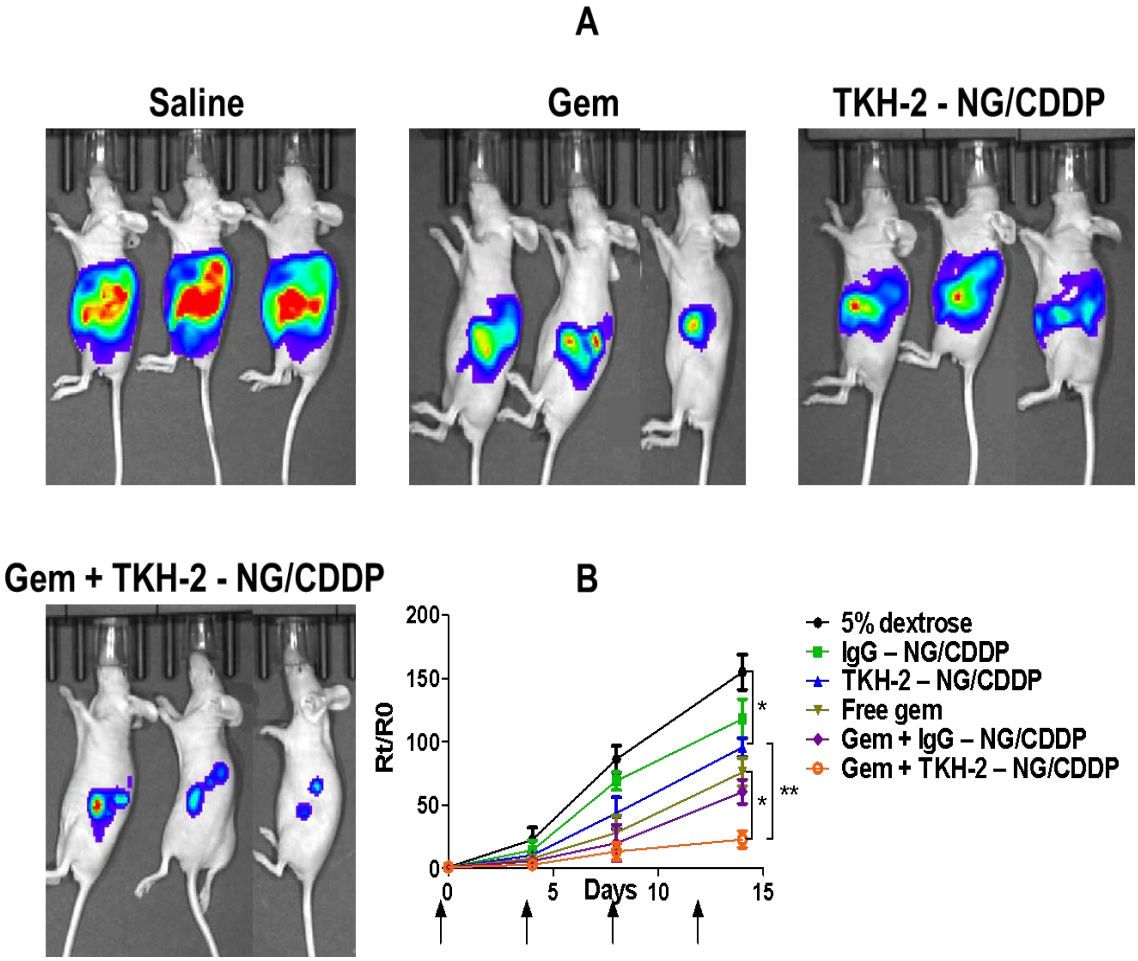

Figure 26. In vivo tumor progression in orthotopic pancreatic cancer across various treatment groups as followed by bioluminescence imaging (A) and quantitation thereof (B).

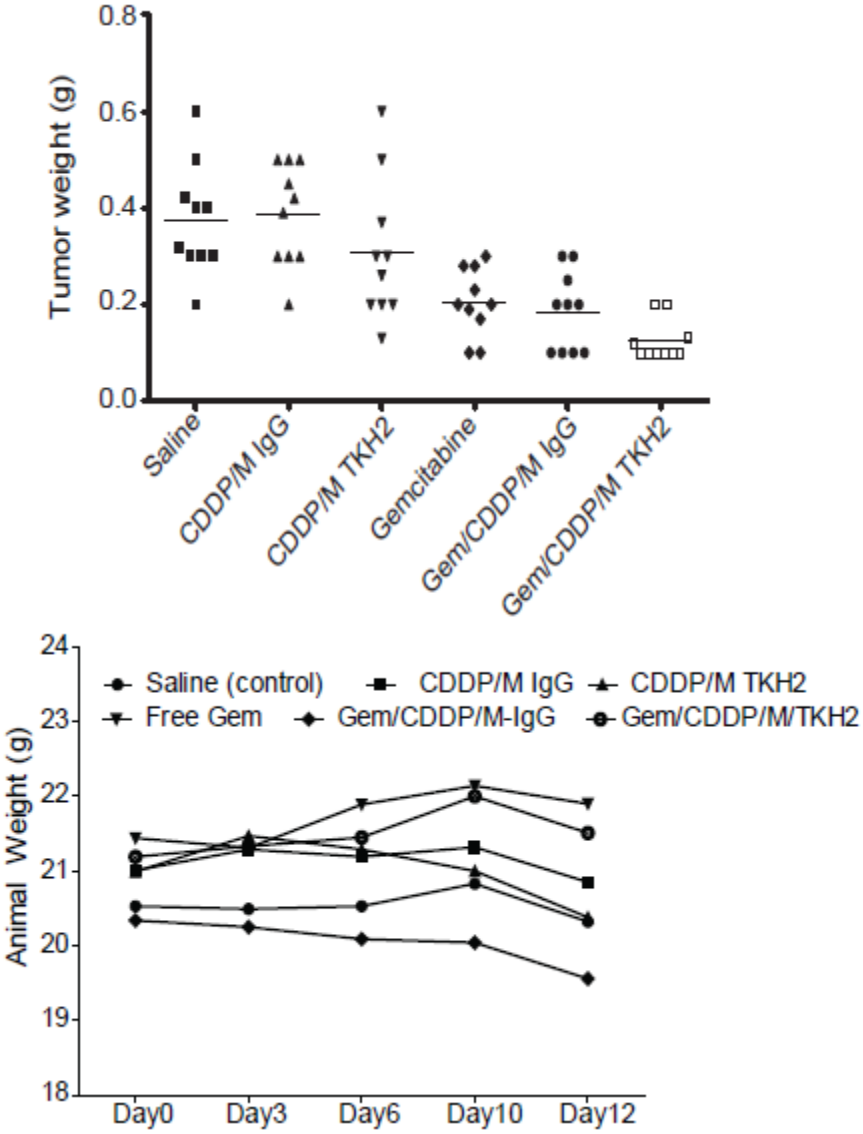

Figure 27. A) Whole tumor weights from animals sacrificed on day 15 of treatment. B) Changes in body weight of animals during the course of treatment.

	Primary Tumor	Peritoneum	Spleen	Liver	Lymph Nodes	Diaphragm
Saline (control)	100	20	60	10	70	30
CDDP/M IgG	100	10	90	10	70	60
CDDP/M-TKH2	100	10	50	0	60	50
Gemcitabine	100	10	80	0	30	20
Gem/CDDP/M-IgG	100	0	30	0	50	20
Gem/CDDP/M/TKH2	100	0	40	0	40	10

Table 20. Tumor metastasis as observed across different treatment arms.

injections at CDDP 4 mg/kg and Gem 20 mg/kg equivalent doses. The tumor progression for each individual treatment is shown in Figure 26. Monotherapy with either TKH-2 – NG/CDDP (targeted formulation) or Gem was successful in retarding tumor growth significantly ($P < 0.05$). Treatment with Gem + TKH-2 – NG/CDDP further retarded the tumor growth as compared with Gem ($P < 0.05$) and TKH-2 – NG/CDDP ($P < 0.01$). Presence of Gem also caused significant suppression of tumor growth in animals treatedwith IgG – NG/CDDP (nontargeted formulation, $P < 0.01$). While Gem + TKH-2 – NG/CDDP was better than Gem + IgG – NG/CDDP, it did not achieve statistical significance. The same trend was also observed in weights of whole tumors post necropsy of animals on day 15 (Figure 27A). While primary tumor was seen in all animals that were inoculated with tumor cells, metastasis was found only in some animals. Notably, peritoneal metastasis was not observed in any of the animals (n = 10) that received combination of both Gem and CDDP/NG, either targeted or nontargeted (Table 20).

Pt content in tumor and other organs

To compare the effectiveness of TKH-2 in delivering CDDP to tumors, tissues from 3 animals randomly selected from each treatment group were digested and checked for Pt content using ICP-MS. It was found that Pt levels in tumors of animals treated with TKH-2 – NG/CDDP were higher than those treated with IgG – NG/CDDP ($P < 0.01$) irrespective of the presence of Gem (Figure 28). An interesting observation, however, was that the presence of Gem itself helped in enhancing the delivery of CDDP to the tumor tissue, as could be seen between animals treated with Gem + TKH-2 – NG/CDDP vs TKH-2 – NG/CDDP ($P < 0.05$). High amounts of Pt were also observed in liver and spleen, organs of the mononuclear phagocyte system, but the effects of targeted delivery due to TKH-2 as well as overall enhanced delivery of Pt due the presence of Gem were observed exclusively in the tumor tissue and not in other healthy organs.

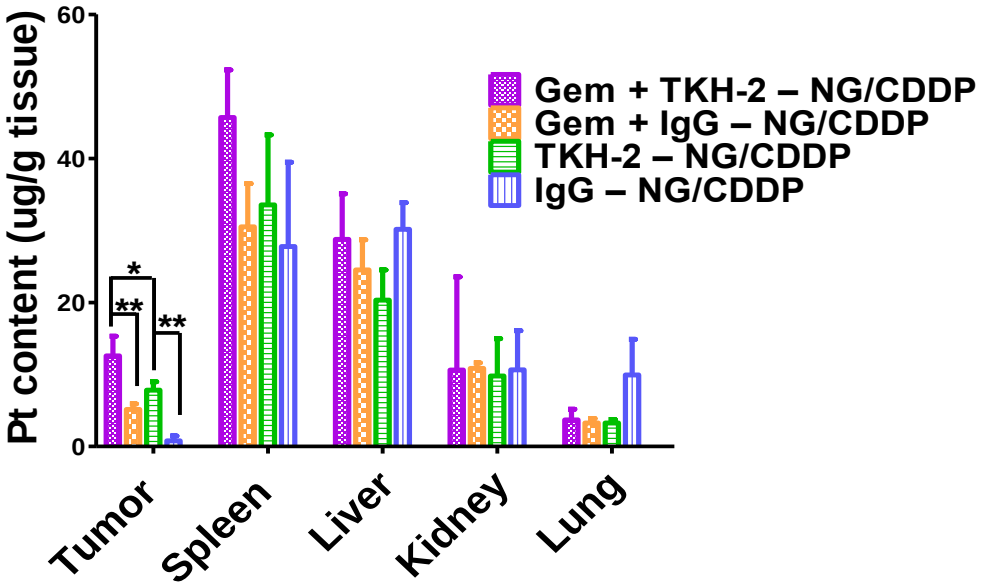

Figure 28. Platinum content in various tissues of animals sacrificed on day 15, as determined by ICP-MS. Animals were treated with TKH-2 – NG/CDDP or Gem + TKH-2 – NG/CDDP or IgG – NG/CDDP or Gem + IgG – NG/CDDP. Data are represented as mean ± SD (n = 3).

Treatment group	ALP (IU/L)	ALT (IU/L)	BUN (mg/dL)
Gem + TKH-2 – NG/CDDP	14.5 ± 0.7	46	17
Gem + IgG – NG/CDDP	13 ± 2.65	50 ± 3	17.6 ± 1.53
TKH-2 – NG/CDDP	15	39.5 ± 5.5	15 ± 1.15
IgG – NG/CDDP	15	38 ± 2.6	15 ± 0.6
Free Gem	15.5± 2.1	45.5 ± 3	15 ± 4
Control	14 ± 0.8	46.5 ± 3.5	17 ± 2.8

Table 21. Clinical chemistry parameters as assessed by whole blood analysis from animals sacrificed on day 15. Data are represented as mean ± SD (n = 3).

Clinical chemistry parameters and toxicity profiles

During the course of the treatment, body weights of animals were routinely monitored, and no significant changes were observed across different treatment groups (Figure 27 B). Blood collected from animals sacrificed on day 15 was subjected to analysis of clinical chemistry parameters indicative of renal and hepatotoxicity. As shown in Table 21 below, parameters across all treatment groups were comparable to control animals, which indicated that no short term toxicity occurred to the animals as a result of the treatment. Furthermore, H & E stained sections of all healthy organs were examined under a microscope by pathologist. No signs of morphological changes were seen in any of the animals, providing additional proof that all treatments were well-tolerated by the animals and no short term toxicity was evident.

3.3 Conclusion

In this study, we demonstrated that TKH-2 decorated nanogels were effective in delivering higher payloads of nanogels encapsulating CDDP. This lead to a better therapeutic efficacy in terms of tumor growth retardation as well as avoidance of acute toxicity, when tested in an orthotopic pancreatic cancer murine model. The sequential administration of Gem followed by CDDP that had the highest synergy was also maintained in vivo for enhanced therapeutic efficacy. Most importantly, this formulation approach allowed for the administration of both the drugs in the same dose and still achieved sequential administration. At the same time, encapsulation of CDDP into tumor-targeted NGs allowed to mitigate the toxicity associated with the combination of Gem and CDDP.

3.5 References

1. Conroy, T.; Desseigne, F.; Ychou, M.; Bouché, O.; Guimbaud, R.; Bécouarn, Y.; Adenis, A.; Raoul, J.; Gourgou-Bourgade, S.; de la Fouchardière, C. FOLFIRINOX versus gemcitabine for metastatic pancreatic cancer. N. Engl. J. Med. **2011**, 364, 1817-1825.

2. Ychou, M.; Conroy, T.; Seitz, J. F.; Gourgou, S.; Hua, A.; Mery-Mignard, D.; Kramar, A. An open phase I study assessing the feasibility of the triple combination: oxaliplatin plus irinotecan plus leucovorin/ 5-fluorouracil every 2 weeks in patients with advanced solid tumors. Ann. Oncol. **2003**, 14, 481-489.

3. Attard, C. L.; Brown, S.; Alloul, K.; Moore, M. J. Cost-effectiveness of FOLFIRINOX for first-line treatment of metastatic pancreatic cancer. Current Oncology **2013**, 21, 41-51.

4. Eastman, A. Activation of programmed cell death by anticancer agents: cisplatin as a model system. Cancer Cells **1990**, 2, 275-280.

5. Hertel, L.; Kroin, J.; Misner, J.; Tustin, J. Synthesis of 2-deoxy-2, 2-difluoro-D-ribose and 2-deoxy-2, 2'-difluoro-D-ribofuranosyl nucleosides. J. Org. Chem. **1988**, 53, 2406-2409.

6. van Moorsel, C. J.; Pinedo, H. M.; Veerman, G.; Bergman, A. M.; Kuiper, C. M.; Vermorken, J. B.; van der Vijgh, W. J.; Peters, G. J. Mechanisms of synergism between cisplatin and gemcitabine in ovarian and non-small-cell lung cancer cell lines. Br. J. Cancer **1999**, 80, 981-990.

7. Yang, L.; Li, L.; Liu, L.; Keating, M.; Plunkett, W. In In Gemcitabine suppresses the repair of cisplatin adducts in plasmid DNA by extracts of cisplatin-resistant human colon carcinoma cells; Proc Am Assoc Cancer Res; 1995; Vol. 36, pp 357.

8. McMahon, M. B.; Bear, M. D.; Kulp, S. K.; Pennell, M. L.; London, C. A. Biological activity of gemcitabine against canine osteosarcoma cell lines in vitro. Am. J. Vet. Res. **2010**, 71, 799-808.

9. Kim, J. O.; Nukolova, N. V.; Oberoi, H. S.; Kabanov, A. V.; Bronich, T. K. Block Ionomer Complex Micelles with Cross-Linked Cores for Drug Delivery. Polym. Sci. Ser. A. Chem. Phys. **2009**, 51, 708-718.

10. Nukolova, N. V.; Oberoi, H. S.; Zhao, Y.; Chekhonin, V. P.; Kabanov, A. V.; Bronich, T. K. LHRH-targeted nanogels as a delivery system for cisplatin to ovarian cancer. Molecular pharmaceutics **2013**, 10, 3913-3921.

11. Arnesano, F.; Natile, G. " Platinum on the road": Interactions of antitumoral cisplatin with proteins. Pure and Applied Chemistry **2008**, 80, 2715-2725.

12. Steinhauser, I.; Spänkuch, B.; Strebhardt, K.; Langer, K. Trastuzumab-modified nanoparticles: optimisation of preparation and uptake in cancer cells. Biomaterials **2006**, 27, 4975-4983.

13. Brown, B. S.; Patanam, T.; Mobli, K.; Celia, C.; Zage, P. E.; Bean, A. J.; Tasciotti, E. Etoposide-loaded immunoliposomes as active targeting agents for GD2-positive malignancies. Cancer biology & therapy **2014**, 15, 851-861.

14. Nukolova, N. V.; Yang, Z.; Kim, J. O.; Kabanov, A. V.; Bronich, T. K. Polyelectrolyte nanogels decorated with monoclonal antibody for targeted drug delivery. React Funct Polym **2011**, 71, 315-323.

15. Ferrari, M.; Fornasiero, M. C.; Isetta, A. M. MTT colorimetric assay for testing macrophage cytotoxic activity in vitro. J. Immunol. Methods **1990**, 131, 165-172.

16. Desale, S. S.; Soni, K. S.; Romanova, S.; Cohen, S. M.; Bronich, T. K. Targeted delivery of platinum-taxane combination therapy in ovarian cancer. J. Controlled Release **2015**.

17. Ferreira, S. A.; Gama, F. M.; Vilanova, M. Polymeric nanogels as vaccine delivery systems. Nanomedicine: Nanotechnology, Biology and Medicine **2013**, 9, 159-173.

18. Soni, K. S.; Desale, S. S.; Bronich, T. K. Nanogels: An overview of properties, biomedical applications and obstacles to clinical translation. J. Controlled Release **2015**.

19. Oberoi, H. S.; Nukolova, N. V.; Laquer, F. C.; Poluektova, L. Y.; Huang, J.; Alnouti, Y.; Yokohira, M.; Arnold, L. L.; Kabanov, A. V.; Cohen, S. M. Cisplatin-loaded core cross-linked micelles: comparative pharmacokinetics, antitumor activity, and toxicity in mice. International journal of nanomedicine **2012**, 7, 2557.

20. Oberoi, H. S.; Laquer, F. C.; Marky, L. A.; Kabanov, A. V.; Bronich, T. K. Core cross-linked block ionomer micelles as pH-responsive carriers for cis-diamminedichloroplatinum (II). J. Controlled Release **2011**, 153, 64-72.

21. Nukolova, N. V.; Oberoi, H. S.; Cohen, S. M.; Kabanov, A. V.; Bronich, T. K. Folate-decorated nanogels for targeted therapy of ovarian cancer. Biomaterials **2011**, 32, 5417-5426.

CHAPTER 4

Summary

Combination therapy remains the mainstay of therapy for cancer. While combinations can be made between various classes of therapeutic agents, the focus of this dissertation remained chemotherapy. Monoclonal antibodies have emerged in recent years to target specific cellular pathways and have shown promising therapeutic efficacy. However, monotherapy always carries a risk of development of resistance and thus our goal was to combine the advantages offered by both small molecules and monoclonal antibodies for the development of novel combination therapies for cancer. To this end, conjugation of nanoparticles loaded with cytotoxic agents to monoclonal antibodies is an attractive strategy. Nanoparticles can be tailored to encapsulate cytotoxic agents of different types. More importantly, with limited points of conjugation to the mAb, nanoparticles can help deliver much higher number of drug molecules per mAb. This can allow for much greater flexibility in terms of adjusting the dose ration between the drugs and the mAbs.

Polypeptides have an inherent property to assemble into supramolecular structures in solution. The formation of supramolecular structures is a controlled and organized process that depends by and large on the nature of the polypeptide and conditions of the solvent it is exposed to. Formation of amphiphilic copolymers based on such polypeptides can allow for tailoring the assembly process to a predefined nanoscale supramolecular structure, which can then be used as drug delivery vehicles. The overall process of self-assembly of such amphiphilic copolymers can then be regarded as a complex phenomenon of structural organization that is governed by the nature of constituent hydrophilic and hydrophobic blocks, their relative lengths, as well as properties of the solvent-phobic block that is the driving force for self-assembly. The inherent biocompatibility and biodegradability of polypeptides is of additional advantage for their

biological applications. For the purpose of the current study, amphiphilic block copolymer with following composition was chosen: polyethylene glycol (PEG) as the hydrophilic, stealth imparting block and polyleucine (PLeu) as the hydrophobic part and the initiator of micelle formation in aqueous environment. The variables explored in the current study were altering the ratio of lengths of constituent blocks as well as chirality of PLeu block and the temperature of solvent used for preparation of micelles via the film rehydration method. The impact of all these variables on the thermodynamic stability as well as type of secondary structures formed and the influence of these attributes on the ability of the micelles to encapsulate a combination of hydrophobic drugs into their core are also described.

The primary purpose of designing this micellar carrier was for combination therapy of ErbB2 positive breast cancer. The receptor tyrosine kinase, ErbB2 is a viable target in 20-25 % breast cancer patients due to its overexpression. Its degradation is associated with slower progression of the disease and increased survival times. While the monoclonal antibody Trastuzumab (Herceptin™) is the first line therapy in such patients, monotherapy with Trastuzumab has shown little benefit and therefore must be given with chemotherapeutic agents. Such combinations also help in delaying the development of resistance to Trastuzumab, since multiple cellular pathways can be targeted simultaneously. ErbB2 is a client protein of heat shock protein 90 and 17-N-allylamino-17-demethoxygeldanamycin (17-AAG) is a potent inhibitor of HSP90. Previous work in our lab has demonstrated strong synergy of action between 17-AAG and a model cytotoxic agent doxorubicin. In order to further improve the efficacy of the therapy, our goal was to replace doxorubicin with a more potent, clinically relevant agent paclitaxel (PTX), which has been shown to have strong synergistic antitumor effect with 17-AAG in ErbB2-driven breast cancers. Since synergy of such therapy is often sequence and dose ratio specific,

co-delivery of the drugs via the same vehicle is desirable as well as beneficial. Dual drug-loaded micelles thus prepared could load 17-AAG and PTX in a ratio 2:1 by weight. The formulation showed a high level of synergy on BT-474 cells that express a high amount of ErbB2 while the synergy was negligible in ErbB2low MCF-7 cells. The strong synergy also observed when the formulation was tested in an orthotopic breast cancer mouse model developed using ErbB2 overexpressing BT-474 cells, and an arrest in the growth of tumors in animals treated with dual drug-loaded micelles was observed, while both 17-AAG and PTX were used at sub therapeutic doses of 10 mg and 5 mg equivalents per kg body weight. The lower doses also helped avoid toxicity associated with the therapy. We also show the importance of simultaneously delivering the two drugs via a single carrier system as opposed to cocktail of individual drug-loaded micelles administered at equivalent doses, which has a better therapeutic outcome than the cocktail therapy. These combination drug-loaded micelles were developed as a platform for chemotherapy with Trast. The triple therapeutic system of Trast with combination drug-loaded micelles containing 17-AAG and PTX exhibited an even stronger anticancer effect, with complete regression of tumors at the end of treatment, which reached a palpable size again after day 45 with much slower progression than other treatment controls.

Chapter 2 was thus focused on the development of antibody conjugates to improve the therapy of ErbB2 positive breast cancer. The goals were to take advantage of synergy of action with multiple therapeutically active components and at the same time explore the scope of dose reduction to avoid the eventuality of increased combined toxicity of the multiple therapeutic agents used. The present study demonstrates the importance of biophysical characteristics of core-forming polyleucine block for the preparation of stable micelles that can load hydrophobic drugs. The self-assembly behavior of the block copolymer PEG-PLeu was dictated not only by the lengths of both constitutive blocks but

also the conditions of preparing these micelles. Thin film rehydration at elevated temperature of 60 ^{0}C lead to the formation of relatively small sized micelles with a low polydispersity index. The nature of polyleucine block was also an important parameter for consideration; racemic poly(D,L)-Leu block had a smaller hydrodynamic diameter and much higher capacity for encapsulation of hydrophobic drugs as compared to the enantiomeric ally pure poly(L)-Leu block. PEG-P(D,L)-Leu micelles were able to encapsulate both 17-AAG and PTX in a weight ratio of 2:1. This ratio showed a high level of synergy of cytotoxic action on ErbB2 overexpressing breast cancer cell line BT-474. When tested in an in vivo orthotopic mouse model of breast cancer, combination delivery via the same carrier had superior anticancer effect as compared to cocktail of individual drug-loaded micelles administered at the same drug ratio. Most importantly, marked antitumor effect was seen at a sub therapeutic doses of both 17-AAG and PTX, which lead to much better tolerability of the therapy and lack of signs of acute toxicity. This combination drug-loaded micellar carrier when conjugated with Trast showed complete retardation of tumor growth for prolonged period of time, without any signs of acute toxicity, which translated into the longest survival time amongst all treatment groups.

Chapter 3 was focused on development of combinatorial therapy for the treatment of pancreatic cancer. The goals of this part were to develop synergy-dependent sequential drug therapy that could be administered as a single dose. Pancreatic cancer (PC) is one of the most lethal malignancies, due to aggressive tumorigenicity, early metastasis and development of drug resistance to standard care chemotherapy. Since its approval in 1997, Gemcitabine (Gem) has been the first-line treatment for advanced disease. However, there is no standard second-line therapy after Gem failure. FOLFIRINOX, a combination of four agents, folinic acid, fluorouracil, irinotecan and oxaliplatin was approved by the FDA in 2010. The rationale for this combination was based on these

drugs having a different mechanism of action, and, more importantly, non-overlapping toxicities. In cases that could tolerate FOLFIRINOX, an overall improvement in the survival times as well as quality of life was noted. However, even the toxicities are non-overlapping, the cumulative toxicity profile for FOLFIRINOX can become the dose limiting factor. In the first trial itself, 50.8% of the patients needed dose adjustment. The common toxicities observed with FOLFIRINOX include Febrile neutropenia, Thrombocytopenic bleeding, ≥ grade 3 platelets, Grade 2 persistent neurotoxicity, Grade 3 persistent neurotoxicity OR Grade 4 neurotoxicity and many more non-hematological toxicities. Most of the toxicities are severe enough to require discontinuation of the treatment or switching to lower doses or alternative agents. The combination of Gem with Cisplatin (CDDP) has been explored in clinical trials for metastatic disease. As a part of FOLFIRINOX, platinum compounds showed significant efficacy. Cisplatin acts by damaging the DNA. It is known to first get converted into the aqua form within the cell, which happens by the replacement of the labile chloro groups with water molecules. This active form is then able to form covalently linked adducts with the DNA. This initial assault then goes on to activate a series of signaling pathways that ultimately lead to apoptosis and cell death. The DNA adducts thus formed can cause distortion of the DNA and subsequent recognition by various cellular proteins. This leads to problems in DNA synthesis and replication and is reported to cause a prolonged G2 cell-cycle phase arrest. However, the exact mechanism of activation of the apoptotic pathways remains unclear. On the other hand, gemcitabine is a deoxycytidine analog. Its mechanism of activation involves conversion into its triphosphate form, which can then be incorporated into the DNA as a false nucleotide. Usually, one more deoxynucleotide can be incorporated into the DNA before the synthesis stops. Another minor mechanism of action of gemcitabine is its ability to inhibit ribonucleotide reductase, which plays a key role in the repair mechanism of the DNA. Many studies report the benefit of administration of gemcitabine prior to that of cisplatin;

the reason cited for this is the increase in the formation of Pt-DNA adducts when the DNA had already been damaged and exposed due to the incorporation of deoxycytidine or active gemcitabine. The gemcitabine in turn inhibits the repair of the formed Pt-DNA adducts as well as reduces the efficacy of nucleotide excision repair by its ability to inhibit the action of ribonucleotide reductase. On the other hand, when Pt compounds are administered prior to gemcitabine, the formed Pt-DNA adducts can no longer allow for the incorporation of gemcitabine and that leaves no scope for gemcitabine to act. Our preliminary in vitro studies with the free drugs on T3M4 Simple Cells (*COSMC* deleted cells) showed that synergy of the combination is schedule-dependent, and Gem administration followed by CDDP showed the most potent cytotoxic activity. However, this combination proved to be only marginally effective in actual practice due to combined increased toxicity of both the agents. We have shown that encapsulation of CDDP in polymeric nanogels with cross-linked ionic cores enhanced its tumor accumulation and improved its safety profile. Additionally, sustained release profile of CDDP from nanogels allows for the administration of free Gem and CDDP loaded nanogels in a single injection while still retaining schedule-dependent synergy of the combination. Pancreatic ductal adenocarcinoma cells are known to express truncated O-glycans (Tn and STn antigens) and it was shown that decorating the nanogels with an antibody directed against this antigen further enhanced their uptake by tumor cells while reducing off-target accumulation in an in vivo pancreatic cancer model. Thus, in this study, we demonstrated that TKH-2 decorated nanogels were effective in delivering higher payloads of nanogels encapsulating CDDP. This lead to a better therapeutic efficacy in terms of tumor growth retardation as well as avoidance of acute toxicity, when tested in an orthotopic pancreatic cancer murine model. The sequential administration of Gem followed by CDDP that had the highest synergy was also maintained in vivo for enhanced therapeutic efficacy. Most importantly, this formulation approach allowed for the administration of both the drugs in

the same dose and still achieved sequential administration. At the same time, encapsulation of CDDP into tumor-targeted NGs allowed to mitigate the toxicity associated with the combination of Gem and CDDP.

LIMITATIONS AND FUTURE DIRECTIONS

The data reported in chapter 2 showed preclinical evaluation of PTX, 17-AAG and Trast in the form of antibody-nanoparticle conjugates. The nanoparticles were micelles made from a biodegradable polymer and showed great therapeutic efficacy at sub-therapeutic doses of both 17-AAG and PTX. This is work demonstrates the advantages of encapsulation of small molecule drugs into nanocarriers, that alters their pharmacokinetics favorably, enabling the system to achieve therapeutic efficacy at sub therapeutic doses. While in the first part of this chapter only the dual drug-loaded nanocarrier was evaluated, the second part consisted of testing the system's efficacy upon conjugation with Trast. Trast acted as a therapeutic as well as targeting ligand, further improving the anticancer response obtained with combination of 17-AAG and PTX. While such actively targeted systems can overcome the drawbacks of relying solely on the EPR effect due to heterogeneity in the tumor vasculature, there is still some variability in responses observed. A major limitation of the diblock copolymer PEG-PLeu is that it can load 17-AAG and PTX in one specific dose ratio only; while that ratio is highly synergistic, the best case scenario would be to have a carrier system that allows for varying the ratio of the two drugs and screen those ratios for efficacy. There is always scope to play with the hydrophobic block to improve the loading capacity for the hydrophobic drugs and achieve smaller sizes of the micellar carriers. The research in our lab is currently focused on the development of novel block copolymers with better loading capacities for hydrophobic drugs as well as being able to manipulate the ratio in which two drugs can be encapsulated into the same carrier. The ErbB2 receptor is known to have impaired endocytosis, which

is known to be improved by inhibition of HSP90 by 17-AAG. The impaired endocytosis also happens to be one of the primary reasons for resistance to Trast that some ErbB2 positive tumors exhibit. While our system shows very good efficacy on Trast-sensitive cell lines, our future work involves testing the efficacy of the system on Trast-resistant cell lines and due modifications therein to achieve better therapeutic response, in terms of the choice of drugs as well as dose ratios. However, this is a model system that can be used as a platform across many cancer types for the development of antibody-nanoparticle conjugates. Additionally, testing of the system in a transgenic mouse model instead of an orthotopic xenograft should provide a better understanding of the working potential of our system.

The current therapy for pancreatic ductal adenocarcinoma remains surgical resection or debulking of the tumor mass followed by chemotherapy and/or radiotherapy. Gemcitabine remains the first line therapy and resistant or relapsed cases are treated with FOLFIRINOX. However, FOLFIRINOX, which is a cocktail of 4 different agents, has severe dose-limiting toxicity and thus our efforts were to develop a combination regimen using Gemcitabine and a platinum drug. We chose cisplatin as our model agent for the proof of concept study. However, the current clinical platinum agent used is oxaliplatin, so our future study will involve using oxaliplatin in combination with gemcitabine. The PEG-b-PMA nanogels used are biocompatible, so our future efforts are directed towards the development of biodegradable carriers. Many recent studies have shown that the particulate system with the size less than 50 nm has profound effect on its tumor accumulation. Although we were able to generate particles with the size less than 100 nm, it wasn't small enough for the very effective tumor accumulation as per recent reports. This is especially true for poorly vascularized cancers like the pancreatic cancer, and may further improve the therapeutic outcome. The targeting antibody, TKH-2 can also be

replaced with a monoclonal antibody that has a therapeutic as well as targeting function. The current clinical trend is towards the use of immunostimulatory monoclonal antibodies and many of them are in clinical trials. Most often, these mAbs inhibit immunosuppressive receptors like that cytotoxic T lymphocyte-associated protein 4 (CTLA4) or programmed cell death receptor 1 (PD1) and so on, that ultimately results in the activation of T lymphocytes or natural killer cells. CTLA4-blocking mAbs, viz., ipilimumab and tremelimumab and PD1 targetign nivolumab are being tested in clinical trials and have shown promising results. One such antibody would be ab ideal candidate to design antibody-nanoparticle conjugates with gemcitabine and oxaliplatin for the therapy of pancreatic cancer.